Numerical and experimental study of semi-transparent photovoltaics integrated into commercial building façades

Leanne Robinson

A thesis

in the Department of

Building, Civil and Environment Engineering

Presented in partial fulfillment of the requirements for the degree of Master of Applied Science (Building Engineering) at Concordia University

Montréal, Québec, Canada

September 2009

Your file Votre référence
ISBN: 978-0-494-67308-9
Our file Notre référence
ISBN: 978-0-494-67308-9

ABSTRACT

Numerical and experimental study of semi-transparent photovoltaics integrated into commercial building façades

Leanne Robinson

Semi-transparent photovoltaics (STPV) have a large potential for integration in fenestration systems, adding the option of solar electricity production while still allowing for satisfaction of daylight needs. In office buildings, where the trends in architecture already include large glazed façades, and lighting loads constitute a significant portion of the overall energy consumption and, the integration of this technology is intuitive.

This thesis studies the potential of using either spaced opaque PV (photovoltaics) or thin-film PV and examines the impact of changing the PV area ratio (ratio of photovoltaics coverage to fenestration area) on the façade. It includes a verification of the workplane illuminance and PV output simulation models through comparison with measured data from an experimental office with a specially built full-scale prototype of a window with spaced solar cells.

The thesis addresses the issue of optimizing the PV area ratio for a simplified model based on a typical office in Montreal with an evenly divided south facing 3-section façade, which is an optimized façade concept that allows for view, adequate daylight and reduced heating/cooling loads. Several parametric variations are taken into consideration including façade orientation, site location, PV efficiency, lighting control strategies and shading device transmittance.

The annual simulation results show that a façade with integrated STPV has the potential to improve the overall energy performance when compared with opaque PV due to the significant daylighting benefits even at low transparency ratios. At approximately 90% PV area ratio in the upper section of the façade, the daylighting needs of the room are met; at higher PV area ratios the lighting loads increase rapidly and at lower ratios, the additional natural lighting does not enhance the performance further.

ACKNOWLEDGEMENTS

I would like express my deepest thanks to my supervisor, Dr. A. K. Athienitis, whose dedication to this field is inspiring and through the vast number of real life projects, we have learned much more than that which is contained in the pages of one thesis. I appreciate the support and encouragement from beginning to end and the opportunities arisen through your supervision.

I would also like to thank Dr. Lisa Dignard-Bailey, whose selfless encouragement and support has allowed me to explore different directions and to remind me to take my dreams into consideration. You have helped more than I believe you can imagine.

Technical support has come from many different people and in many different forms. I would especially like to thank Dr. Thanos Tzempelikos and Constantinos Kapsis for their invaluable input into the content of this thesis, Kwang-Wook Park for his patience and assistance in the experimental set-up, and Yves Poissant for his assistance with the PV measurements.

Last, but definitely not least, I would like to thank my family, my friends, and lab mates- for understanding and for always being there. Of course a special thanks to the fabulous 5.

Financial support from NSERC, FQRNT, NRCan, Eco Canada, and the Solar Buildings Research Network is much appreciated, with special recognition due to Centennial Solar who built the experimental PV system and Unicel Architectural who built and installed the window prototype.

TABLE OF CONTENTS

LIST OF FIGURES

LIST OF TABLES

NOMENCLATURE

a	Fraction after attenuation
a	Modified ideality factor
A_1	Area of the STPV section
ab, bb, cb, db	Derived direct luminous efficacy coefficients used in Perez model
ad, bd, cd, dd	Derived diffuse luminous efficacy coefficients used in Perez model
a_p	Horizon brightness coefficient
A_{PV}	Area ratio of the PV in the STPV window section
AST	Apparent solar time
$A_{workplane}$	Area of the workplane
BIPV	Building-integrated photovoltaics
BISTPV	Building-integrated semi-transparent photovoltaics
b_p	Horizon brightness coefficient
CCR	Ceiling cavity ratio
CU	Coefficient of utilisation of a space
E_b	Exterior beam illuminance incident on surface
E_{bh}	Beam horizontal exterior illuminance
E_d	Exterior diffuse illuminance incident on surface
$E_{desired}$	Desired workplane illuminance
E_{dh}	Diffuse horizontal exterior illuminance
EFF	Efficiency of luminaire
E_g	Exterior ground reflected illuminance incident on surface
$E_{luminaires}$	Illuminance from the luminaires

$E_{required\_lamps}$	Illuminance required by luminaires
E_t	Total exterior illuminance incident on surface
ET	Equation of time
EVA	Ethylene vinyl acetate
$E_{workplane}$	Workplane illuminance
F_1	Circumsolar brightening coefficient
F_{11}, F_{12}, F_{13}	Derived irradiance/illuminance coefficients for Perez model
F_2	Horizon brightening coefficient
F_{21}, F_{22}, F_{23}	Derived irradiance/illuminance coefficients for Perez model
FCR	Floor cavity ratio
FF	Fill factor of PV
f_i	Configuration factor
$F_{i,j}$	Form factor
f_L	Fractional lighting output
f_{L_min}	Minimum electric lighting output
f_p	Fractional electric lighting input
f_{p_min}	Minimum fractional electric lighting input
F_{sa}	Lighting special allowance factor
H	Hour angle
H	Height of room
h_c	Distance of luminaires from ceiling
h_{cav}	Heat transfer coefficient of cavity (radiative + convective)
h_i	Interior heat transfer coefficient (radiative + convective)
h_o	Exterior heat transfer coefficient (radiative + convective)

I	Current
I	Identity matrix
I_b	Exterior beam radiation incident on surface
I_{bh}	Beam horizontal exterior radiation
I_{bn}	Normal beam radiation
I_d	Exterior diffuse radiation incident on surface
I_{dh}	Diffuse horizontal exterior radiation
I_{ex}	Normal extraterrestrial solar radiation
I_g	Exterior ground reflected radiation incident on surface
I_L	Light current
I_{MPP}	Current of PV at maximum power
I_o	Reference irradiance
I_o	Diode reverse saturation current
I_{SC}	Short circuit current
I_t	Total exterior radiation incident on surface
k	Extinction coefficient
k_j	Thermal conductivity of material for i^{th} layer
L / L_j	Material thickness
L	Length of room
Lat	Latitude
LLF	Lighting loss factor
L_{m_tube}	Initial lumens of each tube
Long	Longitude
M_i	Final luminous exitance of surface i

M_o	Initial luminous exitance of surface i
m_{opt}	Relative air mass
n	Day number of the year
N	Inward flowing fraction
n_g	Refractive index
N_{lum}	Number of luminaires required
NOCT	Nominal operating PV cell temperature
N_{tubes}	Number of tubes in the luminaire
P_{lights}	Power required by the lighting
P_{MPP}	Maximum power of PV
P_{PV}	Power output of PV
P_{tube}	Power of each tube
Q_{facade}	Instantaneous heat gain through the façade
Q_{lights}	Instantaneous heat gain from lights
r	Component reflectivity
R_S	Series resistance
R_{SH}	Shunt resistance
RCR	Room cavity ratio
SHGC	Solar heat gain coefficient
STC	Standard test conditions
STM	Standard time meridian
STPV	Semi-transparent photovoltaics
t	Time of the day
T_b	Beam component of matrix used in radiosity method

T_{cell}	Temperature of PV cell
T_d	Diffuse component of matrix used in radiosity method
T_{dp}	Dew point temperature
t_{ext}	Outdoor temperature
t_{int}	Indoor temperature
T_o	Outdoor temperature
T_{STC}	PV cell temperature at standard test conditions
U	U value
V	Voltage
V_{MPP}	Voltage of PV at maximum power
V_{OC}	Open circuit voltage
W	Width of room
WC	Precipitable water content
WPH	Workplane height

Greek letters

β	Tilt angle of surface
Φ	Lumens required to achieve the desired workplane illuminance
$\Phi_{lighting\_required}$	Lumens required by luminaires to augment workplane illuminance
γ	Surface solar azimuth
α	Solar altitude
α	Absorptance of surface
α_j^f	Effective front absorptance through multi-layer glazing
Δ	Sky brightness

δ	Solar declination
ΔT	Longitudinal time correction
$\Delta\eta_{temp}$	Effects of changing cell temperature on PV efficiency
ε	Sky clearness
η	Effective efficiency of PV
η_{power_temp}	Manufacturer's cell temperature coefficient (PV)
η_{STC}	Stated manufacturer's PV efficiency at standard test conditions
θ	Angle of incidence of sun to surface
θ_d	Diffuse incidence angle
θ'	Angle of refraction
ρ	Reflectance of surface
ρ_{grd}	Ground reflectance
$\rho_{i,j}^{f}$	Effective front reflectance through multi-layer glazing
$\rho_{j,i}^{b}$	Effective back reflectance through multi-layer glazing
ρ_{single}	Single layer reflectance
τ	Transmittance of surface
$\tau_{i,j}$	Effective transmittance through multi-layer glazing
τ_{single}	Single layer transmittance
φ	Solar azimuth
ψ	Surface azimuth

1 INTRODUCTION

1.1 BACKGROUND

Canada's building sector is a significant energy user and producer of greenhouse gas emissions. The commercial sector alone accounts for 14% of end use energy consumption and 13% of the country's carbon emissions (NRCan 2009) with office buildings constituting the largest portion of this sector (NRCan 2007). By introducing energy efficient measures and by utilizing the passive solar gains and daylight through windows, the overall energy requirements of the building are reduced. However, all buildings have an energy requirement which cannot be met solely by introducing energy efficient measures. The introduction of active solar technologies into commercial façades to meet the remaining energy requirements is especially appropriate in Canada, where it is ranked second behind the US for total potential production of solar electricity on commercial façades of the countries evaluated by the International Energy Agency (I.E.A. 2002).

Semi-transparent photovoltaics (STPV) are proposed as a technology which will address the issue of reducing the overall energy consumption of commercial buildings. STPV are integrated into the building envelope, substituting conventional building materials, and allow daylight to enter the building while concurrently producing electricity. In office buildings, where recent trends in building design over the last two decades include the use of transparent façades due to an increased appreciation of daylighting, and where lighting loads constitute a significant portion of the overall energy consumption (NRTEE 2009), the integration of this technology is intuitive. Currently, façades with large glazing areas often maximize incoming daylight rather than controlling it appropriately, which could lead to increased thermal loads and thermal/visual discomfort in perimeter building zones (Tzempelikos & Athienitis 2007). However, with a greater understanding of the impact of various façade design parameters, and the use of STPV, these large glazed façades have the potential to have an important positive

impact on building energy performance while concurrently providing a comfortable space for its occupants.

1.2 MOTIVATION

For the use of STPV in highly glazed façades to have a beneficial impact on building energy performance, and to even potentially become a net energy generator, the façade must meet several important requirements:

1. Allow adequate daylighting into the space. With an appropriate lighting and shading strategy, this will provide for both a reduction in lighting energy consumption and improved visual comfort for the occupants (mostly dependant on glare and the quality of the light in a space).
2. Allow a view to the outdoors.
3. Reduce the heat transfer to and from the exterior environment. This will reduce the energy consumption for space heating and cooling, and potentially lead to smaller HVAC equipment (Li et al. 2005).
4. Provide better thermal comfort for the occupants (dependent on the temperature of the indoor window glass layer and affecting the mean radiant temperature felt by the occupants).

The façade used in the study will be a three-section façade with an upper section containing STPV, a middle section with a shade providing a view to the outdoors and glare control, and an opaque bottom section (Figure 1-1).

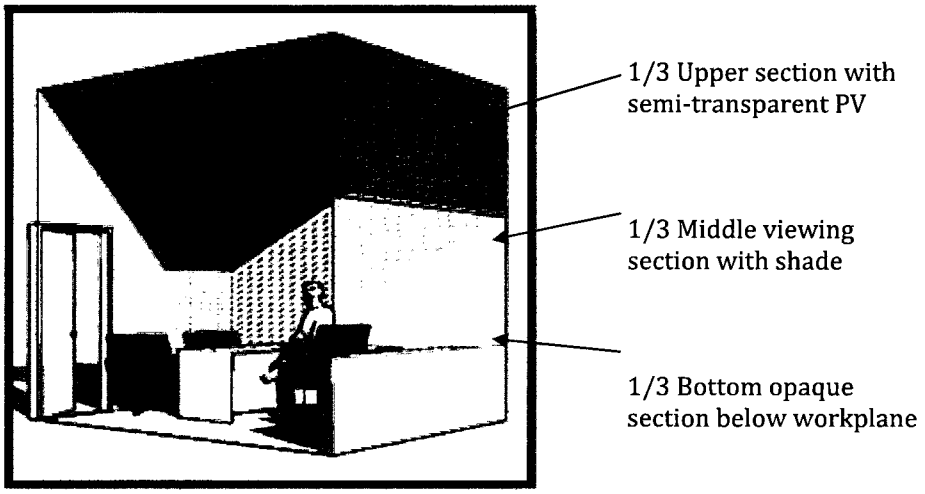

Figure 1-1: Three-section façade used in the study.

The three-section façade concept was used by Tzempelikos (2005) which makes use of each section of the façade for different purposes rather than trying to impose contradicting strategies on the entire façade. The upper section of the façade is used as a daylighting section, allowing daylight to penetrate deep into the room without causing excessive glare on the workplane. The middle section provides an important view to the outdoors and often includes a shading device to control glare. Finally the bottom section is opaque as it is below the workplane level and thus any transparency in this section would create an unfavourable heat transfer without the advantages of daylighting or view.

There has been limited research on the combined performance of STPV, examining both ideal daylight use and maximum electricity generation, while taking into consideration the ideal spacing, or transparency, of the cells. Even less work has been done on the development of guidelines for design/construction of glazed building façades with STPV. By providing an ideal PV area ratio in the semi-transparent PV section of the three-section façade, or by choosing thin film PV with an ideal efficiency/transmittance ratio, both the lighting loads and cooling loads may be kept to a minimum. Of the work done previously in this area, there is much variation in the results and no concrete guidelines given for any deviation from the specific situation studies.

There has been extremely limited work done using STPV in a three-section façade, and most of the daylighting calculations in the studies were conducted using commercial software with generic set-ups, thus limiting the accuracy of the daylighting results.

1.3 Objectives

The objective of this thesis is to develop a methodology for designing a commercial façade which uses STPV as a daylighting and electricity-generating component. The study will include an extensive daylighting study coupled with an artificial lighting strategy, a model of the electricity generated by the PV and a brief discussion on the potential impact of heat gains from both the façade and the artificial lighting. A comprehensive experimental study of an office with a custom-made two-section, double-glazed STPV-integrated window is used to verify the illuminance on the workplane, and to lead the discussion on the heat gains through the window.

The methodology presented will be general enough to be useful for constraints faced in everyday situations in a Canadian climate and not only valuable for a very exact site and façade arrangement. Several important design parameters are taken into consideration including changing façade orientation (South, South-west, South-east, West and East), site location (Montreal, Toronto, Vancouver, St. John's, and Iqaluit), PV efficiency (6%, 10%, 14%, 18%, and 22%), lighting control strategies (passive, active on/off, and continuous dimming) and shading device transmittance (1%, 5%, and 10%).

1.4 Thesis Overview

The thesis is divided into 4 major sections. Chapter 2 presents an overview of existing research conducted on STPV and their potential use in Canadian climate. A review of the modeling techniques for simulating daylighting performance and PV performance is also presented.

The simulation study is introduced in Chapter 3 with a detailed look at the method used for each part of the simulation.

Chapter 4 presents the results of the simulation study for different climatic conditions and different design days. A look at changing parameters and how they affect the ideal arrangement of the STPV in the façade is included and finally a methodology for designers is given.

In Chapter 5 the experimental set-up used to verify the simulation results is discussed and includes a comparison of the simulations and the measured data from the experiment.

Conclusions and recommendations for future work are presented in the concluding chapter 6.

2 LITERATURE REVIEW

2.1 INTRODUCTION

Semi-transparent building-integrated photovoltaic modules (STBIPV) fit directly into the building structure to become the outer skin of the building and incorporate the benefits of both clear glazing and building-integrated photovoltaic (BIPV) systems. They are manufactured by using a transparent material and encapsulating the opaque crystalline in a resin or Ethylene vinyl acetate (EVA) or else by using amorphous cells (Figure 2-1).

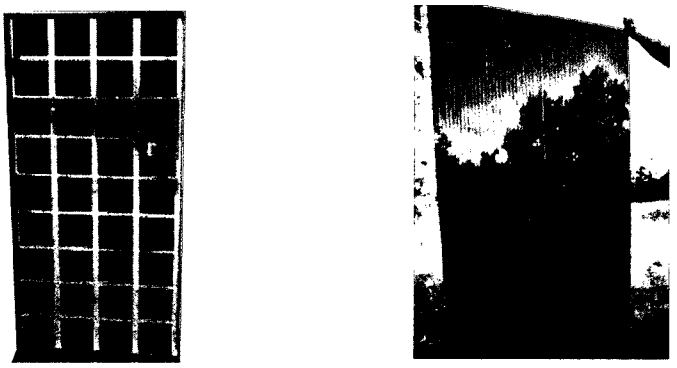

Figure 2-1: Semi-transparent photovoltaics-spaced cell example (right) and thin-film example (left) (Centennial Solar 2004)

The modules can be single, double or triple glazed and the cells can potentially be positioned on any glazing layer, although behind the front glazing is the most common. The transmittance of the semi-transparent photovoltaics (STPV) is determined by the area of the space between the opaque cells or the area of the microscopic holes in the case of the amorphous cells (Figure 2-2). The resulting module is a building element which can be integrated into most façades or roof structures and can be cost effective as it replaces traditional glazing on the building façade.

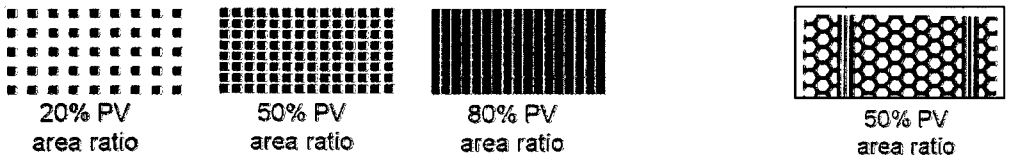

Figure 2-2: Changing transmittance of spaced STPV (left) & amorphous STPV (right) (Takeoka et al. 1993)

2.2 BENEFITS OF ADVANCED SOLAR FAÇADES

Advanced solar façades can be equipped with photovoltaic modules, thermal collectors, air collectors, honeycomb air collectors, transparent heat insulation or even transparent glass glazing with a large surface area. They are designed to effectively use the solar radiation hitting and entering the façade by optimizing between the amount of daylight entering the space, the electricity generated by any active collectors, and the heat passed through or blocked by the façade (Figure 2-3).

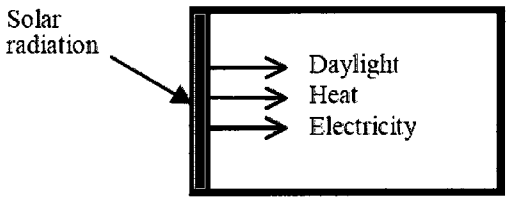

Figure 2-3: Solar façades include daylight, heat and electricity benefits (Vartiainen 2000)

2.2.1 DAYLIGHTING AND ASSOCIATED REDUCTION IN LIGHTING AND COOLING LOADS

The effective use of daylighting in buildings has two major advantages: (i) it can improve the quality of the light in a space, leading to increased worked productivity, and (ii) it can improve the building's performance due to reduced lighting, and potentially, cooling loads. Unfortunately, it is difficult to quantify the cost advantage of increased worker productivity, and thus the main quantifiable argument for daylighting is decreased energy consumption of the building. In this thesis the lighting loads and the associated heat gain reductions are the only energy-related daylighting benefit included, but the very-important increased occupant comfort will also be addressed in this review.

2.2.1.1 PSYCHOLOGICAL EFFECT OF DAYLIGHTING

It has been shown that daylighting has a positive psychological effect on humans. Heschong (2002) reported that rooms lit with daylight increase student performance in comparison with spaces utilizing only artificial lighting. Daylight is a full spectrum source of light to which human

vision is adapted whereas artificial lighting lacks the spectral distribution needed for complete biological functions. As many as 20-30% of the population suffers from problems related to lack of adequate daylight with the problems ranging from sleep disorders to performance difficulties to major depressions (Begemann et al. 1997).

2.2.1.2 ELECTRICAL ENERGY SAVINGS

As lighting and cooling loads constitute the largest portion of the energy consumption of typical commercial buildings, a reduction in either has a large impact on the building's performance. The use of daylighting reduces the need for artificial lighting and consequently the cooling loads as there are less heat gains from the lighting. This reduction could potentially lead to further savings by reducing the initial size of the HVAC equipment (Li et al. 2005). Li et al. (2002) also reported that the use of daylight in a cooling-dominated office building in Hong Kong could result in a 13% decrease in the annual electricity consumption, while when Franzetti et al. (2004) quantified the interaction between lighting and the HVAC for a 5-storey office building in France they found that the global energy needs were reduced by up to half when daylighting was used appropriately. Kapsis et al. (2009) found that for an office building in Montreal, the use of appropriate daylighting (including shading and lighting controls) could result in a lighting energy saving of 32-61%.

2.2.2 SOLAR HEAT GAIN CONTROL & REDUCTION IN COOLING/HEATING LOADS

In commercial buildings, cooling is important for perimeter spaces, even in heating-dominated climates. Maximizing the amount of daylight into a space is not appropriate and could lead to increased thermal loads and thermal discomfort in perimeter building zones (Tzempelikos & Athienitis 2007). For increasing window-to-wall area ratios, both the heating and cooling loads generally increase, although the lighting demand decreases. Shading devices, tinted glass or ceramic frits can help to reduce the solar radiation heat gains through the fenestration, and semi-transparent photovoltaics could be used in much the same way.

In a Montreal-based study conducted by Tzempelikos & Athienitis (2007) they found that if automatic shading control is added to an already controlled office, a reduction in cooling results, but with an increase in both lighting and heating demand. The optimal balance between solar gains and internal gains results in a 12% annual reduction in energy. The importance of optimising the perimeter zone energy balance between daylight admission and solar heat gain rejection was emphasized in Lee et al. (1998) where the use of dimmable lights and controllable daylighting/shading systems lead to significant energy savings and peak demand reductions. Bessoudo (2008) reported that by using a high-quality building envelope in highly-glazed façades, the need for perimeter heating can be eliminated completely and still achieve a high level of thermal comfort.

2.2.3 ELECTRICITY GENERATION

If photovoltaics are included in the advanced fenestration, further electricity savings are possible by the production of electricity from the façade. PV-generated power correlates well with peak summer utilities' daily load patterns as power is available when it is needed most (office hours). The PV potential for Canadian capitals and major cities is favourable when compared with major cities in countries with a high percentage of their electricity generation coming from PV. The yearly potential of the Canadian cities (for latitude tilt) ranges from 1361 kWh/kW in Regina, Saskatchewan, to 933 kWh/kW in St. John's, Newfoundland, both of which are more than the yearly potential for Tokyo, Japan and Berlin, Germany, two world leading photovoltaic countries in terms of installed capacity (Pelland et al. 2006).

Due to the height of the sun in the sky, vertical surfaces are better suited for building-integrated photovoltaics in high latitude rather than low latitude locations. Of the 14 countries studied by the International Energy Agency, Canada is number 2 for total potential production of solar electricity on commercial façades (after the US) and number 5 for ratio of potential production on all types of building façades to electricity consumption (I.E.A. 2002). For commercial and

institutional buildings, Pelland et al. (2006) state that photovoltaics could provide about 15-17% of total electricity consumption (131.7 TWh per year).

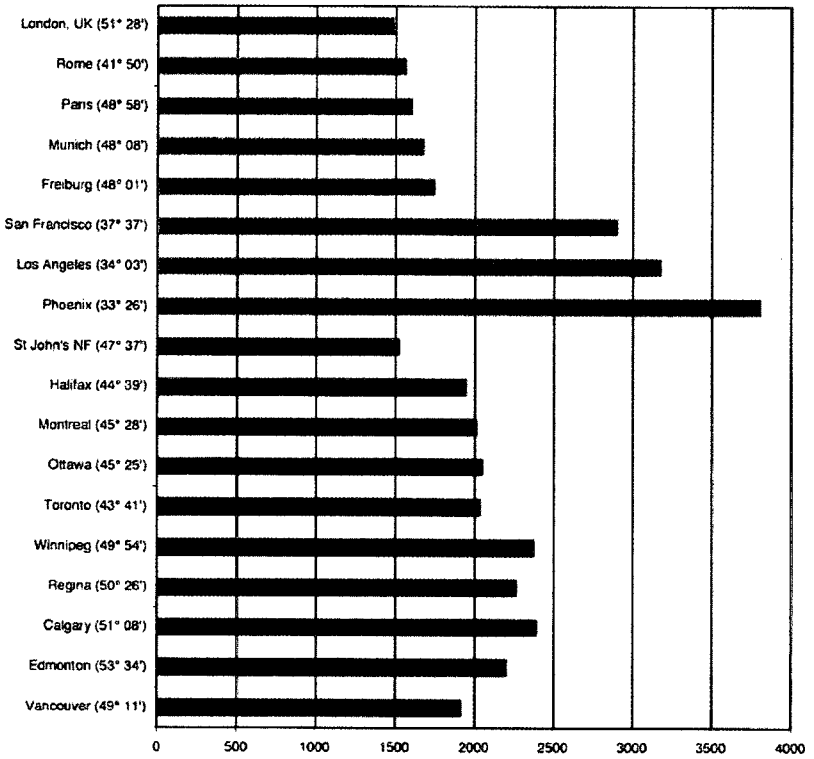

Figure 2-4: Annual sunshine hours for Canadian cities compared with international cities (NRCan 2004).

2.3 Modeling techniques for STPV

2.3.1 Radiation models

The ability to determine the amount of daylight on a workplane or the amount of heat absorbed in a glazing or on a PV cell depends on both the solar radiation (or illuminance) incident on the surface and the solar radiation transmitted through the glazing. The total solar radiation available incident on the surface is evaluated by adding the incident beam component, sky diffuse component and reflected component. The beam and reflected components are fairly straightforward to calculate while the diffuse is harder due to the continuously changing sky

conditions. The amount of radiation transmitted through the glazings will be discussed further in section 3.6.1.

2.3.2 DAYLIGHTING MODELS

In order to determine the illuminance on a workplane, the luminous flux which enters the space and its interactions within the space must be considered. Several advanced methods have been developed to deal with this luminous flux and its interactions with the space, and a brief overview will be given here.

2.3.2.1 RADIOSITY METHOD

The radiosity method is based on the principle of conservation of radiant energy (Siegel & Howell 1982). This method determines the fraction of diffuse radiation leaving each surface and directly reaching the other surfaces with the use of form factors, as well as reflected diffuse radiation reaching all surfaces after infinite reflections. Workplane illuminance after infinite interreflections is calculated using configuration factors relating the illuminance to the workplane point (Athienitis & Tzempelikos 2002), and the final luminous exitances of the surfaces in the room.

Its main weakness is that it models perfectly diffuse reflections for both the non-directional diffuse and directional beam component of the illuminance. This is the model employed in this study and will be described in more detail in section 3.7.

2.3.2.2 RAY-TRACING TECHNIQUES

The ray-tracing technique determines the visibility of surfaces by tracing imaginary rays of light from a viewer's eye to the objects of the rendered scene (Ward & Rubinstein 1994). In a forward ray tracing, the rays are emitted from a light source (or the sun) and strike surfaces in space contributing to the luminances of these surfaces, and in backward ray-tracing, the rays are emitted from a point in the scene and traced back to the source. When a ray with certain intensity strikes a surface, new rays are generated with their intensity depending on the

reflection. The computation time is high and thus it is often combined with a statistical method such as the Monte Carlo technique (Tsangrassoulis & Bourdakis 2003).

Ray-tracing techniques can model complex spaces with a great degree of accuracy and are particularly good for specular refection and refraction effects. However, the complexity and high processing time of ray-tracing limits its use.

2.3.2.3 OTHER TECHNIQUES- DAYLIGHT COEFFICIENT, DAYLIGHT FACTOR, AND LUMEN METHOD

There are several other methods available that will not be examined in detail here. Tregenza & Waters (1983) developed the daylight coefficient approach which related the luminance of an element of sky to the illuminance it produces on the workplane point. It is a complex function and its accuracy and efficiency lie in the number of sky division patches (145 is proposed). However, once the daylight coefficients have been computed for a given space, it takes little effort to calculate the illuminances under a large number of sky luminance distributions.

Two simpler methods are the daylight factor method (developed by Waldram (1950), Hopkinson (1954), and Bryan & Clear (1981)), and the lumen method of sidelighting (developed by Kaufman & Haynes (1981), and in IESNA (2000)) and skylighting (developed by Kaufman & Haynes (1981)). The daylight factor method is expressed as the ratio of the inside illuminance on a point on the workplane to the outside horizontal illuminance under an overcast CIE sky. The inside illuminance is determined as the sum of three components which reach the workplane point: the sky component, the externally reflected component, and the internally reflected component. The precision of this method is low (IESNA 2000) and using the CIE overcast sky underestimates the actual horizontal illuminances (Reinhart & Herkel 2000). The lumen method is similar to the zonal cavity method used for electric lighting and is calculated with the use of a coefficient of utilization, determined from a table of coefficients for different room geometries and sky conditions (IESNA 2000). Its limitations are the use of simplified geometry and that it doesn't consider direct sunlight (Vartiainen et al. 2000).

2.3.3 PHOTOVOLTAIC PERFORMANCE MODELS

Photovoltaic modules are a reliable source of electrical energy but must be properly designed in order to be effective. The manufacturer's stated output or efficiency is given for standard test conditions (25°C temperature, 1000 W/m² irradiance, air mass 1.5, normal incidence and unpolarized light) and does not give a very accurate indication as to the actual operating efficiency or output of a panel in real outdoor conditions. According to Armani et al. (2007), the climatic conditions which most affect the losses of the module while operating under outdoor conditions compared with the STC are: polarization effect, the reflection of unpolarized light, spectral effects, low irradiance level and cell temperature. The PV performance is also affected by system conditions which will not be explored.

For polycrystalline cells, the electrical power is calculated by the product of the current and voltage. The parameter that changes most frequently during a day is the irradiance, which affects predominantly the current of the module. The maximum power point voltage remains fairly constant with changes in irradiance except at very low irradiance levels (Figure 2-5).

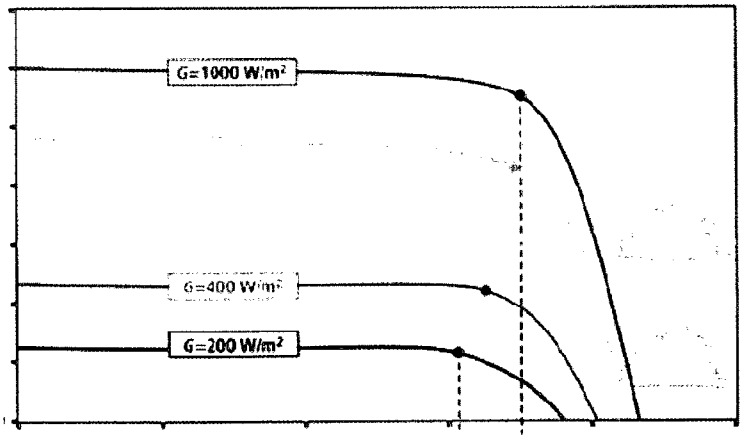

Figure 2-5: Changes in irradiance and the effects on the PV manufactured I-V (current-voltage) curve (German solar energy society 2005). Current is on y axis, voltage on x axis.

The parameter that affects the module voltage the most is the module temperature. The current is hardly affected by changes in module temperature (Figure 2-6). The temperature coefficients

for voltage, current and power change are normally specified on the module data sheets as a percentage per degree Celsius.

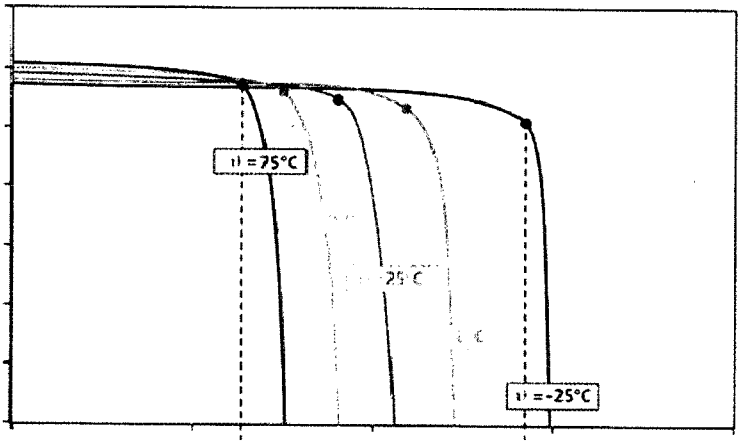

Figure 2-6: Changes in temperature and the effects on the PV manufactured I-V (current-voltage) curve (German solar energy society 2005). Current is on y axis, voltage on x axis.

Much research has been conducted and many software programs are available to predict PV performance and a few will be mentioned here.

2.3.3.1 SIMPLE MODEL

This model is the simplest model for predicting the PV output and is based on the radiation incident on the panel, the area of the PV and the PV area ratio as well as on a simple and widely used expression (Whitaker et al. 1991) which takes into account the effects of changing cell temperature on the stated manufacturer's efficiency. This is the model used in the simulations as it relies only on information available from the manufacturer, and is described further in section 3.9.

2.3.3.2 ONE-DIODE MODEL

The one-diode model is reduced from the two-diode model and is described in detail in Duffie & Beckman (2006).

The equation for the current (I) requires that five parameters be known: the light current (I_L), the diode reverse saturation current (I_o), the series resistance (R_s), the shunt resistance (R_{sh}) and a modified ideality factor (a). Five different conditions required to solve the equations for the five unknown parameters simultaneously at reference conditions. These equations are not easily solved unless good initial guesses and variable limits are used (Duffie & Beckman 2006).

$$I = I_L - I_o\left[exp\left(\frac{V+IR_s}{a}\right) - 1\right] - \frac{V+IR_s}{R_{sh}} \quad (2.3.1)$$

2.3.3.3 SANDIA MODEL

The Sandia model developed by King and others (King et al. 2004) increases the accuracy of the PV output in comparison with the other two models but require information that is not normally provided by the manufacturer and thus its ease of use is reduced.

2.4 ENERGY SAVINGS OF SEMI-TRANSPARENT PV FAÇADES

There have been quite a few studies conducted on semi-transparent photovoltaic façades and their impact on the overall energy consumption. Most studies compare a STPV façade with a base case building, similar in all aspects except the façade itself. They include a look at the influence of the STPV façade on heating and cooling loads based on the solar heat gains through the window and the change in heat gains from artificial lighting. They often include a section on the impact the façade has on the daylighting in the space and the change in electricity consumption due to the changed requirements of the lighting. The daylighting models are normally simplified models using existing software packages. They also look at the electricity generated from the photovoltaics themselves and sometimes link this with peak loads. These studies are all exhaustive and a brief description of the most notable will be presented here.

2.4.1 Overview of previous STPV studies

Japan:

Miyazaki et al. (2005) reported that the optimal solar cell transmittance and window to wall ratio of a STPV façade for an office building in Japan and estimated the potential energy savings, in terms of electricity production, daylighting, and heating and cooling loads. The entire office space was simulated, taking into account all internal heat gains, ventilation and infiltration as well as occupant, lighting and office equipment schedules. A semi-transparent amorphous silicon solar cell was used for the simulation study where the transmittance of the solar cells was adjusted by changing the area of the holes and its resulting power reduction was then almost equal to that transmittance.

Wong et al. (2008) is the only study mentioned in this literature review which explores the use of STPV in residential applications. They looked at the use of STPV as roofing material in 5 climatic regions of Japan for (i) a fully opaque BIPV roof, (ii) a STBIPV roof with 20% radiation transmission, and (iii) a STBIPV roof with 50% radiation transmission; with all roofs designed as 3kW systems. They simulated power generation and the thermal and optical characteristics of STPV and validated it against measurement data.

Spain:

De Boer & Van Helden (2001) conducted a comprehensive study of various STPV applications including a vertical 3-section façade in Madrid, looking at the effect of changing many parameters including: orientation, slope of façade, size of the room, level of internal heat production, ventilation level, transparency of PV module, infiltration of outside air, colour of façade (absorption), percentage of PV modules in façade area, insulation value of modules, and building mass of floors and ceiling. They simulated lighting, heating and cooling demand and power generation.

FINLAND, FRANCE, ITALY:

Vartiainen (2001) studied the electricity benefits of various office façade layouts from the use of daylight and PV for 4 different European locations: Trapani, Paris, Helsinki and Sodankyla. The façades had a minimum window area of 15% of the façade area and a maximum of 63%, with the remaining area covered in PV. He also explored a mosaic PV structure which is essentially STPV.

HONG KONG:

Fung & Yang (2008) has developed a mathematical model which looks at the thermal performance of, and in particular the heat gain through, building-integrated STPV for a base case in Hong Kong. His objective was to look at the total energy performance of the PV modules to evaluate the heat gain through the modules, the power generation of the modules and the resulting indoor illuminance in the room. He looked at the optimal inclination of the surface for the given location of Hong Kong and evaluated the effects of different orientation, solar cell area, solar cell efficiency and module thickness on the heat gains. Fung was using both spaced solar cells and see-through solar cells in his models.

Chow et al. (2007) conducted a performance analysis of a ventilated STPV window in a Hong Kong office building. They too changed the transmittance of the see-through solar cells by changing the area of the cells. They conducted a very comprehensive study of the temperature of the glazings and looked at the effect of changing their extinction coefficients.

Li et al. (2009), compared the difference in energy and cooling requirements of a generic office in Hong Kong with (i) an office with dimmable lighting based on workplane illuminance, (ii) an office with integrated STPV, and (iii) an office with both STPV and dimming lighting control. The study focused on the electricity generation and the reduction of peak cooling demand stemming from both electric lighting energy use and cooling energy use (from both the solar heat gain of the window and heat gain from the electric lighting). Their results included a) the reduction in

peak loads, b) the reduction in emissions and c) the monetary payback for each of the cases. Field measurements of the daylight illuminance, solar irradiance and output power were taken using an amorphous silicon PV module. The visible transmittance of the module and the daily mean PV efficiency along with the yearly measured solar irradiance were then used in the simulations.

2.4.2 Conclusions of previous STPV studies

2.4.2.1 Overall annual energy consumption

Li et al. (2009) reported that when STPV was used along with dimming controls in a large simulated Hong Kong office, an annual building savings of 12% was possible a peak cooling load reduction of 450kW for this office building. However, if taken alone, the STPV resulted in a savings of only 1.6% of the annual building electricity expenditure.

However, Miyazaki et al. (2005) found that an energy saving of 54% was possible when an optimal solar cell transmittance and window-to-wall ratio was used on a building in Japan.

De Boer & Van Helden (2001) found that the largest influences on annual heating and cooling demand for an office in Madrid is the orientation of the building, the infiltration and the internal heat production. They also reported that the transmittance of the STPV façade does not have a large effect on heating or cooling demand for the conditions studied.

In the study conducted by Fung (2006) they reported that the electricity benefits due to the energy savings in air-conditioning systems and electricity generation of PV are higher than energy consumption of artificial lighting for the office building studied in Hong Kong. Also noted was that when the window area is small, the power generated by the BIPV modules dominates the resultant electricity benefit. When the window area increases, the electricity saving from the air conditioning system becomes significant on the resultant electricity benefit. They found that a potential 120kWh/m2 net electricity benefit from the PV façade is possible for a WWR of 0.7 and a PV area ratio of 90%.

2.4.2.2 ENVIRONMENTAL AND FINANCIAL BENEFITS

In Hong Kong, where electricity is largely generated using fossil fuels, it was reported in Li et al. (2009) that emissions of CO_2, SO_2 and NO_x can be reduced by using STPV and dimmable-controls, with a monetary payback of 15 years if an electricity feed-in tariff, chiller plant cost reduction and CO_2 are all taken into consideration.

2.5 STPV FAÇADE DESIGN

2.5.1 SEMI-TRANSPARENT PV VS OPAQUE PV VS CLEAR GLAZING

Miyazaki et al. (2005) found that a PV window with window to wall ratio (WWR) of 50% (the optimal found for STPV) reduced the total electricity consumption by 18% compared to a single glazed window with WWR of 30% (the optimal found for both single and double glazed windows) and by 16% for a double glazed window, if no lighting-control was used. If lighting control is used, this reduces to 13% for single-glazing.

Chow et al. (2007) deemed that the use of semi-transparent a-Si glazing was better that the one with non-transparent c-Si solar cells for a working environment. The savings in electricity consumption of the artificial lighting was slightly higher for the low-iron glass than that for normal window glass.

Wong et al. (2008) found that STPV can result in positive energy savings of up to 8.7% total and 5.3% in heating and cooling when compared to a regular BIPV application if optimised correctly when compared with a BIPV roof. Furthermore they concluded that if STPV are used without optimisation measures, they have the potential to reduce the annual heating load but can result in summer overheating and thus may not offer overall energy savings. For residential applications, STPV did not contribute significantly towards lighting energy savings as the daytime lighting demand is low and already satisfied mostly by daylight from the existing windows.

For Vartiainen's (2001) mosaic façade (PV panels with diffusive glazing between the gaps), he found that it gave the maximum electricity benefit when comparing only lighting loads and electricity generation.

Fung (2006) states that total annual heat gain can be reduced by 30% and 60% for 20% and 80% coverage of total PV modules when compared to ordinary clear glass.

2.5.2 PV AREA RATIO OR TRANSMITTANCE

Miyazaki et al. (2005) report that, for a window-to-wall area ratio of 50%, a solar cell transmittance of 40% achieved the minimum electricity consumption in Japan for an office space of 24m x 24m. Without lighting control, higher solar cell transmittances resulted in smaller heating loads and larger cooling loads. With lighting control, the heating loads increased and cooling load decreased with increasing transmittance until the increase in solar heat gains outweighed the reduced heat from the artificial lighting. A solar cell transmittance of 10% resulted in the minimum electricity consumption when artificial lighting was not controlled by daylighting.

De Boer & Van Helden (2001) found that changing the transmittance of the PV module had little effect on the overall energy balance. For thermal optimization only, the total transparency of the façade should be 15%. For daylighting optimisation, the change from a 10% to 30% transmittance increases the mean workplane illuminance and the penetration level into the room but only slightly, due to the window below the PV façade which already takes care of 75-90% of the transparency of the total façade.

Chow et al. (2007) concluded that the maximum saving can be achieved for cell transmittances of 0.45-0.55 for an office in Hong Kong when taking the PV, lighting and air conditioning loads into consideration.

Wong et al. (2008) determined that for residential applications, a 20% radiation transmittance does not perform as well as the 50% transmittance. These were the only two transmittances explored.

When looking at an optimal glazing to PV ratio, Vartiainen (2001) found that for higher efficiency PV (8%), increasing the glazing area beyond 24% of the total façade area would only reduce the PV electricity but not increase the useful daylight sufficiently. If low-efficiency a-Si PV was used (efficiency of 3.5%) the glazing area should be increased by an additional 10% for all areas except in Trapani, the most southern location.

The solar cell area ratio has a significant impact on the total heat gain of the STPV modules. It was stated by Fung & Yang (2008) that the annual heat gain for this office in Hong Kong is lowered by 30% for a 20% PV area ratio and by 70% for an 80% PV area ratio. When the window to wall ratio is less than 0.5, the optimal solar cell area ratio is 0.7, and when the WWR is equal or greater than 0.5, a 0.9 PV area ratio is optimal (Fung 2006).

2.5.3 ORIENTATION

It was found that the transmittance changed for each orientation in Miyazaki et al.'s (2005) study. The optimal transmittances which give the minimum electricity consumption were: (i) 30% for South, (ii) 30-50% for East, (iii) 80% for North, and (iv) 30-50% for West. If the optimal transmittance was used on all orientations a further reduction of the total electricity consumption of the building, when compared with uniform transmittance was 2.4%.

It was found that of the parameters examined, façade orientation has a very large effect on annual heating and cooling demand and that heating demand is nearly proportional to room volume but cooling demand is roughly the same for small and large room in De Boer & Van Helden's (2001) study.

Fung (2006) found that the total annual heat gain of the east and west orientation was 15.3% and 17.5% less than that of the South orientation. However, the south facing façade still gives

the largest net electricity benefit, with East giving the second largest and the least being for West.

2.6 Examples of STBIPV applications in Canada

Red River College- Winnipeg

The Red River College in Winnipeg is a combination of a renovation and new construction project. It includes a 12.2kWp, 134m^2 STBIPV integrated façade in the south eastern façade. The curtain-wall is double-glazed with spaced polycrystalline cells laminated in the outer glass and a low-e coated inner glass.

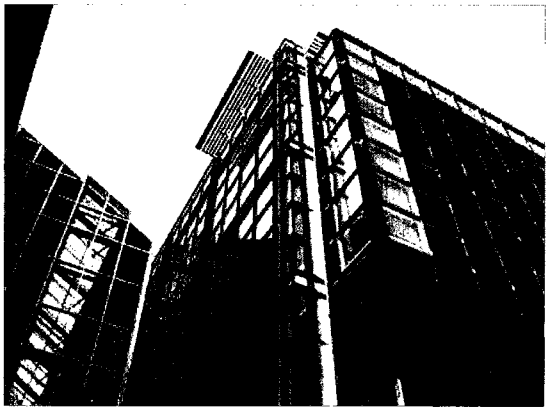

Figure 2-7: Red River college's integrated STPV façade (Boake 2007)

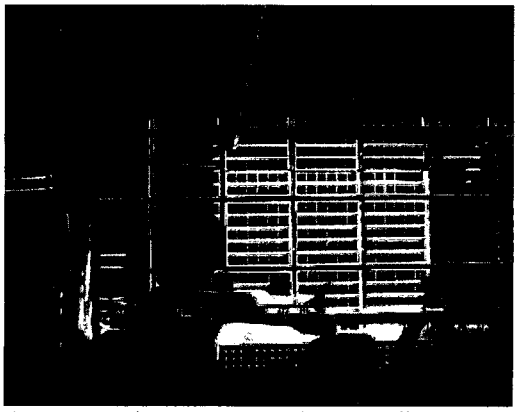

Figure 2-8: Classroom at Red River college with STBIPV (Boake 2007)

Greenstone Building- Yellowknife

The greenstone building is located in Yellowknife and is the Government of Canada's new energy efficient office building, and the largest North of 60 building-integrated photovoltaic system, at 33.5kW rated power. The four-storey office building has 6800m^2 floor area and a total PV area of 304m^2 or 37% of the curtainwall area. The photovoltaic elements are sandwiched between two layers of glass in the exterior element of the four-element glazed curtainwall system.

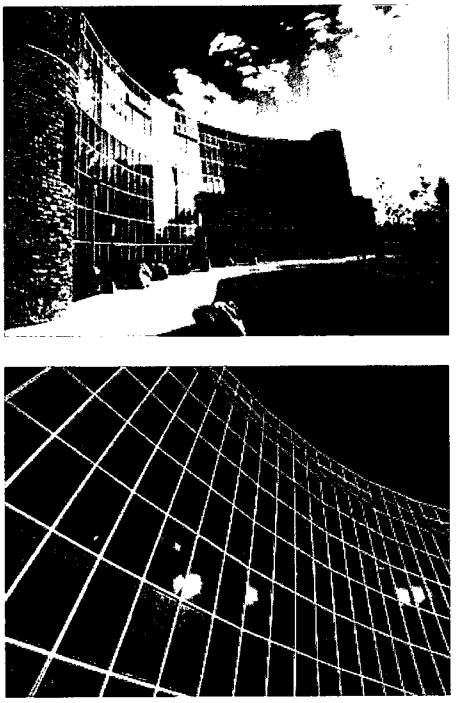

Figure 2-9: The greenstone building in Yellowknife with the STBIPV façade (Reed Construction data 2007, Williams Engineering 2009).

WILLIAM FARREL BUILDING- VANCOUVER

The Telus building was a renovation project which includes a 2.16kWp semi-transparent PV façade. The double-glazed fritted glazing system has operable windows which creates an air-space acting as an insulation in winter and natural ventilation in summer. The spaced poly-crystalline cells are incorporated into the northwest and southwest curtain wall façade (Boake 2007).

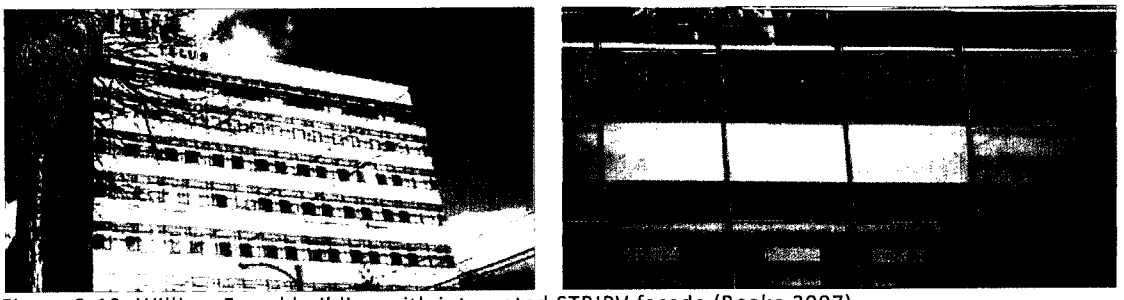

Figure 2-10: William Farrel building with integrated STBIPV façade (Boake 2007)

CENTRE FOR INTERACTIVE RESEARCH ON SUSTAINABILITY- VANCOUVER

The proposed center for interactive research on sustainability is a research center that will accommodate 4 academic institutions in downtown Vancouver that is scheduled to be completed in August 2010. It includes a semi-transparent BIPV south-facing, 30° skylight which is double-glazed. The system planned power output is 41kWp with a cell coverage of 85% (Cole et al. 2007).

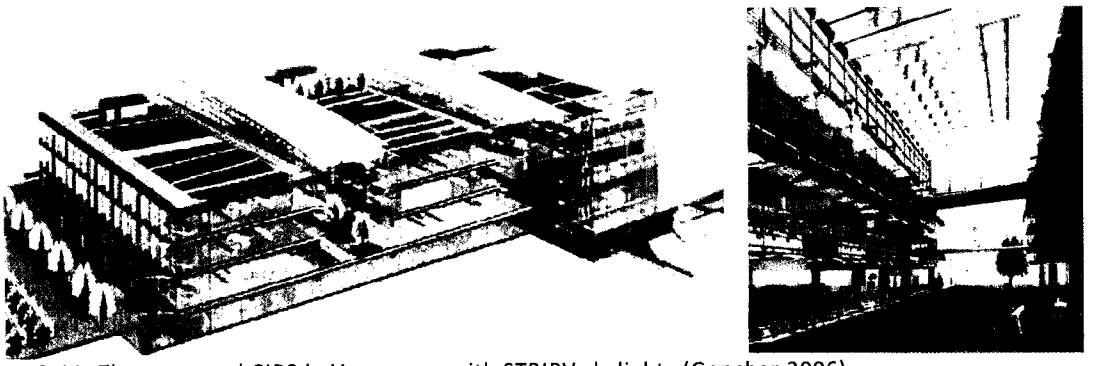

Figure 2-11: The proposed CIRS in Vancouver with STBIPV skylights (Gonchar 2006)

2.7 NEED FOR FURTHER WORK

As can be seen, some work has been done in this area but there is much variation in the results and there has been little in the way of proposing a methodology for designing a façade which incorporates semi-transparent photovoltaics taking into consideration the constraints faced in real situations. How does the designer integrate the selection of PV and its transparency into the overall design of the façade system taking into account the total energy picture but also the quality of the indoor environment? For Northern hemisphere locations, a southern façade is ideal for maximum PV electricity generation and daylight utilization and a vertical façade is ideal for minimizing cooling loads in the summer and heating loads in the winter. However, in reality, true-South facing façades are not always possible and the importance of understanding the implications of designing for a different orientation, or a different PV efficiency than that given in the previously mentioned studies is important. There has also been limited work done using STPV in a three-section façade, and with detailed daylighting models.

3 NUMERICAL MODEL

3.1 INTRODUCTION

The numerical simulation model was created in MathCAD and calculates the net electricity generation of an office with a semi-transparent photovoltaic façade. It is adaptable for different façade and room configurations as well as a range of design variables such as lighting control strategy, shade transmittance, and PV efficiency.

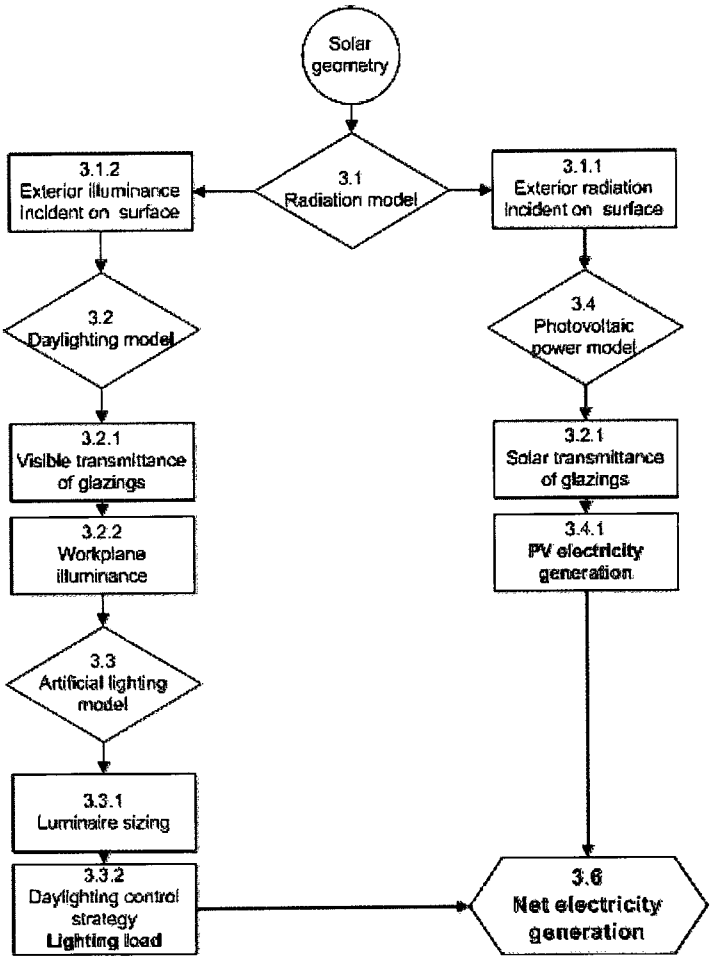

Figure 3-1: Steps in the numerical electricity generation model

The model steps are presented in (Figure 3-1). It was created for a Montreal based office using typical meteorological year data (TMY2) derived from the 1961-90 National solar radiation

database and converted by TRNSYS16 hourly weather observations, but by changing the input weather data, the model can be used for any location. As the weather data is hourly, all calculations are also performed hourly.

The first step in the model is to define the solar angles in order to calculate the radiation and illuminance incident on the inclined surface. The calculation of the solar angles is presented in Appendix I using well used expressions. Next the exterior radiation and illuminance incident on the inclined surface is calculated using the Perez all weather sky model (Perez et al. 1990). Using Fresnel derived expressions, the optical and solar properties of the glazing are determined, giving the total amount of solar radiation and illuminance passing through the façade.

In the daylighting portion of the model, the workplane illuminance is calculated after infinite interreflections using the Radiosity method (IESNA 2000, Murdoch 2003). The principal assumption made with this method is that all reflections are perfectly diffuse and that the inside surface of the STPV and window act as perfectly diffuse luminous sources. Figure 3-2 demonstrates the diffuse and direct portions of light which are modelled in the simulation.

The artificial lighting load is then determined using the lumen method of interior lighting design and by applying the appropriate lighting control strategy.

In the PV performance portion of the model, the output of the PV is calculated using a simple but widely used expression which takes into account the effects on the overall efficiency of the module from the variation in PV cell temperature from the standard test conditions.

Finally, the net electricity generation is calculated by subtracting the lighting load from the electricity generated by the PV. The simulations are performed on a yearly basis as well as for specific design days. The heat transfer through the façade is not taken into consideration in the simulation model.

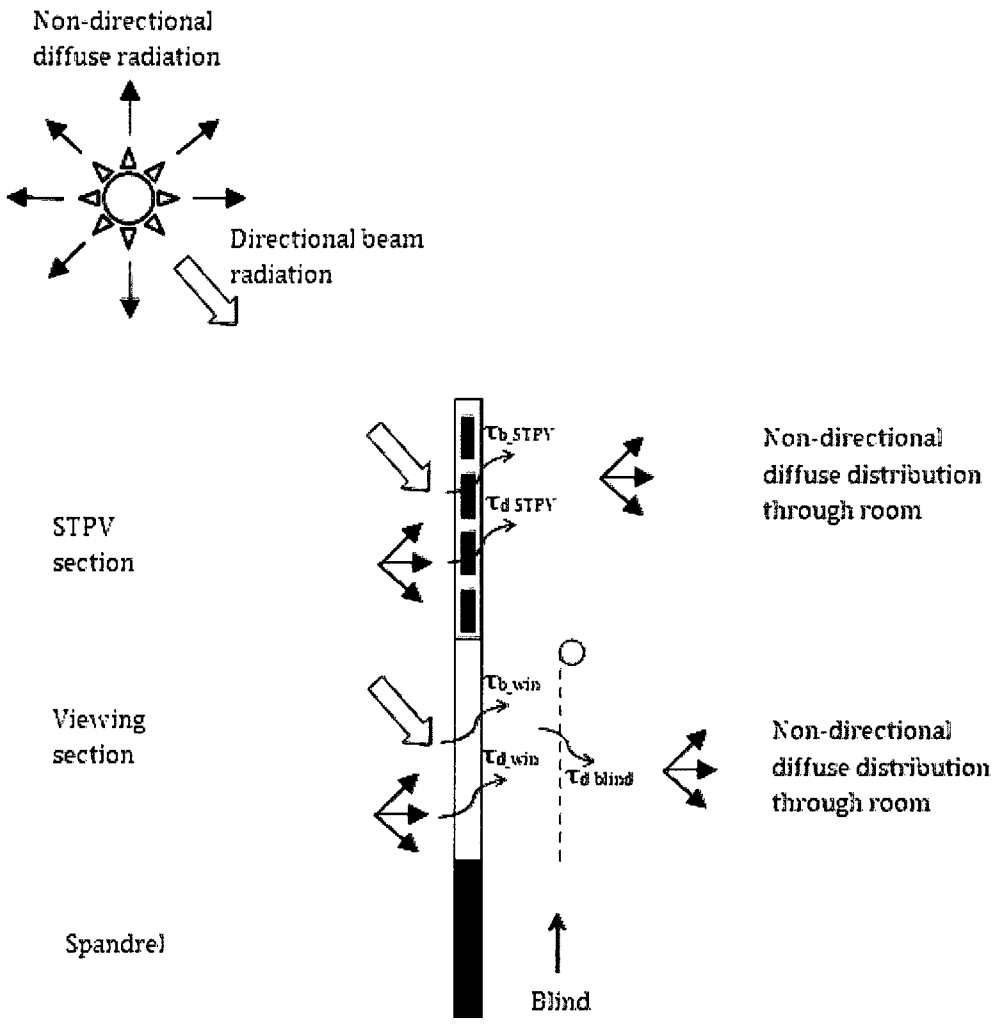

Figure 3-2: Diffuse and direct light as used in the façade simulation model for each of the façade sections.

However, the heat gain through the STPV façade and the impact of changing the PV area ratio or transmittance of the façade on the building's heating and cooling loads is an important design consideration. The experimental office and the resultant heat gains through the experimental STPV window will serve to lead the discussion on the heat gains through STPV façades in Chapter 5. The calculation of the U-values and solar heat gain coefficients for the experimental STPV window are presented with this numerical model overview (Figure 3-3).

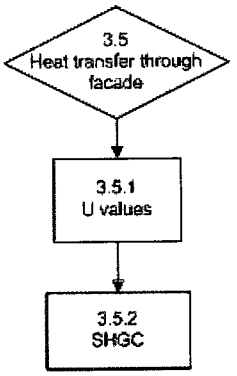

Figure 3-3: Steps in the façade heat transfer calculation for the experimental window

3.2 AUTHOR CONTRIBUTIONS

The work creating the mathematical model was done for the most part by the author, with a few notable exceptions. The solar angles were calculated using well-known expressions (Murdoch 2003) but input into MathCAD by author. The conversion of the TMY2 data and the development of the Perez model in MathCAD was done previously by Dr. Tzempelikos (Tzempelikos 2005). The model of the transmitted radiation and illuminance into the room was created for very specific window set-us, including the experimental window and the base case window by the author from the well-defined Fresnel expressions.

The daylighting model is an extension of a model developed Dr. Tzempelikos (Tzempelikos 2005). The model was adapted for this specific façade and room set-up. The configuration factors and form factors were redone for this set-up.

The artificial lighting model, the PV output model and the heat transfer through the façade were all created by the author using well-known and documented expressions (IESNA 2000, German Solar Energy Society 2005, Athienitis 1999).

3.3 MODEL ASSUMPTIONS

As the weather data is not real data but rather derived as a normal, errors will occur if comparing with an actual year of data. The Fresnel equations have limitations with complex

fenestration systems but are widely used for this type for calculation. Also, we are considering only 1-dimensional interactions of the light, where in fact it is 3-dimensional.

The principal assumption made with the daylighting model is that all reflections are perfectly diffuse and that the inside surface of the STPV and window act as perfectly diffuse luminous sources. For both glazing components- the STPV and the window viewing section, the transmittances are calculated for both the directional light passing as an angle of incidence of the sun on the window and the non-directional diffuse light. For the window viewing section, all light passes through a shade, when more than $100W/m^2$ direct light is incident on the exterior surface and the light becomes non-directional. If there is less than $100W/m^2$ direct light, the light is essentially all diffuse anyways and so our assumption of the window acting as a perfectly diffuse luminous source is not unreasonable. For the STPV the case is slightly different as there is no shade when direct light is present. In this case an area weighted average of the transmittance of the PV and the EVA is used. Thus the assumption that the STPV acts as a perfectly diffuse luminous source introduces errors, but which are much lower for high PV area ratios.

The control strategies of the lighting assumes that there is no human interaction with the lights and that if the workplane illuminance is at the desired level, this will be sufficient. The required illuminance from daylighting is set as the same as that required by artificial lighting, which may or may not be a reasonable assumption as in reality the quality of light is not the same. Both the artificial lighting model and the use of the control strategies were coded by the author.

The PV model takes only the effects on the overall efficiency of the module from the variation in PV cell temperature from the standard test conditions with the polarization, reflectance of unpolarized light, spectral and low irradiance effects not being taken into consideration. Also, an estimate of the PV cell temperature is used as no full heat transfer calculations were made.

The heat transfer through the façade is not taken into consideration in the simulation model.

3.4 BASE CASE

The base case used in the simulation study is the 'ideal, realistic' case based on one of Concordia's single offices. It is 3m wide x 4m deep x 4m high with the façade being equally divided into three sections: (i) a top section covered by STPV, (ii) a middle section used for view, and (iii) an opaque spandrel section. The spandrel goes up to the workplane height (0.8m) and continues for another 0.8m below the floor. It has been found that, for south-facing façades, a 30% window-to-wall ratio ensures that daylight provides enough light a similar space for 76% of the working time of the year; and larger window areas do not result in a significant increase in useful daylight in the room (Tzempelikos & Athienitis 2007). The window is full width across, save 10cm on each side for the frame. The reflectances of the walls are 0.6 (with some clutter, cork boards etc), ceiling 0.8, floor 0.2 as given in (IESNA 2000).

The desired workplane illuminance is 400lx, a balance between the recommended illuminance for common visual tasks and below the maximum for use with video display terminals (VDT) (IESNA 2000). The workplane point is in the center of the room and a control loop is added to account for activation of an interior roller shade whenever the incoming direct radiation is higher than 100 W/m^2. In this way, the occupant will be protected from glare when sunlight is present. There is no shade on the STPV section. The lighting used in the simulation study is 3 lamp 32-W, T-8 rapid-start fluorescent system with electronic ballast and based on Sylvania's F032W/31K 830 warm white deluxe (Sylvania 2007). The lighting is controlled by a continuous dimming control strategy and calculated hourly for typical office hours (from 8am to 5pm standard time).

The window make-up is a clear 6mm low-iron glass front glass, PV cells, EVA and then a clear 6mm back glass. The PV cells are based on Centennial Solar's transparent crystalline solar module- CS140VG (based on CS 140) (Centennial Solar 2004).

All weather data is taken from the TMY2 files derived from the 1961-90 National solar radiation database and converted by TRNSYS16 hourly weather observations. The ground reflectance is assumed to be 0.2 for no snow cover and 0.7 for ground snow cover of over 2.5cm (Liu, Jordan 1963). The snow cover was taken from the normalised historical data from the Environment Canada's website (Environment Canada 2008). The weather data for locations other than Montreal were converted using an excel macro provided on TRNSYS website (University of Wisconsin 2006).

All inputs used in the simulations are given in Appendix II.

3.5 NET ELECTRICITY GENERATION

The net electricity generation of the semi-transparent façade and its associated artificial lighting is equal to the electricity generated from the PV, less the energy consumption of the lights. It is calculated for the office based on changing PV area ratio of the semi-transparent photovoltaic façade.

$$Net\ electricity\ generation = P_{PV} - P_{lights} \tag{3.5.1}$$

The heat gains through the façade are not taken into consideration in the simulations. However, temperature distributions through the experimental window were measured and are discussed in sections 5.6.3 and 6.2.

3.6 RADIATION MODEL

The total solar radiation available incident on the surface is evaluated by adding the incident beam component, sky diffuse component and reflected component. The Perez all weather sky model (Perez et al. 1990) has been widely accepted as the most accurate model for treating diffuse radiation on an inclined surface. The model uses derived coefficients to control the horizon or zenith anisotropy which are calculated from horizon brightness, optical air mass, sky brightness and sky clearness. The beam normal, diffuse horizontal , beam horizontal radiation

components as well as outdoor temperature, and dew point temperature are taken from a typical meteorological year (TMY2) derived from the 1961-90 National solar radiation database and converted by TRNSYS16 hourly weather observations. The calculation of the exterior radiation and illuminance are presented in Appendix I.

3.6.1 TRANSMITTANCE, REFLECTANCE AND ABSORPTANCE OF GLAZINGS

For each layer, the visible and solar transmittance and reflectances are calculated for both beam and diffuse light. The beam components are calculated as a function of the angle of incidence of the sun on the surface while the diffuse components are assumed constant for all angles of incidence. The diffuse incidence angle (θ_d) is calculated based on the slope of the surface (β) from the expression used in (Brandemuehl & Beckman 1980).

$$\theta_d = 59.68 - (0.1388\beta) + (0.001497\beta^2) \tag{3.6.1}$$

3.6.1.1 SINGLE LAYER

The transmittance, reflectance and absorption are functions of the incoming radiation, and the properties of the material- thickness, refractive index and extinction coefficient. The angle of refraction is calculated using Snell's law. The component reflectivity is determined from the Fresnel expressions. For each layer, the transmittances, reflectances and absorption will be calculated for both beam and diffuse components. These equations can equally be used for both solar and visible transmittances and reflectances. The equations are given in Appendix I.

3.6.1.2 MULTIPLE LAYERS

To calculate the effective transmittances through multiple glazing layers, Fresnel derived expressions are used which include both a parallel and perpendicular reflection component of radiation from one layer to the next.

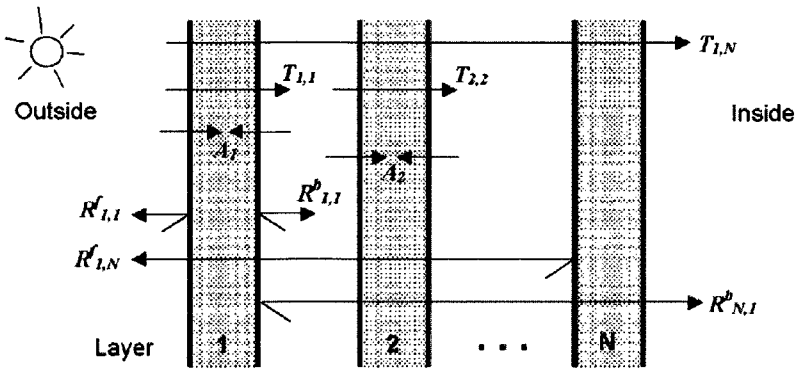

Figure 3-4: Transmittance, reflectance and absorptance of radiation or illuminance within a multi-layer glazing system (University of Illinois & Lawrence Berkeley National Laboratory 2008)

The effective transmittance is the transmittance through all layers of a multi-layer system is calculated using the effective reflectances of each layer. Layer 1 is the outermost layer and layer N is the innermost layer. The effective front absorption is the absorption of j after having passed through the other layers. The calculation is given in Appendix I.

3.6.1.3 DOUBLE GLAZED WINDOW USED IN SIMULATION

For the simulations, the window is treated as three 2-layer systems (Figure 3-5): a) the double glazed window viewing section (front glazing (g1)+ back glazing(g2)), b) the EVA in the STPV section (EVA & front glazing (EVA) + back glazing (g2)), and c) the PV in the STPV section (PV, EVA, and front glazing (PV) + back glazing (g2)).

For the absorptance of the PV, the front layer is further divided into 2 layers for a more accurate prediction of the PV output. In the simulations however, as the PV efficiency given by the manufacturer includes the front glazing but is not given as a function of angle of incidence. As the goal for the PV model was to predict the output using only manufacturer's data, the absorptance is assumed constant for all angles of incidence.

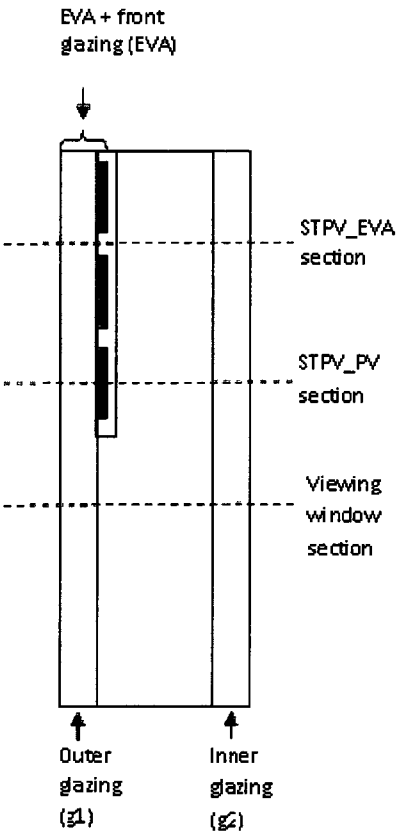

Figure 3-5: The window used in the simulations. The window is treated as 3 double-glazed sections.

The effective transmittance (τ_{win}) and reflectance (ρ_{win}) into the room for the double glazed **window viewing section** (front glazing (g1)+ back glazing(g2)) are calculated for a 2 layer system. They are calculated for both the solar and visible ranges. The absorptance of the outer glazing (α_{g1_win}) and inner (α_{g2_win}) glazing are used for the heat transfer calculation and is thus calculated only for the solar range.

The EVA and outer glazing are considered 1 layer in our analysis. The effective transmittance (τ_{STPV_EVA}) and reflectance (ρ_{STPV_EVA}) into the room for the EVA and outer glazing in the double glazed **STPV section** (EVA & glazing (EVA) + back glazing (g2)) and the absorptance of the outer (α_{EVA}) and inner (α_{g2_EVA}) glazing layers are calculated similarly to those in the window viewing section.

Window viewing section:

$$\tau_{win} = \frac{\tau_{g1} * \tau_{g2}}{1 - {\rho_{g2}}^{f} * {\rho_{g1}}^{b}} \quad (3.6.2)$$

$$\rho_{win} = {\rho_{g2}}^{b} + \frac{(\tau_{g2})^2 * {\rho_{g1}}^{b}}{1 - {\rho_{g1}}^{b} * {\rho_{g2}}^{f}} \quad (3.6.3)$$

$$\alpha_{g1\_win} = (1 - \tau_{g1} - {\rho_{g1}}^{f}) + \frac{\tau_{g1} * {\rho_{g2}}^{f} * (1 - \tau_{g1} - {\rho_{g1}}^{b})}{1 - {\rho_{g2}}^{f} * {\rho_{g1}}^{b}} \quad (3.6.4)$$

$$\alpha_{g2\_win} = \frac{\tau_{g1} * (1 - \tau_{g2} - {\rho_{g2}}^{f})}{1 - {\rho_{g2}}^{f} * {\rho_{g1}}^{b}} \quad (3.6.5)$$

STPV section:

$$\tau_{STPV\_EVA} = \frac{\tau_{EVA} * \tau_{g2}}{1 - \rho_{EVA} * \rho_{g2}} \quad (3.6.6)$$

$$\rho_{STPV\_EVA} = \rho_{g2} + \frac{(\tau_{g2})^2 * \rho_{EVA}}{1 - \rho_{EVA} * \rho_{g2}} \quad (3.6.7)$$

$$\alpha_{EVA} = (1 - \tau_{EVA} - {\rho_{EVA}}^{f}) + \frac{\tau_{EVA} * {\rho_{g2}}^{f} * (1 - \tau_{EVA} - {\rho_{EVA}}^{b})}{1 - {\rho_{g2}}^{f} * {\rho_{EVA}}^{b}} \quad (3.6.8)$$

$$\alpha_{g2\_EVA} = \frac{\tau_{EVA} * (1 - \tau_{g2} - {\rho_{g2}}^{f})}{1 - {\rho_{g2}}^{f} * {\rho_{EVA}}^{b}} \quad (3.6.9)$$

The effective transmittance (τ_{STPV_PV}) and reflectance (ρ_{STPV_PV}) into the room for the PV in the double glazed STPV section (front glazing, PV & EVA (PV) + back glazing (g2)) is calculated based on a 2-layer system which is reasonable considering the cells are opaque. However the absorptance of the PV cells (α_{PV}) and the front glazing in front of the PV cells (α_{g1_PV}) is calculated using a 2 layer system of the front glazing and PV cells.

$\tau_{STPV\_PV} = 0$ The cells are opaque

$$\rho_{STPV\_PV} = \rho_{g2} + \frac{(\tau_{g2})^2 * \rho_{PV\_back}}{1 - \rho_{PV\_back} * \rho_{g2}} \quad (3.6.10)$$

$$\alpha_{PV\_eff} = \frac{\tau_{g1} * \alpha_{PV}}{1 - {\rho_{PV}}^{f} * {\rho_{g1}}^{b}} \quad (3.6.11)$$

$$\alpha_{g1\_PV} = (1 - \tau_{g1} - {\rho_{g1}}^{f}) + \frac{\tau_{g1} * {\rho_{PV}}^{f} * (1 - \tau_{g1} - {\rho_{g1}}^{b})}{1 - {\rho_{PV}}^{f} * {\rho_{g1}}^{b}} \quad (3.6.12)$$

$\alpha_{g2\_PV} = 0$ The transmittance is 0

The overall transmittance (τ_{STPV}) and reflectance (ρ_{STPV}) of STPV section is an area weighted average based on the area ratio of the PV in the semi-transparent PV section (A_{PV}).

$$\tau_{STPV} = \tau_{STPV\_EVA} * (1 - A_{PV}) + \tau_{STPV\_PV} * (A_{PV}) \quad (3.6.13)$$

$$\rho_{STPV} = \rho_{STPV\_EVA} * (1 - A_{PV}) + \rho_{STPV\_PV} * (A_{PV}) \quad (3.6.14)$$

$$\alpha_{STPV} = \alpha_{STPV\_EVA} * (1 - A_{PV}) + \alpha_{STPV\_PV} * (A_{PV}) \quad (3.6.15)$$

3.7 Daylighting Model

To determine the horizontal workplane illuminance, a radiosity model is employed. It is based on the principle of conservation of radiant energy (Siegel & Howell 1982). This method determines the fraction of diffuse radiation leaving each surface and directly reaching the other surfaces with the use of form factors, as well as reflected diffuse radiation reaching all surfaces after infinite reflections. Workplane illuminance after infinite interreflections is calculated using configuration factors relating the illuminance to the workplane point (Athienitis & Tzempelikos 2002), and the final luminous exitances of the surfaces in the room.

The radiosity method models perfectly diffuse reflections for both the non-directional diffuse and directional beam component of the illuminance. It is generally an adequate daylighting model except for the directional beam component. A ray tracing technique would be a more realistic model for the behaviour of the beam component being distributed in the space, as it takes its direction into account. In the simulations for a clear day, there is always a shade on the viewing section if the radiation exceeds 100W/m^2 and thus all light will be diffuse and the radiosity model again accurate.

3.7.1 Workplane Illuminance

The illuminance of the STPV is divided into beam and diffuse components (E_{b_STPV}, E_{d_STPV}, E_{g_STPV}) and multiplied by the appropriate visible transmittances. The beam and diffuse transmittances are separated (τ_b, τ_d) and if a shade is required (for our model whenever the

beam component incident on the surface is greater than 100W/m^2), the window visible transmittances are multiplied by the shade transmittance.

$$E_{b\_STPV} = E_b * \tau_{b\_STPV} \tag{3.7.1a}$$

$$E_{d\_STPV} = E_d * \tau_{d\_STPV} \tag{3.7.1b}$$

$$E_{g\_STPV} = E_g * \tau_{d\_STPV} \tag{3.7.1c}$$

The illuminance of the window viewing section is also divided into beam and diffuse components (E_{b_win}, E_{d_win}, E_{g_win}) and multiplied by the appropriate visible transmittances.

$$E_{b\_win} = E_b * \tau_{b\_win} \tag{3.7.2a}$$

$$E_{d\_win} = E_d * \tau_{d\_win} \tag{3.7.2b}$$

$$E_{g\_win} = E_g * \tau_{d\_win} \tag{3.7.2c}$$

For this particular 8 surface room, there are only two surfaces having initial beam and diffuse luminous exitances, (M_{o_beam}, $M_{o\_diffuse}$) the window section containing the PV, and the window viewing section. These initial luminous exitances are equal to the illuminance coming through the respective surfaces and are separated into beam and diffuse components.

$$\begin{bmatrix} M_{o1_{beam}} \\ M_{o2_{beam}} \\ M_{o3_{beam}} \\ M_{o4_{beam}} \\ M_{o5_{beam}} \\ M_{o6_{beam}} \\ M_{o7_{beam}} \\ M_{o8_{beam}} \end{bmatrix} = \begin{bmatrix} E_{b_{STPV}} \\ E_{b_{win}} \\ 0 \\ 0 \\ 0 \\ 0 \\ 0 \\ 0 \end{bmatrix}; \qquad \begin{bmatrix} M_{o1\_diffuse} \\ M_{o2\_diffuse} \\ M_{o3\_diffuse} \\ M_{o4\_diffuse} \\ M_{o5\_diffuse} \\ M_{o6\_diffuse} \\ M_{o7\_diffuse} \\ M_{o8\_diffuse} \end{bmatrix} = \begin{bmatrix} E_{d\_STPV} + E_{g\_STPV} \\ E_{d\_win} + E_{g\_win} \\ 0 \\ 0 \\ 0 \\ 0 \\ 0 \\ 0 \end{bmatrix} \tag{3.7.3a,b}$$

The final beam and diffuse luminous exitances (M_{i_beam}, $M_{i\_diffuse}$) of the room are calculated after infinite interreflections by multiplying the reflectance of each surface (ρ_i) by the form factors of the room (F_{ij}).

$$\begin{bmatrix} M_{i1\_beam} \\ M_{i2\_beam} \\ \vdots \\ M_{i8\_beam} \end{bmatrix} = \begin{bmatrix} M_{o1\_beam} \\ M_{o2\_beam} \\ \vdots \\ M_{o8} \end{bmatrix} + \begin{bmatrix} F_{11}\rho_{1\_beam} & \cdots & F_{18}\rho_{1\_beam} \\ F_{21}\rho_{2\_beam} & \cdots & F_{28}\rho_{2\_beam} \\ \vdots & \ddots & \vdots \\ F_{81}\rho_8 & \cdots & F_{88}\rho_8 \end{bmatrix} \begin{bmatrix} M_{i1\_beam} \\ M_{i2\_beam} \\ \vdots \\ M_{i8\_beam} \end{bmatrix} \tag{3.7.4a}$$

$$\begin{bmatrix} M_{i1\_diffuse} \\ M_{i2\_diffuse} \\ \vdots \\ M_{i8\_diffuse} \end{bmatrix} = \begin{bmatrix} M_{o1\_diffuse} \\ M_{o2\_diffuse} \\ \vdots \\ M_{o8} \end{bmatrix} + \begin{bmatrix} F_{11}\rho_{1\_diffuse} & \cdots & F_{18}\rho_{1\_diffuse} \\ F_{21}\rho_{2\_diffuse} & \cdots & F_{28}\rho_{2\_diffuse} \\ \vdots & \ddots & \vdots \\ F_{81}\rho_{8} & \cdots & F_{88}\rho_{8} \end{bmatrix} \begin{bmatrix} M_{i1\_diffuse} \\ M_{i2\_diffuse} \\ \vdots \\ M_{i8\_diffuse} \end{bmatrix} \quad (3.7.4b)$$

The final workplane illuminance ($E_{workplane}$) is calculated using the final luminous exitances of the room and the configuration factors (f_i). It is the sum of the portion coming from beam (first term) and diffuse (second term) components.

$$E_{workplane} = \sum M_{b_i} f_i + \sum M_{d_i} f_i \quad (3.7.5)$$

Once again, the principal assumption made with this method is that all reflections are perfectly diffuse and that the inside surface of the STPV and window act as perfectly diffuse luminous sources. As all direct light passes through a shade on the window viewing section our assumption of the window acting as a perfectly diffuse luminous source is not unreasonable. However, there is no shade present on the STPV section when direct light is present and thus the assumption that the STPV acts as a perfectly diffuse luminous source introduces errors, but which are much lower for high PV area ratios. More work is required to determine the exact transmittance in which a shade would be required on this section so that our assumptions are reasonable.

3.8 ARTIFICIAL LIGHTING

3.8.1 LUMINAIRE SIZING

The lumen method of interior lighting design was used to size the luminaires for our space from IESNA (2000). The illuminance from the luminaires ($E_{luminaires}$) is calculated using the lumens produced from the luminaire system, the coefficient of utilization (CU) of the space taken from tables in IESNA (2000) and based on cavity ratios, and the lighting loss factor (LLF).

$$E_{luminaires} = \frac{(\#of luminaires)*\left(\frac{lamps}{luminaire}\right)*(lamp\ lumens)*CU*LLF}{Workplane\ Area} \quad (3.8.1)$$

The effective reflectances of the ceiling and floor cavities are calculated using table in IESNA (2000) and the room, ceiling and floor cavity ratios (RCR, CCR, FCR).

$$RCR = \frac{5(H-WPH-h_c)(L+W)}{L*W} \quad (3.8.2a)$$

$$CCR = \frac{5(h_c)(L+W)}{L*W} \quad (3.8.2b)$$

$$FCR = \frac{5(WPH)(L+W)}{L*W} \quad (3.8.2c)$$

The number of luminaires (N_{lum}) is based on the lumens required from the artificial lighting ($\Phi_{lighting\_required}$) to supplement the daylighting and the characteristics of the luminaires: number of tubes in luminaire (N_{tubes}), lumens per tube (Lm_{tube}) and the efficiency of the luminaire (EFF).

$$\Phi = \frac{E_{desired}*A_{workplane}}{CU*LLF} \quad (3.8.3)$$

$$N_{lum} = \frac{\Phi_{lighting\_required}}{N_{tubes}*Lm_{tube}*EFF} \quad (3.8.4)$$

3.8.2 DAYLIGHTING CONTROL STRATEGIES

Two different lighting control strategies are explored in the study. For active on/off lighting control, the lights all turn on if the workplane illuminance ($E_{workplane}$) falls below the desired workplane illuminance ($E_{desired}$), and the lights all turn off if the workplane illuminance goes above the desired value. For continuous dimming control, the lighting adds only enough to achieve the desired illuminance on the workplane. The simplified models are based on the hourly data and thus this action can be performed hourly. The fractional lighting input is calculated based on the EnergyPlus model (University of Illinois & Lawrence Berkeley National Laboratory 2008).

3.8.2.1 ACTIVE ON/OFF CONTROL:

For active on/off control, the lights are either fully on or fully off. This means that if the lights are off, both the fractional electric lighting input (f_p) and the illuminance required by the lamps

($E_{required\_lamps}$) are both 0, or if the lights are on the fractional electric lighting input is 1 and the illuminance required by the lamps is equal to the desired illuminance.

$$E_{required_{lamps}} = 0 \quad if\ E_{workplane} \geq E_{desired} \tag{3.8.5}$$

$$= E_{desired}\ otherwise$$

$$f_p = 0\ if\ E_{workplane} \geq E_{desired} \tag{3.8.6}$$

$$= 1\ otherwise$$

3.8.2.2 AUTOMATIC DIMMING CONTROL:

For continuous dimming control, the lighting adds only enough to achieve the desired illuminance on the workplane. There is a minimum fractional electric lighting input (f_{p_min}) which occurs for a specific minimum electric lighting output (f_{L_min}).

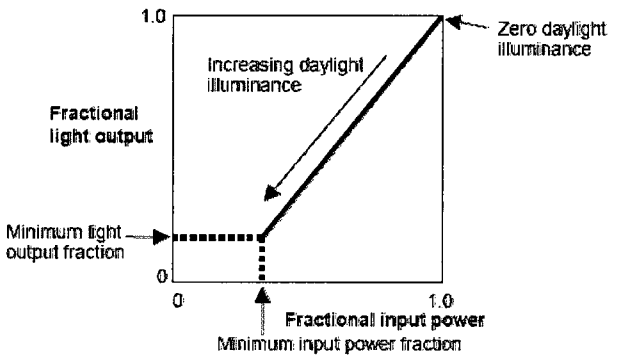

Figure 3-6: Continuous dimming control action (University of Illinois & Lawrence Berkeley National Laboratory 2008)

The illuminance required by the lamps is equal to 0 if the workplane illuminance is greater than the desired workplane illuminance and equal to the difference if it less. The fractional electric lighting input (f_p) is never equal to zero for continuous dimming (Figure 3-6).

$$E_{required_{lamps}} = 0 \quad if\ E_{workplane} \geq E_{desired} \tag{3.8.7}$$

$$= E_{desired} - E_{workplane} \quad otherwise$$

$$f_p = f_{p\_min} \; if \; f_L < f_{L\_min} \tag{3.8.8}$$

$$= \frac{f_L + (1 - f_L) * f_{p\_min} - f_{L\_min}}{1 - f_{L\_min}} \; otherwise$$

$$\text{Where } f_L = \max\left(0, \left(\frac{E_{desired} - E_{workplane}}{E_{desired}}\right)\right) \tag{3.8.9}$$

3.8.3 POWER REQUIRED FOR LIGHTING:

The power required by the lighting (P_{lights}) is thus equal to the power of the luminaires (number of luminaires ($N_{lum\_required}$), the number of tubes per luminaire (N_{tube}), and the power of each tube (P_{tube})) multiplied by the fractional electric lighting input(f_p).

$$P_{lights} = N_{lum\_required} * P_{tube} * N_{tube} * f_p \tag{3.8.10}$$

In the simulations, a minimum workplane illuminance is required and the daylight is augmented with artificial lighting. A shade is employed when beam radiation is over 100W/m^2 but there is no check for a maximum workplane illuminance. Glare may be an issue.

3.9 PHOTOVOLTAIC POWER OUTPUT

The power output of the PV (P_{PV}) is calculated based on the radiation incident on the panel (I_t), the area of the PV (A_1) and the PV area ratio (A_{PV}) as well as on a simple and widely used expression (Whitaker et al. 1991) which takes into account the effects of changing cell temperature ($\Delta\eta_{temp}$) on the stated manufacturer's efficiency (η_{STC}).

$$P_{PV} = I_t * A_{PV} * A_1 * \eta \tag{3.9.1}$$

$$\eta = \eta_{STC} - \Delta\eta_{temp} \tag{3.9.2}$$

The manufacturer's stated output or efficiency is given for standard test conditions (25°C temperature, 1000 W/m^2 irradiance, air mass 1.5, normal incidence and unpolarized light) and is calculated based on the maximum power (P_{MPP}). The fill factor (FF) is used to describe the

quality of the cells, comparing the voltage (V_{MPP}) and current (I_{MPP}) at maximum power with the open circuit voltage (V_{OC}) and short circuit current (I_{SC}).

$$\eta_{STC} = \frac{P_{MPP}}{A * I_t} \tag{3.9.3}$$

$$P_{MPP} = V_{OC} * I_{SC} \tag{3.9.4}$$

$$FF = \frac{V_{MPP} * I_{MPP}}{V_{OC} * I_{SC}} \tag{3.9.5}$$

According to Messenger (2000), for variations in ambient temperature and irradiance from the standard test conditions, the cell temperature can be estimated quite accurately using the outdoor temperature (T_o), the nominal operating cell temperature (NOCT), the irradiance (I_t) and the reference irradiance (I_o = 800W) using a linear approximation.

$$\Delta\eta_{temp} = \eta_{STC}[\eta_{power\_temp} * (T_{cell} - T_{STC})] \tag{3.9.6}$$

$$T_{cell} = T_o + I_t * \left(\frac{NOCT - 20}{I_o}\right) \tag{3.9.7}$$

The temperature of the cell calculated using an estimate and this assumption may introduce errors. In reality the temperature of the cell is dependent on more than just the outside temperature and irradiance; it is also dependant on the window absorption and the temperature of the glazings. As a detailed thermal model was not created, this estimate was used instead but has been deemed acceptable in the literature (Messenger 2000).

3.10 HEAT GAINS THROUGH FAÇADE

The heat gain through the STPV façade and the impact of changing the PV area ratio or transmittance of the façade on the building's heating and cooling loads is an important design consideration. The equations for the heat gains through the façade and due to the lighting would be:

$$Net\ heat\ gain = Q_{lights} + Q_{facade} \tag{3.10.1}$$

The heat gains would be converted to a load (either through coefficient of performance or other) and would then either be added or subtracted from the net electricity generation, depending on

whether it was the heating or cooling season. Again this would be based on the PV area ratio of the upper section of the façade.

The total energy through the window is equal to the heat transfer due to temperature difference between inside and outside + solar radiation transmitted through glazing + inward flow of solar radiation absorbed in glazing (Athienitis & Santamouris 2002). The instantaneous heat gain from the façade will only give an indication of how the façade configurations will affect the heating and cooling loads.

The U-values and SHGC are calculated for design days of the experimental office only and not in the simulations. They are presented in Chapter 5 for discussion purposes only.

ASHRAE (2001) gives a basic equation for the instantaneous energy flow through fenestration due to indoor-outdoor temperature difference (t_{int}, t_{ext}) and due to solar radiation (I_t). The instantaneous heat gain from the window (Q_{facade}) is based on the instantaneous performance indices- thermal transmitance (U value) and the solar heat gain coefficient (SHGC) of the entire window.

$$Q_{facade} = U * A(t_{ext} - t_{int}) + SHGC * A * I_t \qquad (3.10.2)$$

3.10.1 FAÇADE U VALUE

The U value of the center of glass (U) is calculated for each separate section of the window and includes the conductive, convective and radiative heat transfer. The convective and radiative heat transfer are combined for the exterior, interior and cavities (h_o, h_i, h_{cav}) and a calculation for the window prototype is given in Appendix VII. The conductive heat transfer for each separate layer j is calculated by dividing the thickness of the material (L_j) by its thermal conductivity (k_j).

$$U = \frac{1}{\frac{1}{h_o} + \frac{1}{h_i} + \frac{1}{h_{cav}} + \frac{L_j}{k_j}} \qquad (3.10.3)$$

3.10.2 SOLAR HEAT GAIN COEFFICIENT

The solar heat gain coefficient (SHGC) is calculated as a function of angle of incidence. The SHGC is calculated based on the solar transmittance of the entire glazing system ($\tau(\theta)$) and for each layer, the inward flowing fraction (N) and the effective solar absorptance of the entire layer($\alpha_{eff\_k}(\theta)$). For a double glazed window, two inward flowing fractions for the exterior and interior layers (N_1), (N_2) are needed and defined in ASHRAE (2001). The equations for the calculation of the solar transmittances and absorptances are given in section 3.6.1, Appendix I.

$$SHGC(\theta) = \tau_{1,j}{}^{f}(\theta) + \sum_{k=1}^{j} N_k * \alpha_{eff\_k:(1,j)} \tag{3.10.4}$$

$$N_1 = \frac{U}{h_o},\ N_2 = \frac{h_o+U}{h_o} \tag{3.10.5a,b}$$

The effective solar absorptance (α_{eff_k}) as a function of the angle of incidence of the sun is an area weighted average of the 3 sections. The first term in the effective solar absorptance of the outer layer (α_{eff1}) is the solar absorptance of the front glazing in the window viewing section as a function of angle of incidence (α_{g1_win}) and is multiplied by the area of the front glazing in the window viewing section (A_2). The second term is the effective solar absorptance of the area occupied by the PV cells (A_1*A_{PV}). The effective absorptance of the PV cells (α_{PV}) is reduced by the amount which is converted to electricity; here the calculated efficiency of the cells (η). In the second term is also the solar absorptance of the front glazing in front of the PV cells (α_{g1_PV}). The third term consists of the solar absorptance of the combined EVA and front glazing (α_{EVA}), which is multiplied by the area in the STPV section not occupied by the cells (A_1*(1-A_{PV})).

$$\alpha_{eff_1} = \frac{[\alpha_{g1\_win}*(A_2)]+\left[[\alpha_{PV\_eff}*(1-\eta)+\alpha_{g1_{PV}}]*(A_{PV}*A_1)\right]+[\alpha_{EVA}*A_1*(1-A_{PV})]}{A_1+A_2} \tag{3.10.6}$$

The effective solar absorptance of the inner layer (α_{eff2}) contains only 2 terms: the absorptance of the back glazing behind the window viewing section (α_{g2_win}) and the absorptance behind the EVA in the STPV section (α_{g2_EVA}).

$$\alpha_{eff_2} = \frac{\alpha_{g2\_win}*(A_2)+[\alpha_{g2\_EVA}*A_1*(1-A_{PV})]}{A_1*(1-A_{PV})+A_2} \tag{3.10.7}$$

4 DESIGN OF STPV FAÇADES

4.1 INTRODUCTION

The objective of this thesis is to develop a methodology for designing a commercial façade which uses STPV as a daylighting and electricity-generating component. The results of the simulation study are presented in this section and should be useful for designers of STPV façades facing everyday constraints in a Canadian climate. Several important design parameters are taken into consideration including changing façade orientation and site location, as well as design variable such as PV efficiency, lighting control strategies, and shading device transmittance. Table 4-1 presents all the design parameters and variables taken into consideration.

Table 4-1: Parametric variations used in the simulation study.

Design parameters	**Base case**	**Variation from base**			
Orientation	South	SouthEast	SouthWest	East	West
Location	Montreal	Toronto	Vancouver	St. John's	Iqaluit
PV efficiency	14%	6%	10%	18%	22%
Lighting control strategy	Continuous dimming	Active on/off		Passive	
Shade transmittance	5%	1%		10%	

All simulations are conducted for varying PV area ratio in the upper façade section. Results are presented either annually or for specific design days.

4.2 BASE CASE

The base case is described in section 3.4 and is based on a typical small office (3m wide x 4m deep x 4m high) in Montreal with a south facing three section façade. The annual net electricity generation is calculated by deducting the annual lighting load from the annual electricity generated from the photovoltaics.

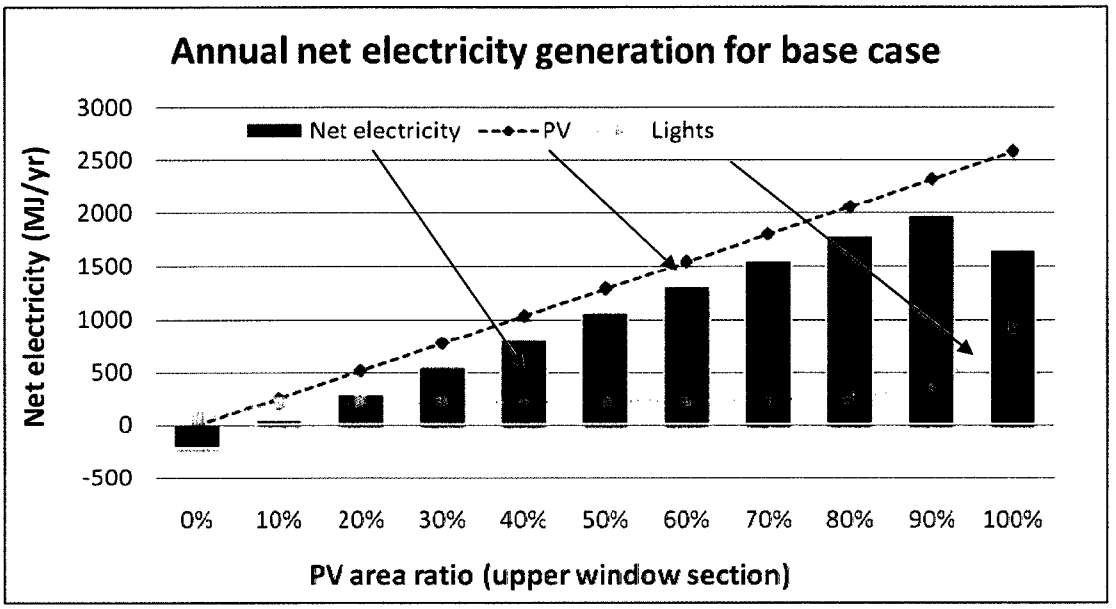

Figure 4-1: Annual net electricity generation results for base case for varying PV area ratio in the upper façade section.

For the base case, it can be seen that the most favourable PV area ratio is about 90%. In general, the more PV in the upper section, the higher the net electricity generation, until 100% where is drops significantly. By leaving a 10% transmittance in the upper façade section, the lighting loads are significantly reduced and the net electricity is increased by approximately 16%.

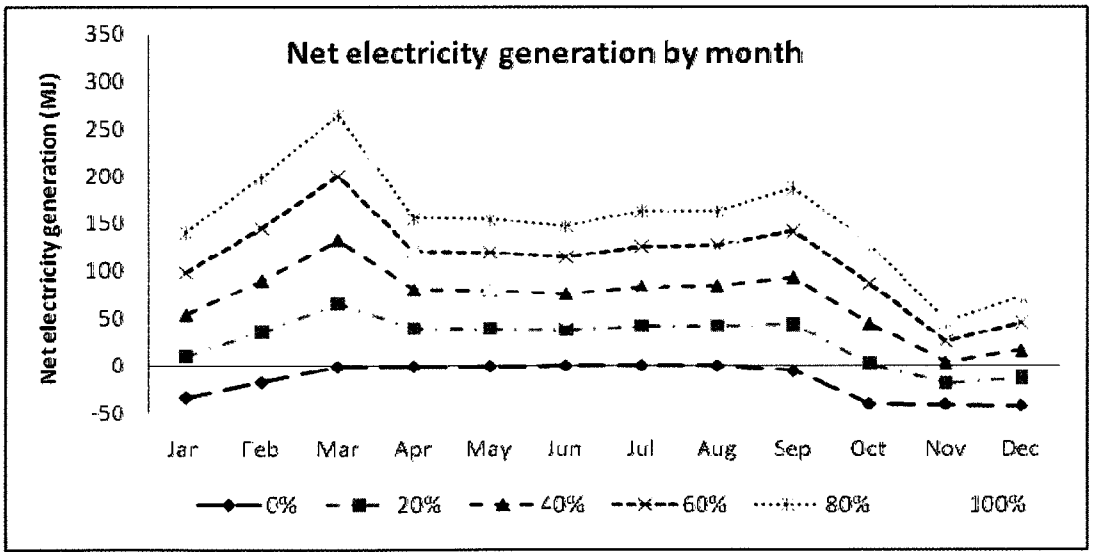

Figure 4-2: Net electricity generated by STPV base case per month of the year.

Examining the base case on a per month basis, it can be seen that the 100% PV area ratio performs well during the winter months and poorly during the summer months.

To get a better idea of how the STPV performs under specific outdoor conditions, design days are used (Figure 4-3).

Winter season

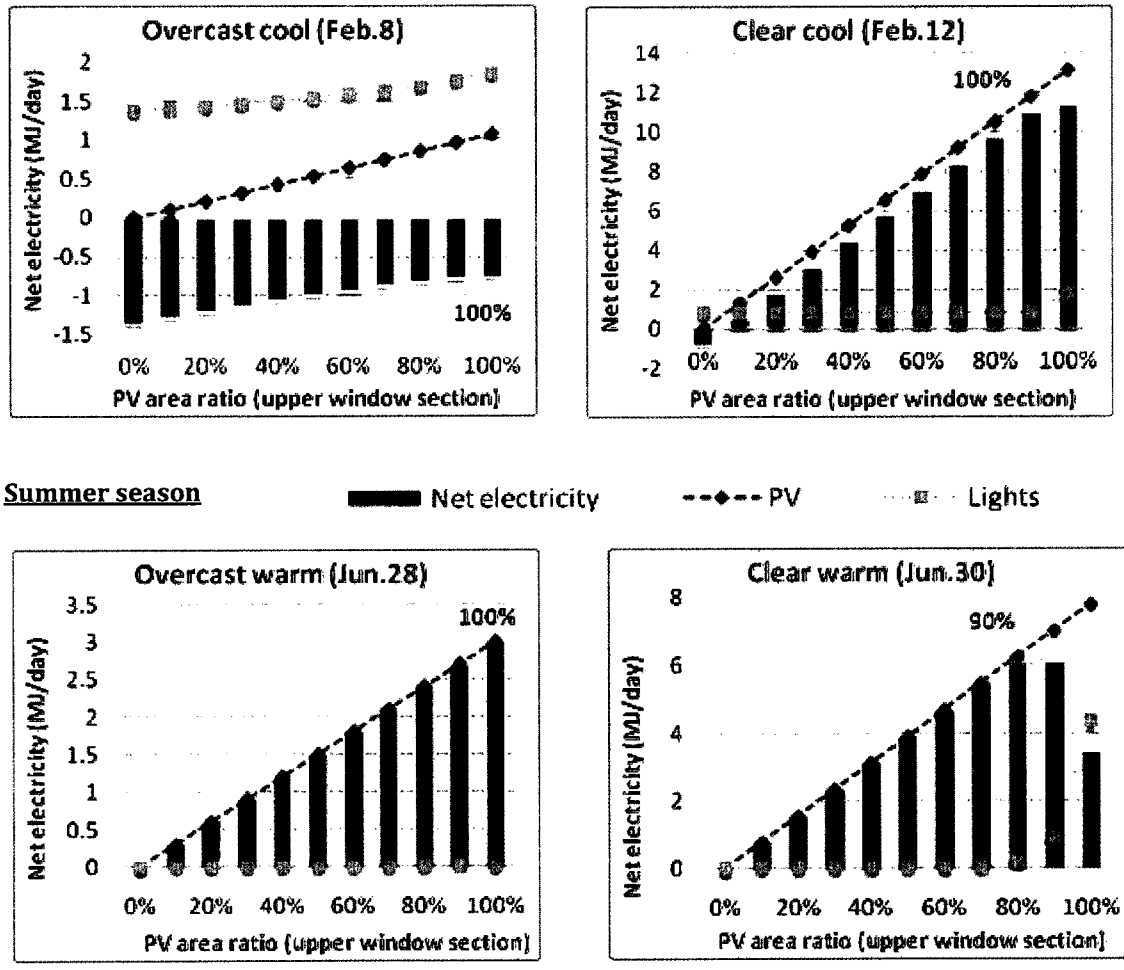

Figure 4-3: Representative design days for base case for varying PV area ratios in the upper section.

Interestingly, the design days give a different picture of the ideal PV area ratio in the upper façade section. For the clear overcast, clear cool and overcast warm days, the most favourable in terms of net electricity generation is the 100% PV area ratio. 90% is still ideal for the clear warm day. These results could be very useful when designing to reduce peak loads. If the goal is to reduce the high summer cooling loads, the façade should be designed using the hot clear day while the cold overcast day should be used if designing to reduce winter heating loads.

4.3 CHANGING ORIENTATION

For Northern hemispheres, a southern façade is ideal for maximum PV electricity generation and daylight utilization and a vertical façade is ideal for minimizing cooling loads in the summer and heating loads in the winter. However, in reality, true-South facing façades are not always possible and the intent is this section is to show to what extent a change of 45 degrees (SW, SE) and 90 degrees (W, E) has on the net electricity generation.

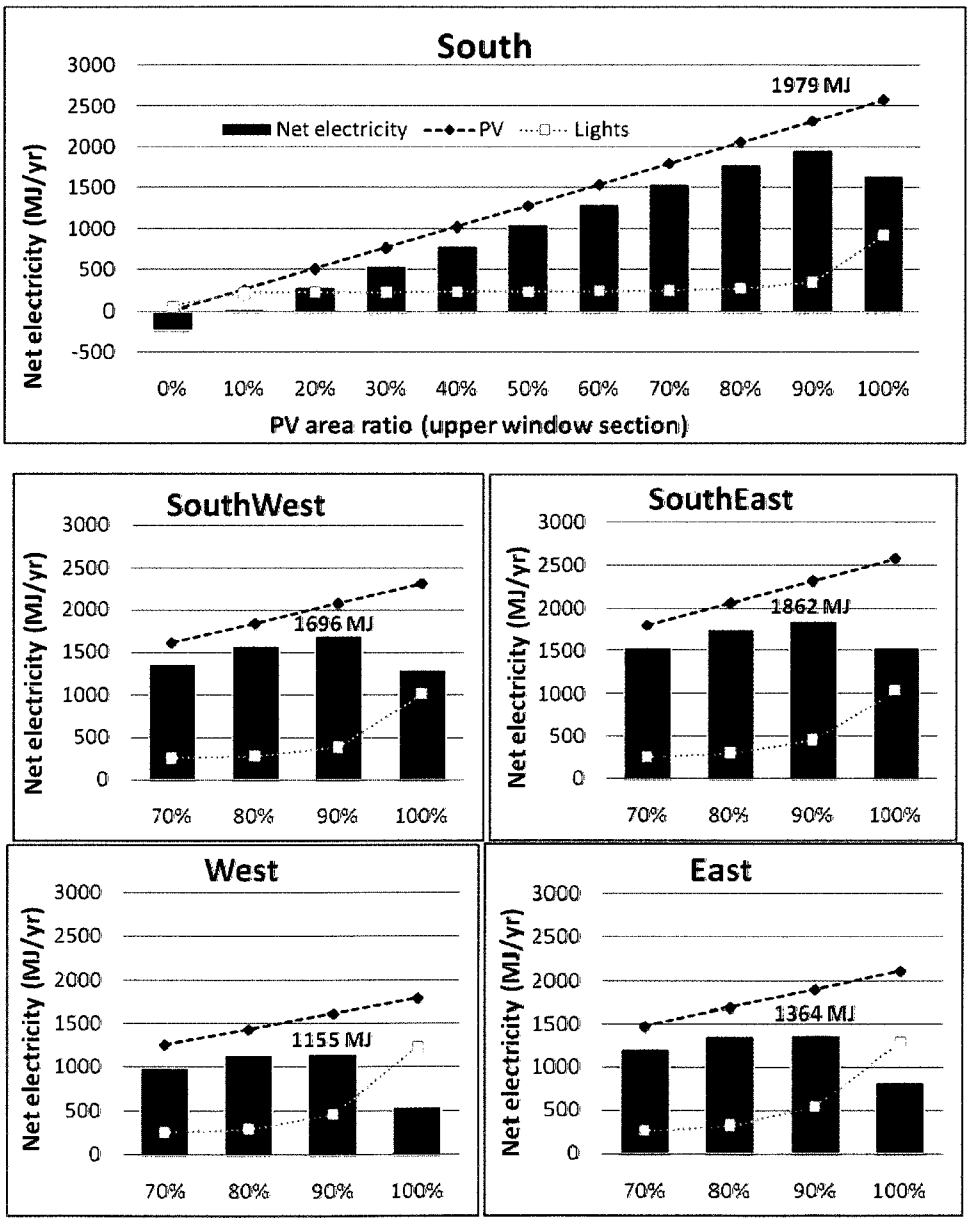

Figure 4-4: Annual net electricity generated by STPV façades for different orientation and PV area ratios

Of the orientations explored, all orientations have an ideal PV area ratio of 90% when looking at annual results. South facing façades produce up to 60% more annual net electricity than the other orientations. For office hours of 8am to 5pm standard time, East and South-East facing façades performed better than West and South-West facing façades. This is extremely dependant on the office hours chosen. A quick calculation revealed that if office hours of 9am to 5pm standard time are chosen, West performs better than East.

A change of 45 degrees from South (either East or West) does not produce an extreme reduction in annual net electricity (5 to 13%) but a change of 90 degrees does (28 to 38%).

4.4 CHANGING PV EFFICIENCY

The PV efficiency used in the base case of 14% was taken from an on the market polycrystalline PV module. The efficiency of different PV technologies varies greatly and can be as low as 5% and potentially as high as 27% (German solar energy society 2005). As the efficiencies of the modules changes significantly from one to the other, it is important to examine this difference on the net electricity generation. How does a lower or higher efficiency change the ideal PV area ratio?

As can be seen in the figures on the next page, changing the PV efficiencies drastically changes the values of the net electricity generated for a year but the ideal PV area ratio remains the same. The impact of changing from 90% to 100% PV area ratio in the upper section is very pronounced for low efficiencies and much less so for the higher efficiencies. In the future, should PV efficiencies reach significantly higher values than those explored here, this conclusion may change.

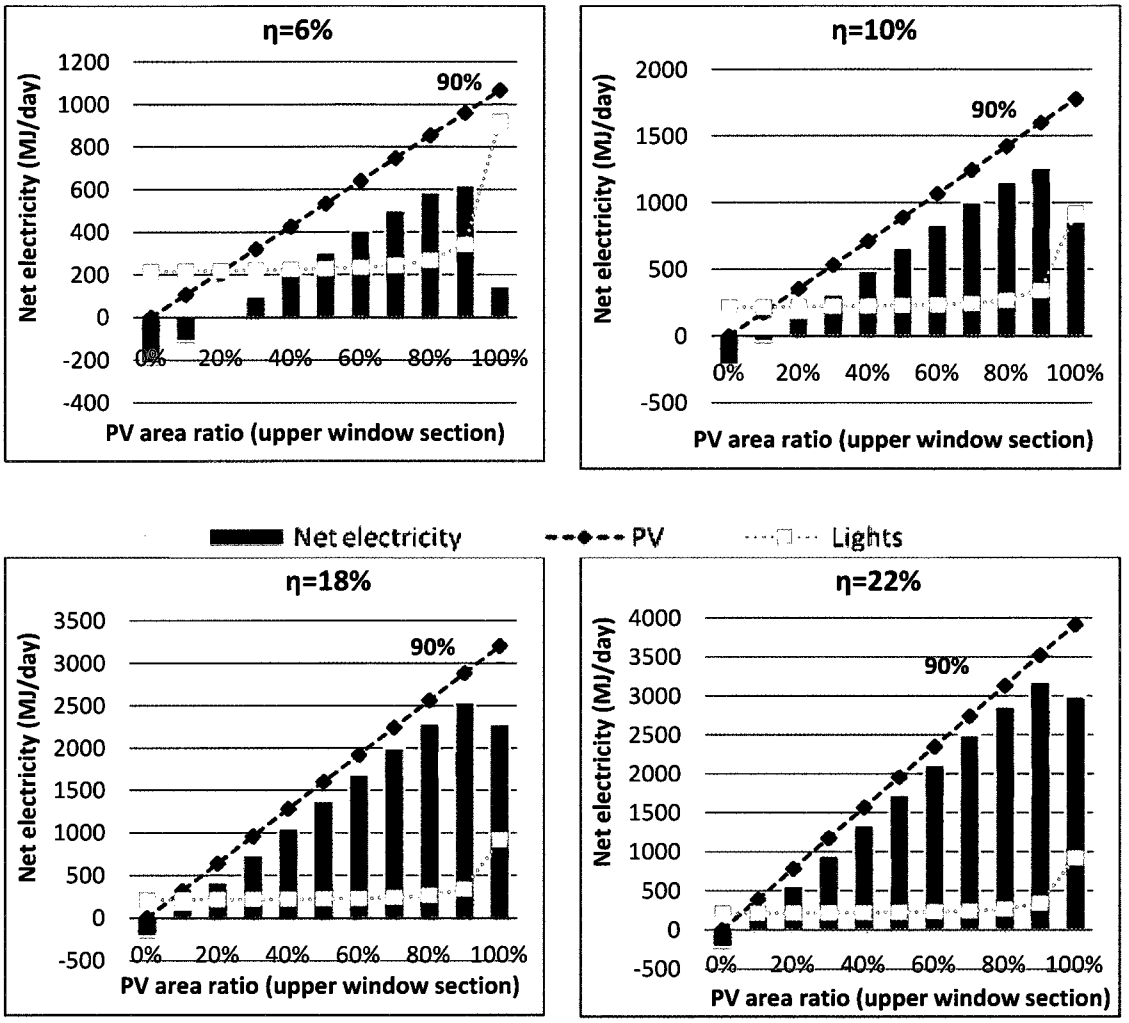

Figure 4-5: Varying PV efficiencies

The concept of semi-transparent photovoltaics includes both spaced opaque cells and uniform thin-film photovoltaics. Thin-film photovoltaics have an advantage over spaced PV cells as the natural light coming in through this technology would be uniform. Even though the efficiencies of this technology are low, the above conclusions demonstrated that the ideal transmittance would be similar to the spaced cells and this methodology can provide value even for this different PV technology.

4.5 CHANGING LOCATION

For this methodology to be useful for a Canadian climate, locations other than just the base case need to be explored. 5 locations were chosen- major cities situated at different longitudinal and to an extent, latitudinal locations, as well as a city in Canada's North (Figure 4-6).

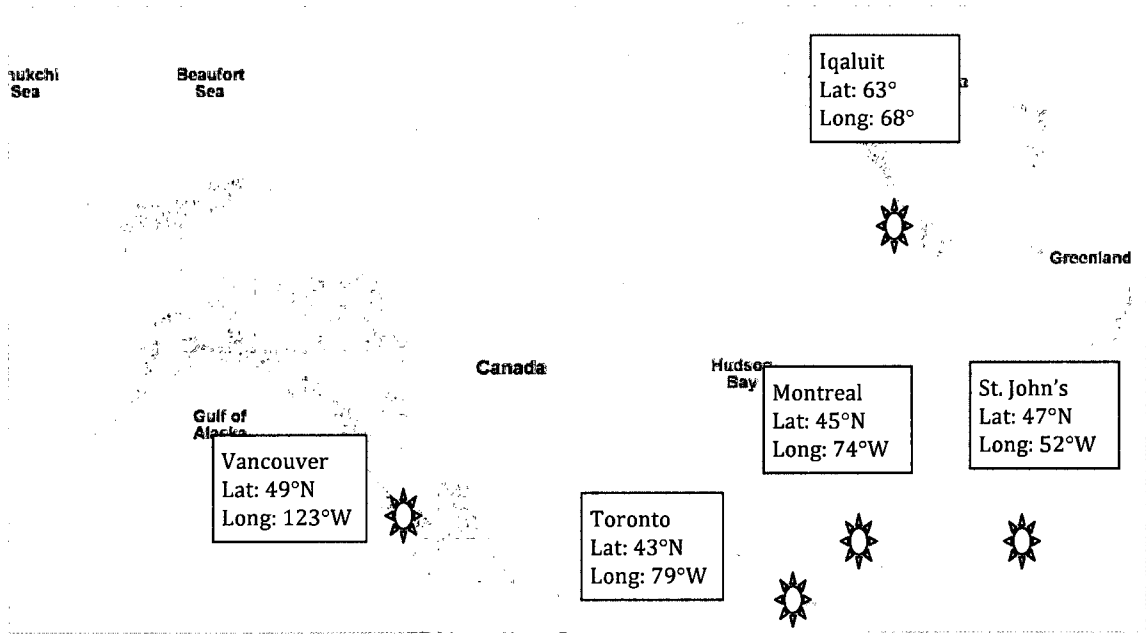

Figure 4-6: Locations used in the study

John's to 2580 MJ/yr in Montreal. The lighting load varies from 883 MJ/yr in Toronto to 1123MJ/yr in Iqaluit. Our base case produces the most electricity from the PV and consumes a mid-range of lighting. Interesting to note is the electricity generated by the PV in Iqaluit, which is the second highest of the cities studies, due to the low sun on the vertical façade and the lower outdoor temperatures. St. John's has the lowest annual net electricity generation while Montreal has the highest. All façade locations experience the highest annual net electricity generation at 90% PV ratio in the upper section of the façade (Figure 4-6, Table 4-2).

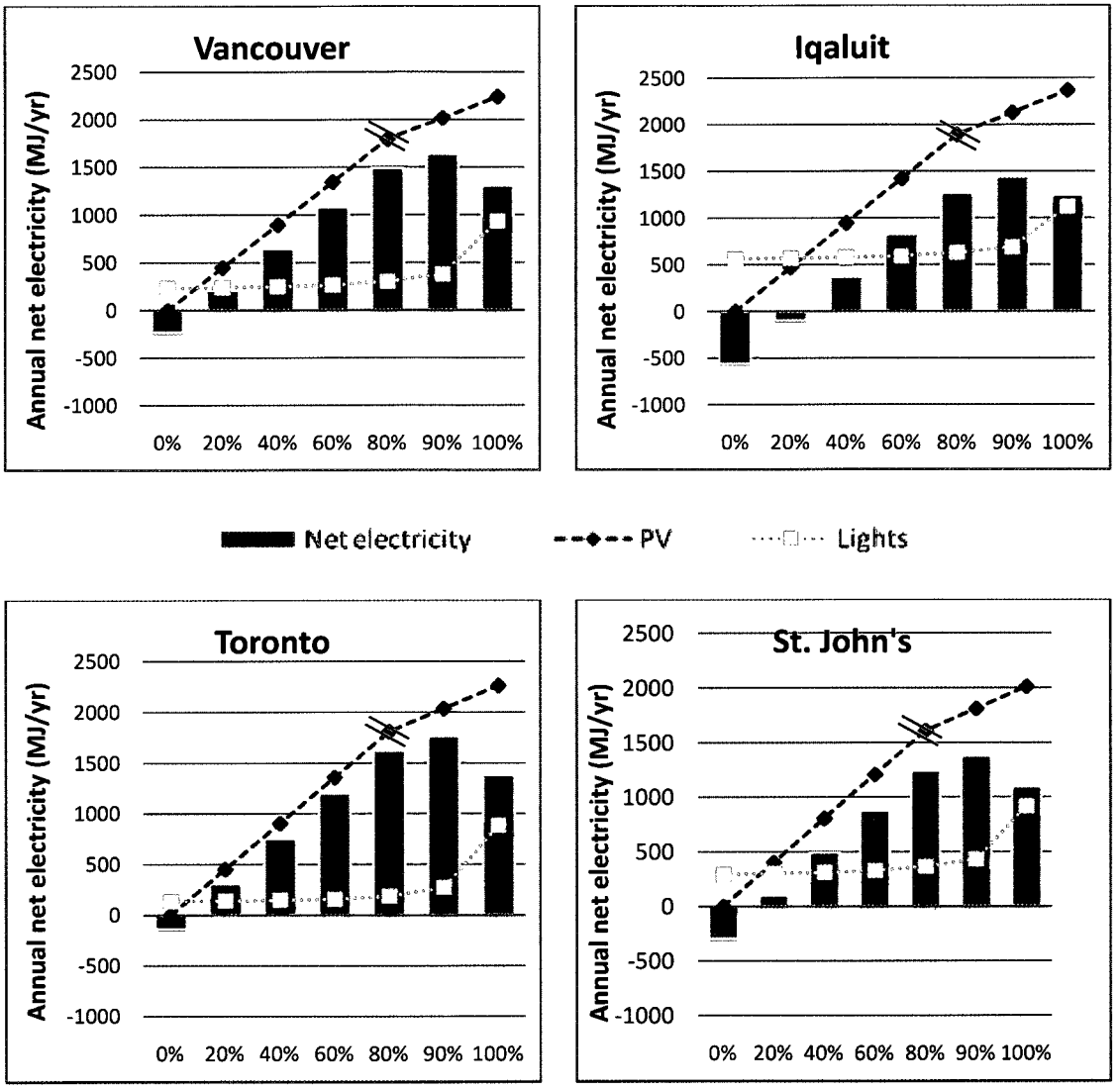

Figure 4-7: Changing location in Canada

Table 4-2: Results for various locations in Canada

Location	Max PV output	Max. lighting load	Max net electricity	PV area ratio giving max electricity generation
Montreal	2580 MJ/yr	922 MJ/yr	1979 MJ/yr	90%
St. John's	2013 MJ/yr	918 MJ/yr	1379 MJ/yr	90%
Toronto	2263 MJ/yr	883 MJ/yr	1764 MJ/yr	90%
Vancouver	2242 MJ/yr	937 MJ/yr	1637 MJ/yr	90%
Iqaluit	2367 MJ/yr	1123 MJ/yr	1440 MJ/yr	90%

4.6 CHANGING SHADE TRANSMITTANCE

In order to protect the occupant from glare, an interior roller shade is present whenever the incoming direct radiation is higher than 100 W/m^2. The shade in the base case has a transmittance of 5%. The effect of changing this transmittance to 1% or 10% is explored here for both annual results (Figure 4-8) and design day results (Figure 5-9).

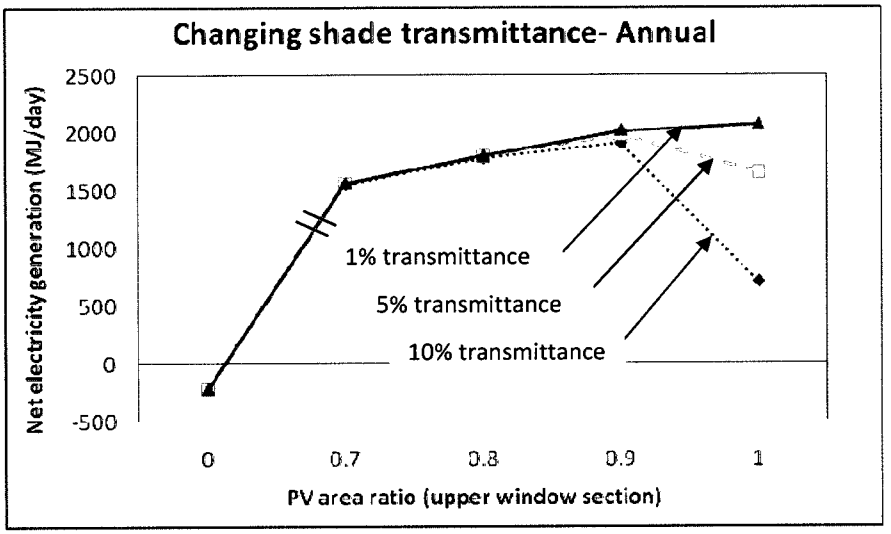

Figure 4-8: Annual results for net electricity generation for changing shade transmittances

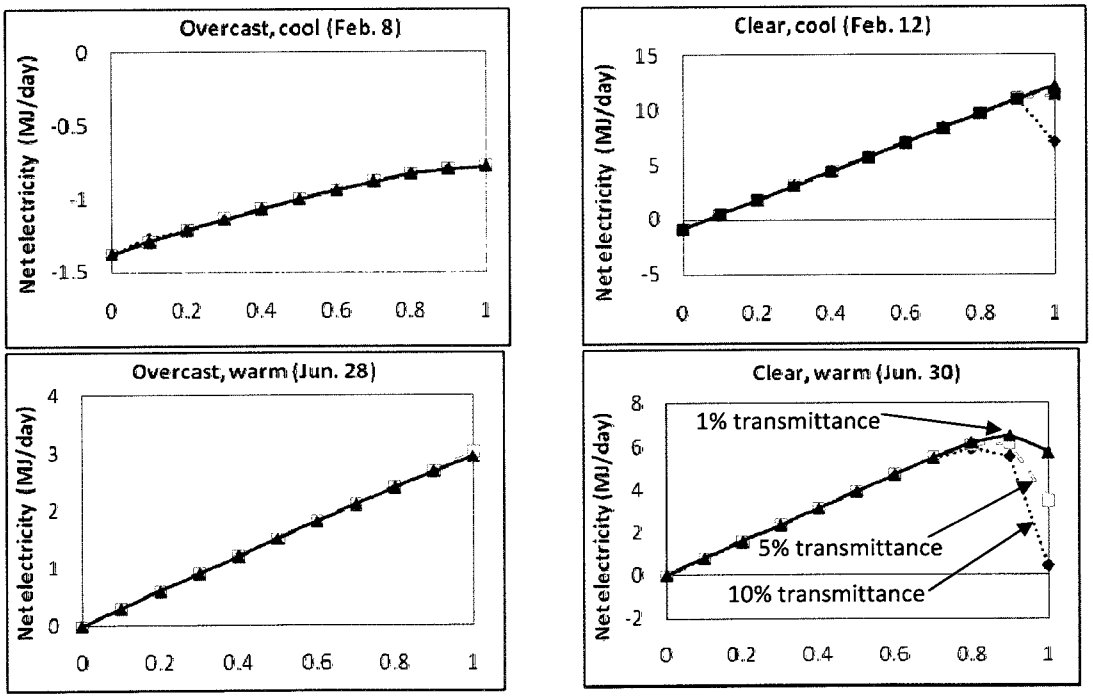

Figure 4-9: Shade transmittances- design days

Changing the shade transmittance over the window viewing section does not have a significant effect on the annual net electricity generation for all PV area ratios except 100%. For 90% coverage the difference between the 1% and 10% is 5% and for 100% coverage this difference increases to 65%

For the design days, the results are quite different than the annual results. As expected, there is no change in net electricity generation for the overcast days, as the shade is only employed when beam radiation is present. For the clear cool day, there is little difference in the results with the exception of a slight decrease for the 1% shade transmittance at 100% PV area ratio. Te clear warm day gives results similar to the annual results, but with greater differences.

These results demonstrate that the choice of shade transmittance as a design variable is not very significant if using STPV in a three-section façade for anything but a 100% PV area ratio. However, for hot clear climates, choosing a shade with an appropriate transmittance is extremely important.

4.7 CHANGING LIGHTING CONTROL STRATEGY

The lighting in the base case is controlled by a continuous dimming control strategy in which the lighting adds only enough output to achieve the desired illuminance on the workplane. Two other control strategies were explored- active on/off control and passive control. In active on/off control the lights all turn on if the workplane illuminance falls below the desired workplane illuminance and the lights all turn off if the workplane illuminance goes above the desired value. In passive control, the lights are on continuous during office hours. The effect of changing this control strategy is again explored for both annual results (Figure 4-10) and design day results (Figure 4-11).

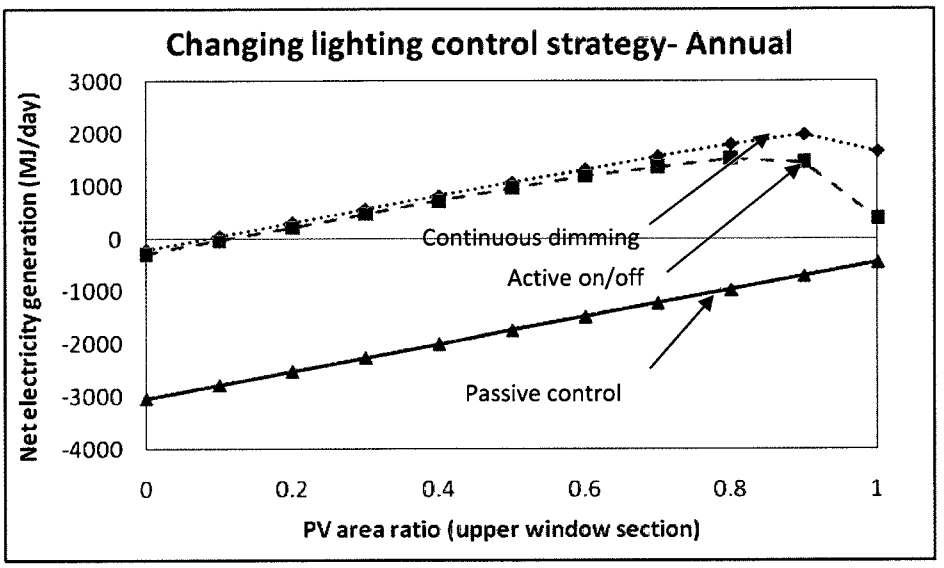

Figure 4-10: Annual results for net electricity generation for changing lighting control strategy

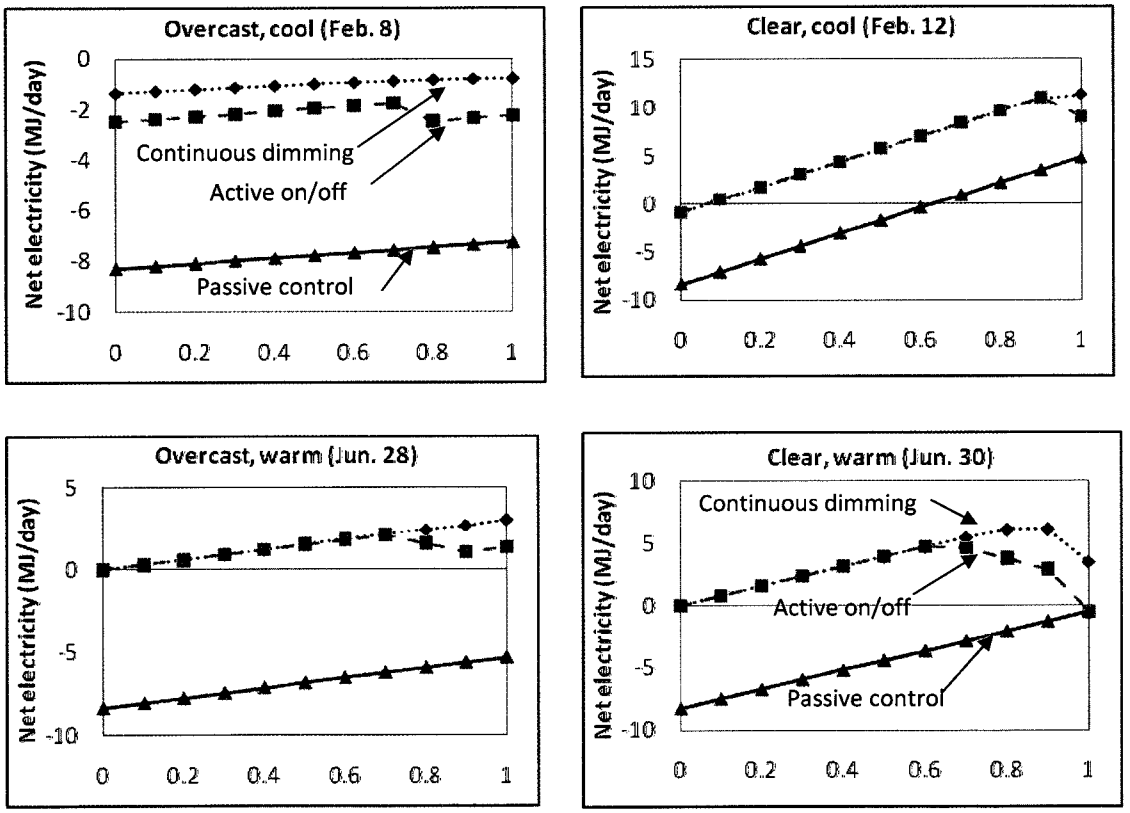

Figure 4-11: Changing lighting control strategy

The continuous dimming control and active on/off control give similar results up to 80% PV area ratio. For the active on/off control, the ideal PV area ratio becomes 80% instead of 90%.

Active on/off control reduces the net electricity generation by 27% when compared with continuous dimming for a 90% PV area ratio and 77% for 100% PV area ratio. For the passive control, the lighting load is the same, regardless of the PV area ratio and the net electricity generation is always negative, meaning that the PV can never cover the lighting loads required.

For the design days, the results are quite similar to the annual results. The continuous dimming and active on/off control act similarly for a clear, cool day, an overcast warm day, and a clear warm day. The largest differences between the two occur for a clear warm day with a 100% PV area ratio, where the net electricity generation for the active on/off control actually becomes negative. The passive control always results in less net electricity when compared with the other two strategies.

These results demonstrate the importance of using an appropriate lighting control strategy when integrating STPV into the façade. Significant electricity savings are achieved by using an automatic continuous dimming control and to a lesser extent, active on/off control.

5 EXPERIMENTAL OFFICE SET-UP AND NUMERICAL MODEL VERIFICATION

5.1 INTRODUCTION

A custom-made prototype semi-transparent window was designed and constructed to be used as a parametric comparison of the results of the numerical model with measured data. The window was designed and built specifically for this study and was coordinated by the author, bringing two different manufacturers together. The experimental set-up is fully instrumented with illuminance meters, thermocouples and PV output monitors. As an existing space was used, the parameters, dimensions and façade configuration are not the same as those used in the simulation model. The experiment was not meant to duplicate the numerical model but was to serve as a verification of the results of the model.

Both the daylighting and PV output models were verified from March 2009 to June 2009 using the experimental office set-up. The numerical model was adapted for the specific experimental space. For the daylighting model, 9 illuminance meters were placed throughout the room to verify the illuminance levels on an imaginary workplane for both a clear and overcast day. For the PV output model, the output was verified before the window was installed on a cold clear day, with the PV facing the direction of the sun. As the window is shaded a large portion of the time, the continuous output of the PV was not measured but the PV was always producing power throughout the experiments.

The temperatures of each side of the glazings were also measured continuously with 39 thermocouples, installed in the window during manufacturing. These temperatures were taken to give an indication of the impact the semi-transparent photovoltaics on the heat transfer through the window, compared with a normal double glazed window. They were also used to verify the temperature of the PV cells.

The experimental set-up was also used to gain experience in measurements and comparison of real models with simulated models. It was used to advance knowledge in the manufacturing of semi-transparent photovoltaic windows practical limitations and difficulties which may occur.

5.2 EXPERIMENTAL OFFICE SET-UP

The experimental office is a 3m x 3.3m x 2.3m room and is integrated in the 'Northern Light' solar house, now located in Montreal at Concordia University's Loyola campus (Lat. 45° 30'N, Long. 73° 35'W) (Figure 5-1). The window is south-facing and replaced the existing window with a total window to wall ratio of 32%.

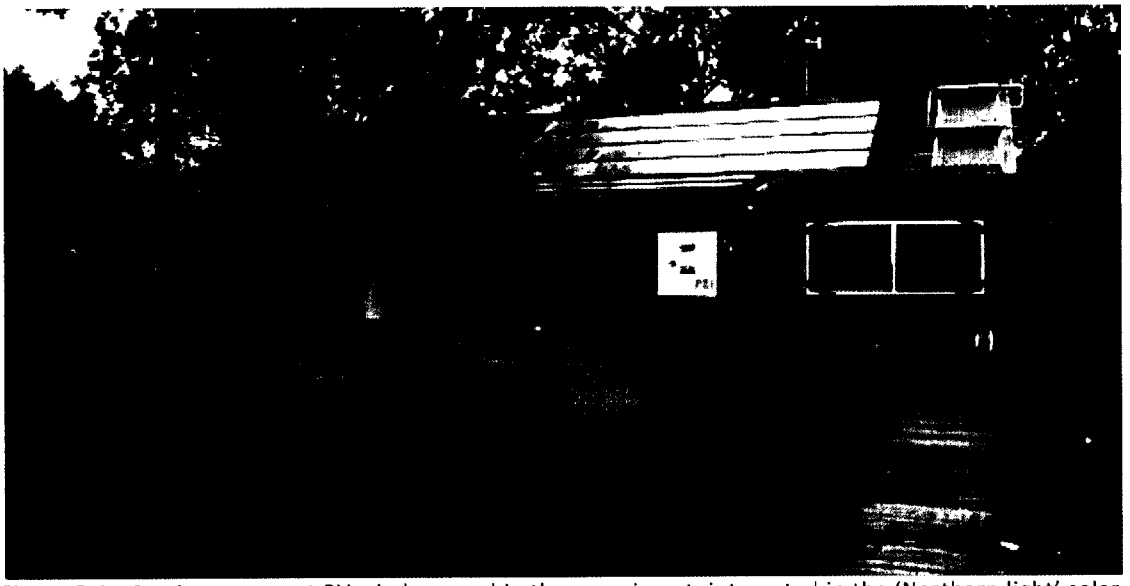

Figure 5-1: -Semi-transparent PV window used in the experiment, integrated in the 'Northern light' solar house in Montreal

The window is not centered on the façade and the room serving as the office is empty except for the data acquisition system. The walls are white with reflectance of 0.85, the ceiling is white with a reflectance of 0.83 and the wooden floor has a reflectance of 0.28. All reflectance measurements were taken with a Gigahertz-Optik LCRT-2004-02 AC.

There is a large building to the East shading the window during the morning and part of the house to the West which shades the window in the afternoon (Figure 5-2)

Figure 5-2: Obstructions in front of window- to the East (left), and to the West (right)

5.3 Window Description

The custom-made window was manufactured by two different Quebec-based companies. The photovoltaic cells were placed by a Montreal-based photovoltaic manufacturer, Centennial Solar, (http://www.centennialsolar.com). The framing and installation of the window was conducted by a Longueil-based specialty-glass and custom aluminum structure company, Unicel Architectural (http://unicelarchitectural.com). The window was manufactured as two windows, each 1.2m x 1m, but placed in the same aluminum frame.

The semi-transparent photovoltaics are spaced opaque poly-crystalline cells with an overall coverage of the upper section of approximately 70% (Figure 5-3). There are 60 cells in series in each window and both windows have either alkali-etched cells (reflective finish) or acid-etched cells (matt finish). The make-up of the window (from outside to inside) is: a) 6mm tempered glass, b) poly-crystalline photovoltaic cells, c) Ethylene vinyl acetate (EVA) encapsulate, d) 2" air gap, e) 6mm glass with low-e coating (Figure 5-4). The window properties used in the mathematical model in order to compare with the experimental results are presented in Appendix II.

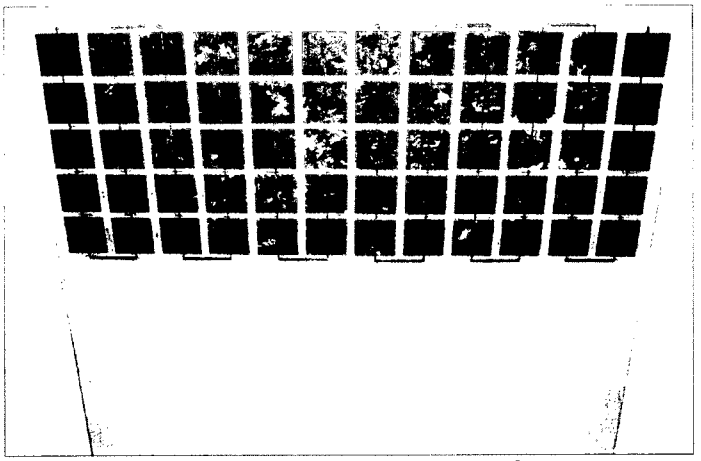

Figure 5-3: 61% cell coverage in upper section of PV-integrated window

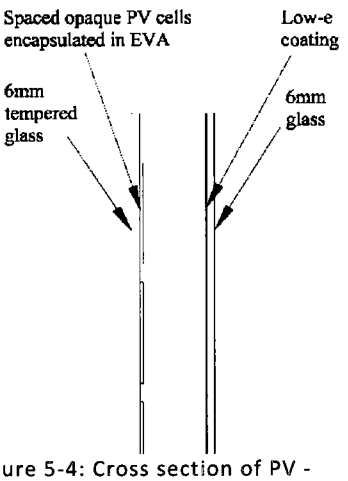

Figure 5-4: Cross section of PV - integrated window

5.4 Transmittance of the Window

5.4.1 Individual window layers

The transmittance of each individual layer of the window was measured on both a sunny and overcast day in January. The measurements were taken indoors with both pyranometers (solar radiation) and photometers (illuminance) placed in front and behind each of the clear glazing, the low-e glazing and the EVA layer (Figure 5-5).

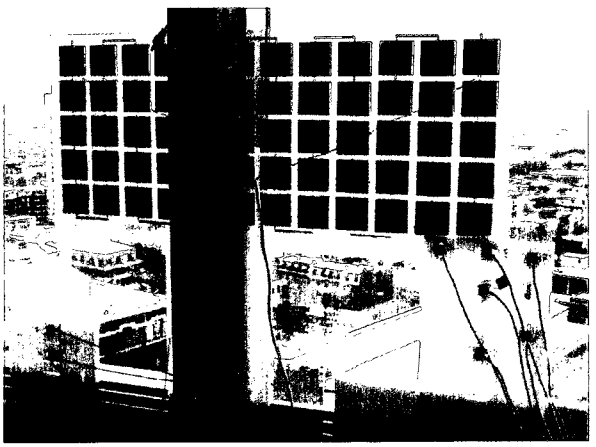

Figure 5-5: Measuring transmittances (radiation and illuminance) of each individual window layer.

The diffuse solar and visible transmittances are calculated using the results of the overcast day. The beam solar and visible transmittances as a function of angle of incidence are calculated by removing the diffuse portion from the results on a clear day. The results of the individual layer transmittances are presented in (Appendix III and Table 5-1 to Table 5-4).

5.4.1.1 DIFFUSE TRANSMITTANCE

The diffuse visible and solar transmittances of the individual layers are essentially constant and will be used as such in the comparison with simulated results. The measurements were taken on January 7, 2009.

Table 5-1: Diffuse visible transmittances of each individual layer, taken on an overcast day. See Appendix III for graphical results

Visible transmittance	Illuminance	
	Average	Standard deviation
Clear glazing	91%	0.4%
Low-e glazing	81%	0.5%
EVA + clear glazing	84%	0.3%

Table 5-2: Diffuse solar transmittances of each individual layer, taken on an overcast day. See Appendix III for graphical results

Solar transmittance	Radiation	
	Average	Standard deviation
Clear glazing	85%	1.1%
Low-e glazing	69%	1.1%
EVA + clear glazing	77%	1.3%

5.4.1.2 BEAM TRANSMITTANCE

The beam transmittance of the individual layers varies significantly for all angles of incidence. For the clear glazing and the low-e coating on the clear glazing, the beam transmittance is approximately constant for angles of incidence of 0 to 60° and then linear for 60 to 75°. The EVA + clear glazing is approximately linear for all angles measured. The beam transmittance is calculated by subtracting the diffuse portion from the overall transmitted radiation and illuminance. The measurements were taken on January 10, 2009.

Table 5-3: Beam visible transmittances as a function of angle of incidence of the sun on the window for individual layers-taken on a clear day. See Appendix III for graphical results.

Visible transmittance	Illuminance			
	Average; θ = 0-60°	Standard deviation	$\tau(\theta)$; (θ in radians), θ = 60-75°	R^2
Clear glazing	95%	1.0%	$=-.5781\theta+1.5943$	0.9042
Low-e glazing	84%	0.8%	$=-.4331\theta+1.3106$	0.767
EVA +clear glazing	$=-0.3603\theta^2+0.3152\theta+0.8364$ for all angles			0.9072

Table 5-4: Beam solar transmittances as a function of angle of incidence of the sun on the window for individual layers-taken on a clear day. See Appendix III for graphical results.

Solar transmittance	Radiation			
	Average; θ = 0-60°	Standard deviation	$\tau(\theta)$; (θ in radians), θ = 60-75°	R^2
Clear glazing	86%	0.9%	$=-.5084\theta+1.4384$	0.767
Low-e glazing	$=-0.6368\theta^3+1.28873\theta^2-.6835\theta+0.8462$ for all angles			0.9535
EVA +clear glazing	82%	1.0%	$=-.4229\theta+1.3027$	0.7426

5.4.2 Overall window transmittance

As the window was manufactured and installed all within a few days, no transmittance measurements were taken of the overall double glazed window before it was installed. In-field measurements of the diffuse visible and solar transmittance were calculated on an overcast day in May (Figure 5-6, Figure 5-7). Accurate beam transmittances were not attainable, as only a limited range of solar angle of incidences were available, as the sun is high in the sky in May and buildings shaded the early morning and late afternoon sun. The diffuse measurements were correct as diffuse light is non-directional and thus not dependant on the angle of incidence of the sun on the window.

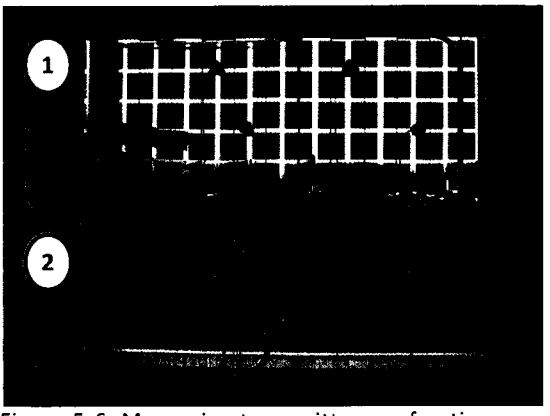

Figure 5-6: Measuring transmittance of entire experimental window (view from interior). 1-EVA & front glazing, 2-Low-e & front glazing

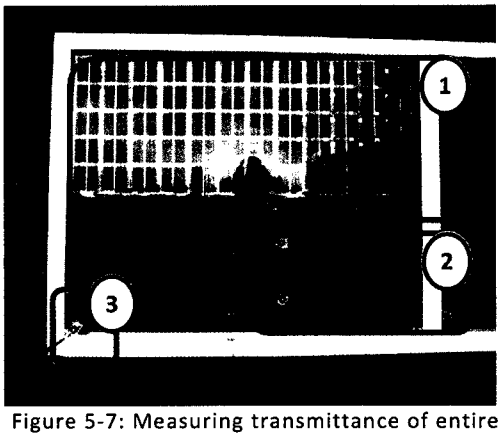

Figure 5-7: Measuring transmittance of entire experimental window (view from exterior). 1-EVA & front glazing, 2- Low-e & front glazing, 3- Exterior on façade.

5.4.2.1 DIFFUSE TRANSMITTANCE

The overall diffuse visible and solar transmittances are essentially constant and will be used as such in the comparison with simulated results. The measurements were taken on May 14, 2009.

Table 5-5: Diffuse visible transmittances of each entire experimental window, taken on an overcast day. See Appendix III for graphical results

Visible transmittance		**Illuminance**	
		Average	Standard deviation
Clear front glazing/EVA & low-e	Average	35%	3.1%
Clear front glazing & low-e glazing	Average	81%	2.5%

Table 5-6: Diffuse solar transmittances of each entire experimental window, taken on an overcast day. See Appendix III for graphical results

Solar transmittance		**Illuminance**	
		Average	Standard deviation
Clear front glazing/EVA & low-e	Average	28%	1.6%
Clear front glazing & low-e glazing	Average	50%	5.8%

5.4.2.2 BEAM TRANSMITTANCE

The beam transmittances for this double glazed window were harder to measure as only a limited range of solar angle of incidences were available, as the sun is high in the sky in May and buildings shaded the early morning and late afternoon sun. This is especially true for the EVA + front glazing results as the cells were partially blocking the incoming radiation and illuminance.

The overall beam transmittance through the double glazed window was thus calculated using the Fresnel expressions described in section 3.6.1. Values of the refractive index, and extinction coefficient for each individual layer were approximated using the individual layer transmittances. Appendix III presents the calculation and comparison of the estimated and calculated transmittances.

Table 5-7: Beam visible transmittances of each entire experimental window, using the Fresnel expressions. See Appendix III for graphical results.

Visible transmittance	**Illuminance**
	$\tau(\theta)$; (θ in radians)
Clear front glazing & low-e glazing	$= -0.7979\theta^3 + 1.3828\theta^2 - 0.8429\theta + 0.9875$
Clear front glazing/EVA & low-e	$= -0.655\theta^3 + 1.1017\theta^2 - 0.6909\theta + 0.9075$

Table 5-8: Beam solar transmittances of each entire experimental window, using the Fresnel expressions. See Appendix III for graphical results

Solar transmittance	**Radiation**
	$\tau(\theta)$; (θ in radians)
Clear front glazing & low-e glazing	$= -0.7102\theta^3 + 1.1406\theta^2 - 0.6738\theta + 0.8771$
Clear front glazing/EVA & low-e	$= -0.6418\theta^3 + 1.0008\theta^2 - 0.5789\theta + 0.8233$

5.5 Sensors and Measurements

The experimental office was used to verify the daylight and PV output models as well as to make some basic conclusions about the heat transfer through this type of façade.

5.5.1 Weather Data

Irradiance data components (global horizontal, diffuse horizontal and beam normal) were taken from NRCAN's weather station in Varennes QC (loc: 45°37'35"N; 73°22'52"W). Exterior temperatures and total vertical irradiance and illuminance were taken on site. Dew point temperature was taken from Environment Canada's online climate database (Environment Canada 2008).

5.5.2 ILLUMINANCE

The illuminance on the workplane was measured with calibrated photometric sensors (LI-210) manufactured by LICOR at 9 locations in the room. They are placed at a representative workplane height of 0.8m from the floor, at 0.25m, 0.5m, 1.0m, 1.5m, 2.0m, 2.5m, and 2.75m from the window, and 2 are placed at 0.55m from right wall and 1.5m from window, as well as 0.55m from left wall and 1.5m from window (Figure 5-8). One photometer and one pyranometer (LI-200) are placed at each of the following places: a) exterior, vertical in window-plane, b) inside the room behind the EVA, and c) inside the room behind clear viewing section (Figure 5-9, Figure 5-10).

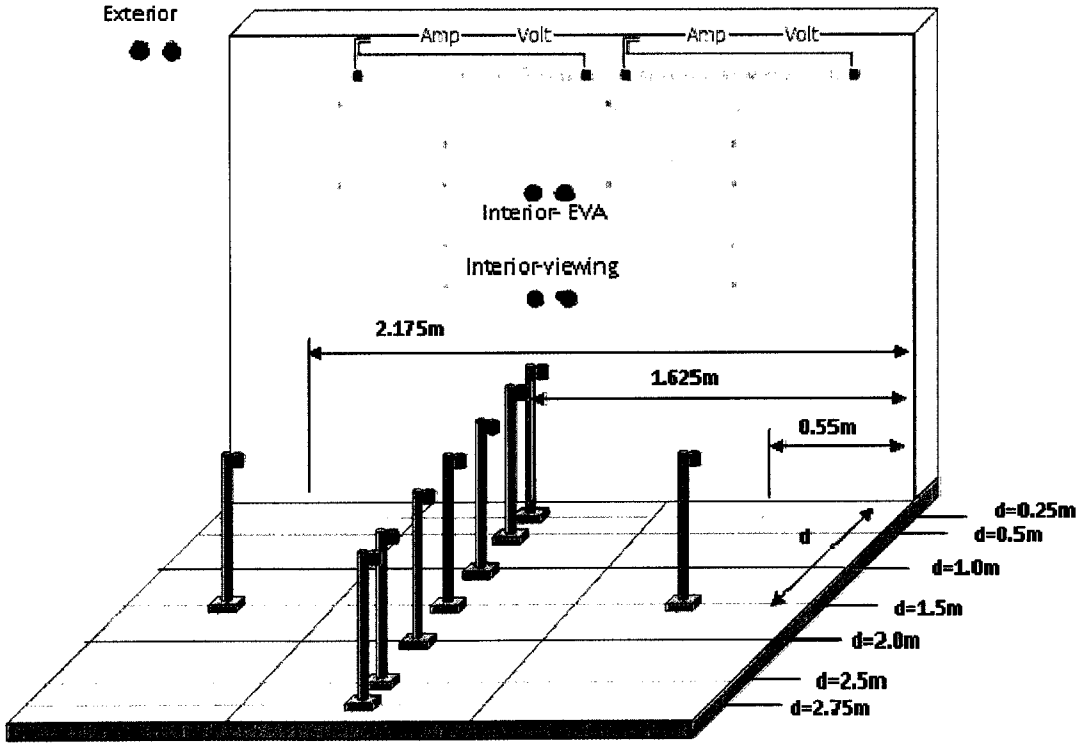

Figure 5-8: Placement of photometers and pyranometers used in experiment

Figure 5-9: Daylight and radiation sensors inside room, behind EVA and clear viewing section

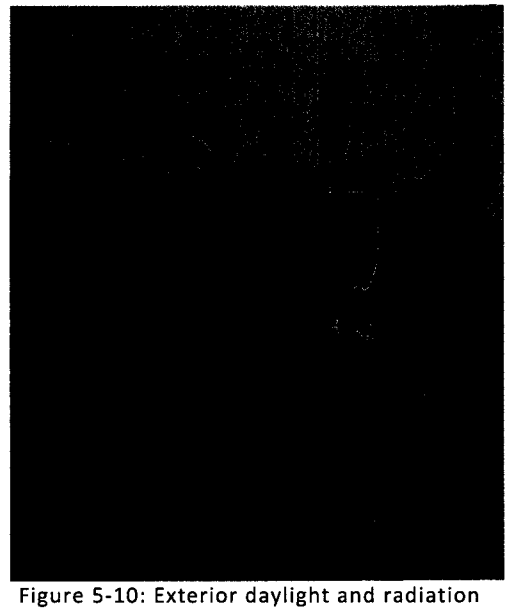

Figure 5-10: Exterior daylight and radiation sensor. Note that for specific day measurements, sensors were placed directly on the façade.

The inner sensors are used to measure the transmittance through each of the EVA and clear viewing section. The measurements are taken over a 3-month period (mid March 2009 – mid June 2009). An inside view of the office with the sensors is shown in (Figure 5-11).

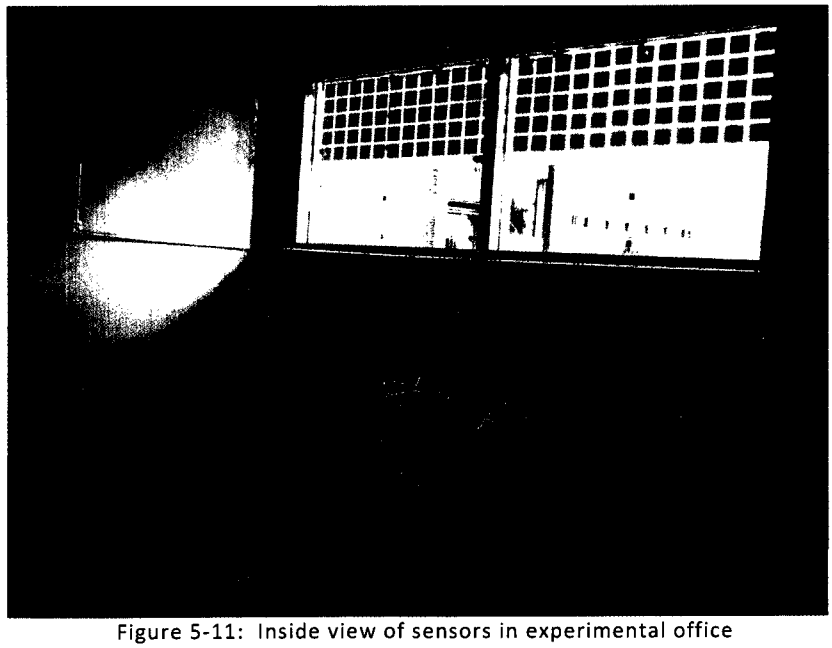

Figure 5-11: Inside view of sensors in experimental office

5.5.3 PHOTOVOLTAIC OUTPUT

The I-V curves of both PV windows were measured using a Daystar Inc. DS-100C I-V curve tracer (Daystar Inc. 2006) at CanmetENERGY in Varennes, QC. "The DS-Tracer obtains an I-V curve by varying the electrical impedance connected across the PV array output terminals. Varying the impedance from zero to infinity causes the array operating point to change from Isc to Voc. The DS-Tracer accomplishes this impedance change by connecting the array to a capacitive load. As the capacitor charges, the array moves through its operating range and presents a set of current and voltage values that form the I-V curve. When the capacitor load reaches Voc, data sampling stops." (Daystar Inc. 2006)

The measurements were taken on January 11, 2009 between 11:30 and 14:00 with global normal irradiance values between 900W/m^2 and 950W/m^2 and an outdoor temperature of -2°C to -4°C (Figure 5-12).

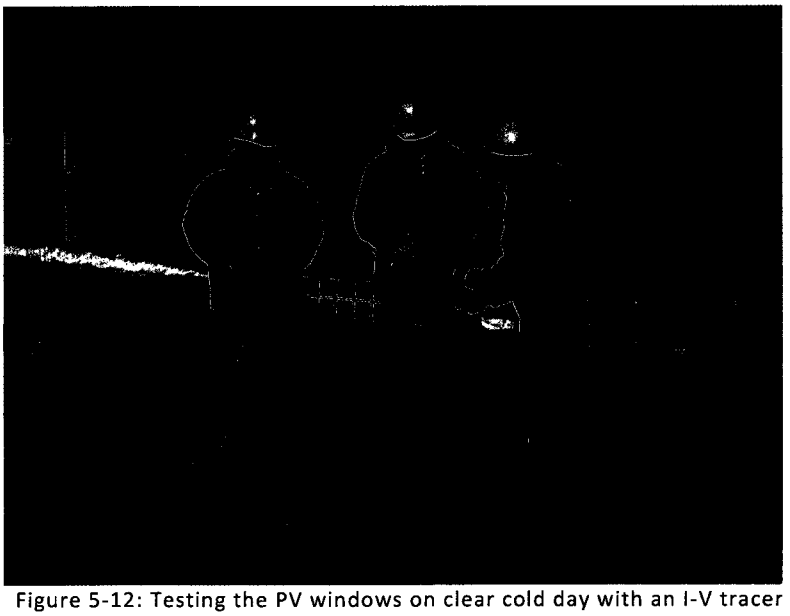

Figure 5-12: Testing the PV windows on clear cold day with an I-V tracer

On-site measurement of the PV output was not conducted as the windows are shaded a large percentage of the time from both East in the morning and West in the afternoon. Ideally, a maximum power point tracker would have been used to measure the output of the PV but even then, the results would not add anything to the analysis as the conditions are less than ideal.

Furthermore, the cells were all connected in series without a diode-bypass in case of shadows, so that if any part of the module is shaded, the output is greatly affected.

In order to have accurate temperatures of the PV cells under real conditions, the PV needed to generate electricity. A variable resistor was attached across the PV (Figure 5-13) in order to allow the PV to generate electricity.

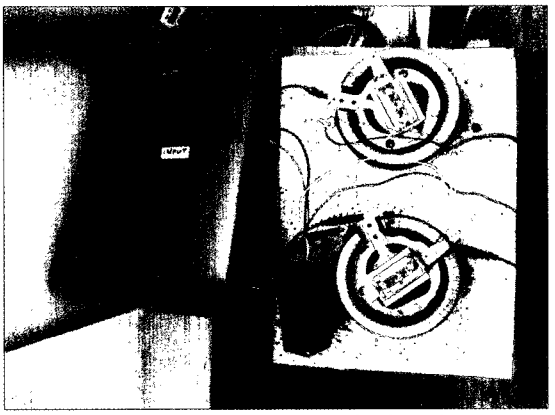

Figure 5-13: Resistor attached to the PV

Data was collected during this time but will not be used in the analysis. Fairly accurate and well tested models are available to determine the output of the PV.

5.5.4 TEMPERATURE

Thermocouples on the window are used to measure the temperature distribution in the window, enabling a calculation of the overall U-value and SHGC coefficients of each section of the window. The thermocouples behind the PV cells are used to verify the PV cell temperature estimation used in the simulations. The thermocouples are machine calibrated to 0.3°C. In this study we were interested only in the difference in temperatures and not the absolute temperatures.

The thermocouples were attached on the layers of the windows before they were manufactured (on the back of PV cells, behind front glazing, and on the interior of the low-e glazing surface). There are 37 thermocouples distributed through the window, as well as one inside the room, and one outdoors (39 total). See (Figure 5-14) for the placement of the thermocouples on the

windows and Appendix IV for a full description of placement of the thermocouples on each layer.

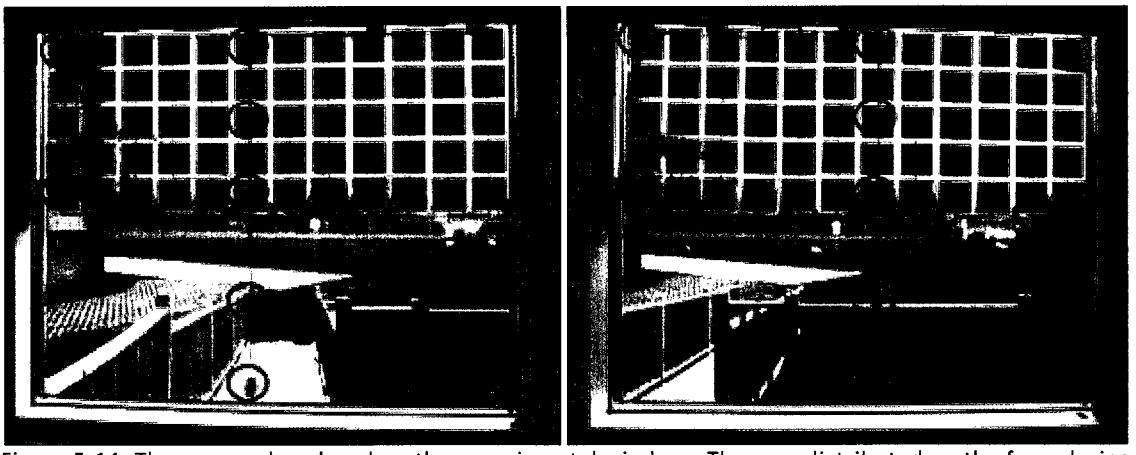

Figure 5-14: Thermocouples placed on the experimental window. They are distributed on the four glazing surfaces (outside of outer glazing, inside of outer glazing (behind PV cells), outside of inner glazing and inside of inner glazing)

Measurements were again taken for 3 months and a typical hot and cold day, both overcast and clear are presented in the comparison section.

The temperature distribution of the inner glazing was also measured using a ThermaCAM S60 infrared camera (Flir Systems) on both an overcast (May 14, 2009) and a clear day (May 13, 2009). The results will be used to extrapolate the temperatures which were not measured by thermocouples (i.e. the EVA) and are presented in Appendix IV. Only the differences in temperature will be used and not their absolute values.

5.6 Comparison of Measured Results and Simulations

5.6.1 Illuminance on the workplane

A representative overcast and sunny day were used to measure the illuminance on the workplane. The illuminances were taken during the entire day on May 16, 2009 (overcast) and May 18, 2009 (sunny) (Figure 5-15) and (Figure 5-16) show the room during these two days at solar noon (close to 13:00 standard time), the time which is used for comparison of simulated and measured results. At this time of the day it was raining on May 16 (overcast) (Figure 5-17), and fairly clear on May 18 (clear) (Figure 5-18). For the clear day, the sensor closest to the window (at 0.25m) had a sunspot, whereas none of the other sensors did. It appeared on the floor only.

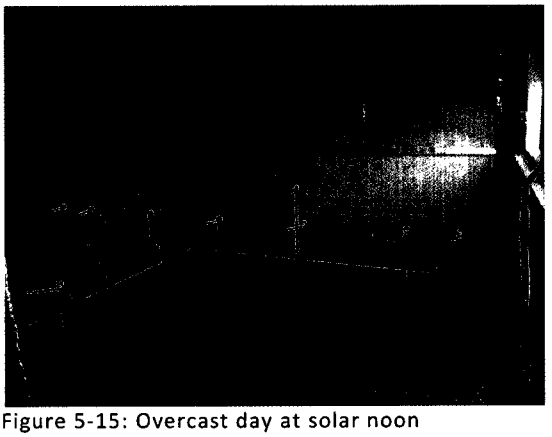

Figure 5-15: Overcast day at solar noon

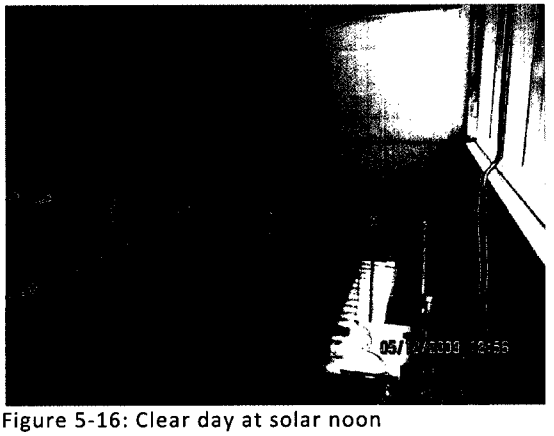

Figure 5-16: Clear day at solar noon

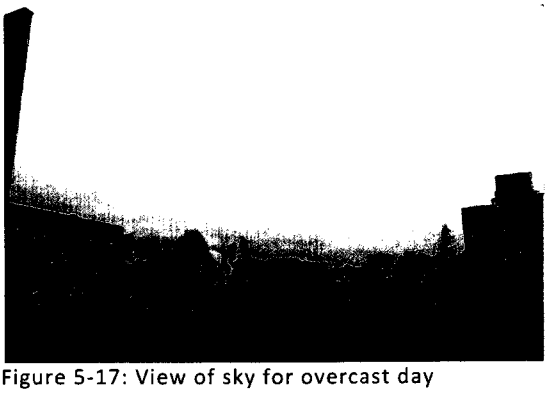

Figure 5-17: View of sky for overcast day

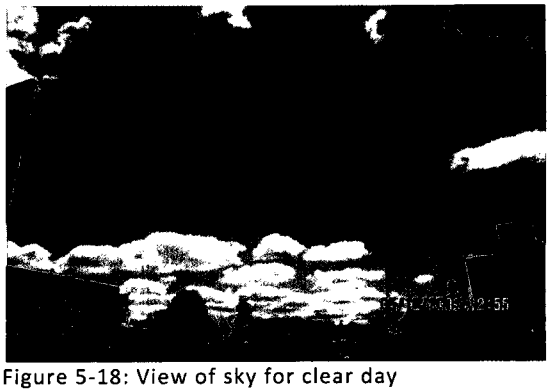

Figure 5-18: View of sky for clear day

5.6.1.1 DIFFUSE DAY

On this day, it was raining and thus there is no possibility of having a direct component influencing the results. Comparing the weather data with the NRCAN data (section 5.5.1), the vertical illuminances were quite different and thus the measured on-site data was used.

The simulated values of workplane illuminances on this overcast day are underestimated close to the window and overestimated near the back of the room (Figure 5-19). The overall error is as high as 17% near the center of the room, but this represents an absolute error of a maximum of 30lx. (Table 5-9)

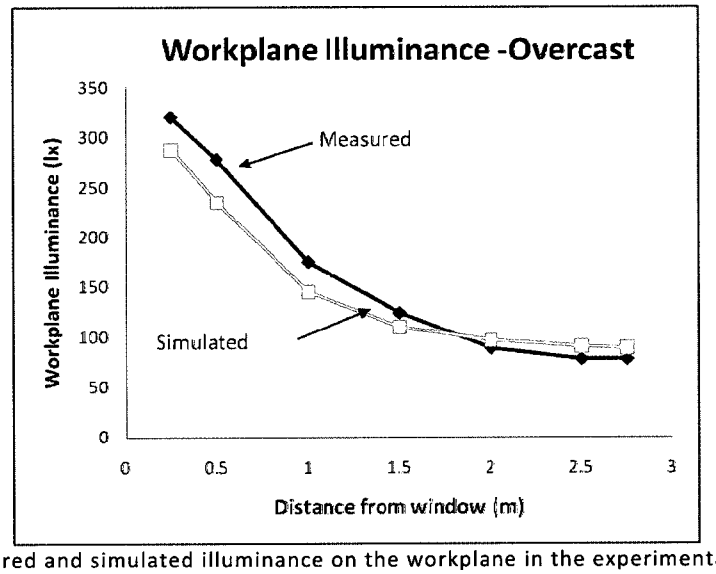

Figure 5-19: Measured and simulated illuminance on the workplane in the experimental office for a typical overcast day (May 16, 2009) at solar noon

Table 5-9: Summary of illuminances- simulated and measured for an overcast day.

Illuminance	Distance from window						
	0.25m	0.5m	1.0m	1.5m	2.0m	2.5m	2.75m
Measured	320 lx	278 lx	175 lx	124 lx	89 lx	78 lx	78 lx
Simulated	288 lx	235 lx	145 lx	110 lx	97 lx	91 lx	89 lx
Error	10.0%	15.4%	17.1%	11.3%	-9.0%	-16.7%	-14.1%

(IESNA 2000) warns that generally the differences between detailed analysis methods and field measurements are as high as 20% when dealing with basic lighting from luminaires. Daylighting adds another degree of complexity to this.

5.6.1.2 CLEAR DAY

The radiosity model used in the simulations models perfectly diffuse reflections and is generally an adequate model. However, we know that the beam component is not non-directional. A ray tracing technique would be a more realistic model for the distribution of the beam component in the space, as it takes its direction into account. As is seen above, for the overcast day, the radiosity model gives satisfactory agreement, as the assumption that the light is diffuse is close to reality for our daylighting model. If we compare our clear day measurements results with the simulated results using the radiosity method, the difference is great (Table 5-10).

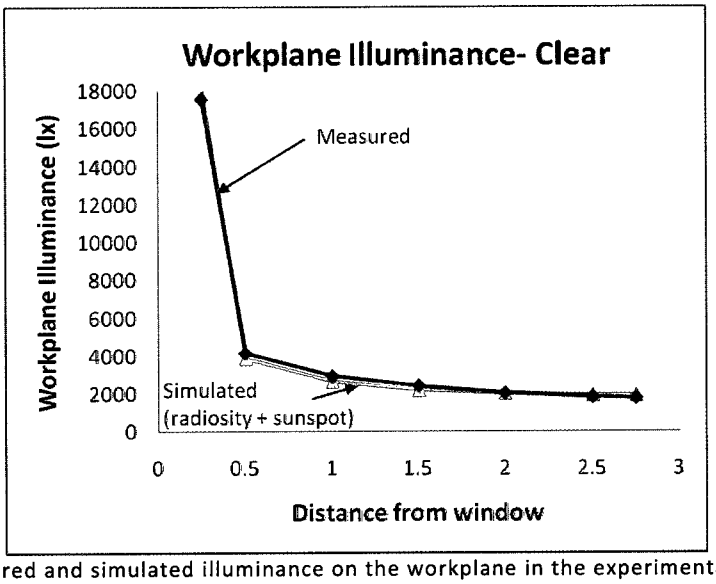

Figure 5-20: Measured and simulated illuminance on the workplane in the experimental office for a typical clear day (May 18, 2009) at solar noon

Table 5-10: Summary of illuminances, simulated and measured for a clear day.

Illuminance	Distance from window						
	0.25m	0.5m	1.0m	1.5m	2.0m	2.5m	2.75m
Measured	17569lx	4155lx	2936lx	2437lx	2052lx	1829lx	1783lx
Simulated (radiosity)	11350lx	9204lx	5644lx	4324lx	3803lx	3576lx	3513lx
Error1	-35%	122%	92%	77%	85%	96%	97%
Simulated (radiosity +sunspot)	18140lx	3877lx	2649lx	2199lx	2023lx	1945lx	1924lx
Error2	3.3%	6.7%	9.8%	9.8%	14.1%	6.3%	7.9%

The first sensor, closest to the window is underestimated by the simulations and all other sensors are overestimated. Looking at the photo taken from that day (Figure 5-16), the first sensor only has a sunspot. As the radiosity method assumes that this beam component of the illuminance is distributed through the room rather than directly on this sensor and accounts for the reason why the first the illuminance is underestimated at this spot and overestimated everywhere else.

In order to verify that the diffuse light is behaving as anticipated in the room, a quick calculation was made (called simulated- radiosity + sunspot in table and graph) which looked at the illuminance coming from diffuse and direct components separately. It was observed that at the time in question, there was a sunspot on the first sensor and the floor only (as shown in Figure 5-16). The workplane illuminances were recalculated using the radiosity method with the diffuse portion of the illuminance and adding an initial luminous exitance equally distributed on the floor. Ideally, a 9th surface should be added to the room, which would treat the sunspot as a luminaire; but as a quick calculation, it is assumed that the sunspot is equally distributed across the floor. The initial luminous exitance of the sunspot was taken as the measured value on the first sensor less the illuminance expected from the diffuse light. To be equally distributed on the floor it is multiplied by the area of the sunspot and divided by the area of the floor. Taking this sunspot into account, the simulated illuminances are very close to the measured (Table 5-10).

In the simulations for a clear day, there is always a shade on the viewing section if the radiation exceeds 100W/m^2 and thus all light entering the space will be diffuse. Our radiosity model without the sunspot calculation will again be sufficient. In practice, the shade could also cover the top section of the STPV, particularly for transmittances higher than 10%.

5.6.2 PHOTOVOLTAIC OUTPUT

A clear day in January was used to measure the output of both STPV windows. The I-V (current-voltage) curves in (Figure 5-21, Figure 5-22) are representative curves of each of the two

windows. The experimental set-up was used to verify that the PV model used in the simulation model was being calculated within an acceptable degree of error. The PV output model is accurate for the days measured to within 2%. However, due to the constraints of the set-up, only 1 point in time measurements were taken with high irradiance levels, low temperatures, clear sky and with a close-to-zero angle of incidence. Ideally, more measurements would have been taken for varying conditions.

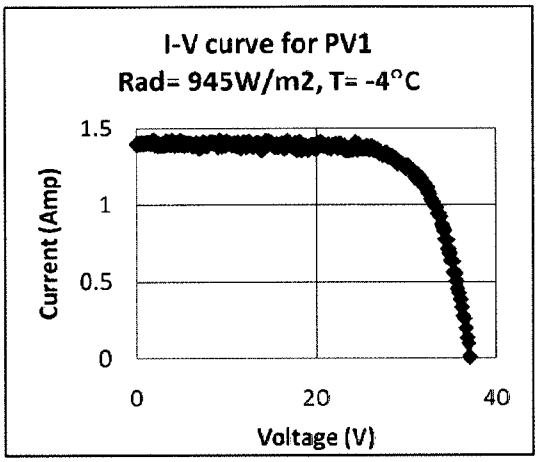

Figure 5-21: I-V curve for PV1 (West)

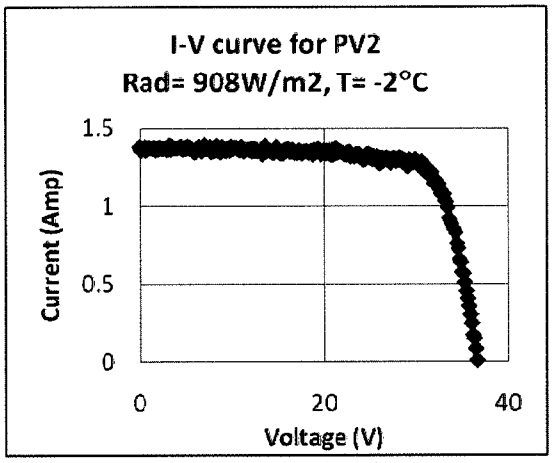

Figure 5-22: I-V curve for PV2 (East)

For both windows, at high irradiance levels and outdoor temperatures of -2 to -4 °C, the simulated values, as calculated per the change in efficiency due to changing cell temperature (section 3.9) and measured values are within 1.5% (Table 5-11).

Table 5-11: Comparison of simulated and measured PV power output

	PV1-measured	PV1- simulated	PV2-measured	PV2- simulated
I_{t_ref}	945.7 W/m²		907.7 W/m²	
P_{PV}	37.86W	37.73W	39.26W	38.68W
Error	0.34%		1.48%	
	Using the following values for simulated results			
$A_{PV}*A_1$		*0.365m²*		*0.365m²*
η_{PV}		*10.97%*		*11.84%*
$T_{o,\ NOCT}$		*25℃*		*25℃*
η_{cell_temp}		*0.55%/℃*		*0.55%/℃*
T_o		*-4℃*		*-2℃*
NOCT		*45℃*		*45℃*
I_o		*800W/m²*		*800W/m²*

The stated efficiency and the fill factor of each PV window is calculated by using the expressions described in section 3.9 (Table 5-12).

Table 5-12: Calculated PV efficiency and fill factor, for each window

	PV1 (West)	PV2 (East)
Rad_{ref}	945 W/m^2	908 W/m^2
V_{oc}	37.00V	36.54V
I_{sc}	1.26A	1.38A
P_{max}	37.86W	39.26W
A_c	0.365m^2	0.365m^2
η_{PV}	10.97%	11.84%
FF	73.38	77.73%

5.6.3 TEMPERATURE DISTRIBUTION THROUGH WINDOW

37 thermocouples were placed throughout the STPV window in order to give an indication of the impact of STPV on the heat transfer though the window. An infrared camera was used to measure the missing temperatures.

The goal was not to conduct an extensive heat transfer analysis but rather to examine the temperature differences and changes in U values and SHGC for varying outdoor conditions. From these results, an estimate of the heat transfer through the façade is presented. In addition the measured PV cell temperature is compared with the estimated temperature.

5.6.3.1 THERMOCOUPLES

Representative hot clear (Jun17, 2009), hot overcast (Jun 11, 2009), cold clear (Mar 12, 2009), and cold overcast (Apr 7, 2009) days were used to measure the temperature distribution through the window. Ideally hotter and colder days would be used, but data with the largest temperature variation was chosen from the data available.

Table 5-13: Weather data for design days- taken at solar noon (13:00 standard time)

	Cold		Hot	
	Mar 12, 2009	Apr 7, 2009	Jun 11,2009	Jun 17, 2009
Sky cover	Mainly clear	Cloudy	Cloudy	Mainly clear
Outdoor temperature	-7.5°C	2.0°C	21.9°C	24.2°C
Wind speed	28km/h	37km/h	4km/h	11km/h

Cold days

The maximum temperature difference on the inner glazing (g4) for the cold mainly clear day is 4.9°C, with the maximum temperature being in the viewing section and the minimum temperature being in the STPV section. For the cool cloudy day, the maximum temperature difference reduces to 1.4°C, again with the maximum temperature occurring in the viewing section. The temperature behind the PV is significantly higher than the rest of the glazing layers for the clear cold day (Figure 5-23, Figure 5-24).

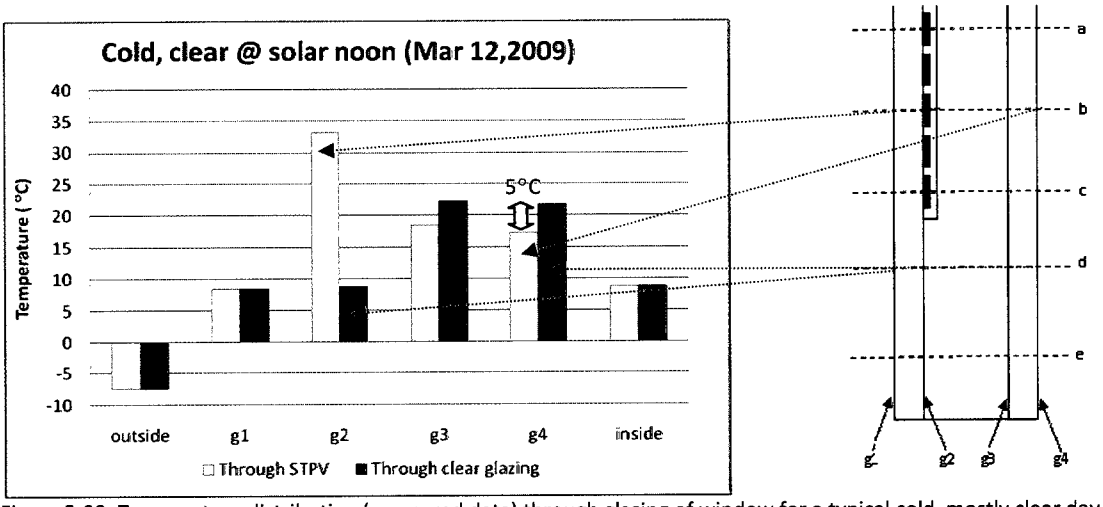

Figure 5-23: Temperature distribution (measured data) through glazing of window for a typical cold, mostly clear day (Mar12, 2009). Two cross sections are shown: grey-through STPV section (b), black-through clear viewing section (d)

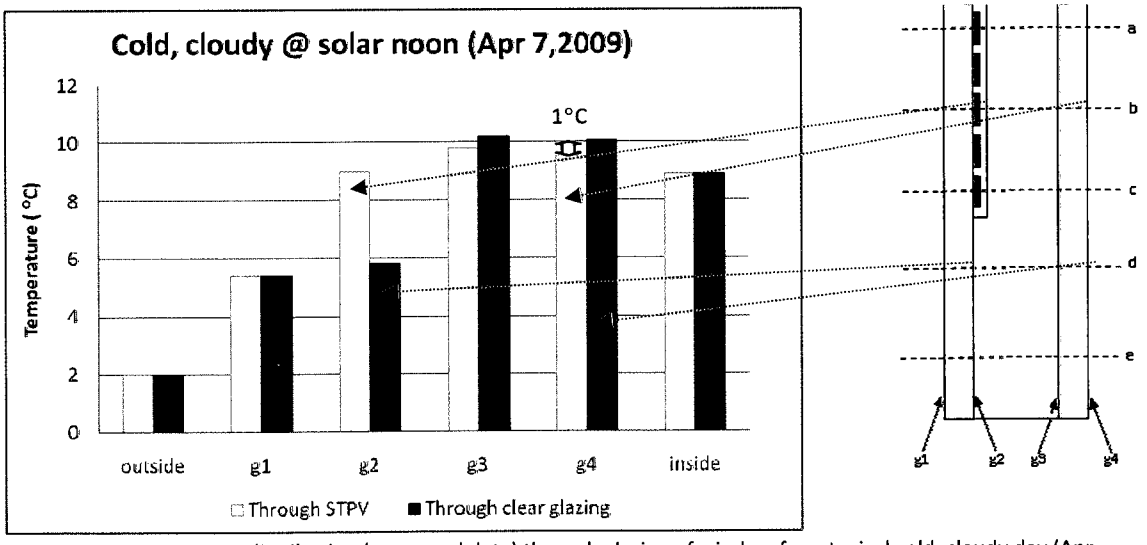

Figure 5-24: Temperature distribution (measured data) through glazing of window for a typical cold, cloudy day (Apr 7, 2009). Two cross sections are shown: grey-through STPV section (b), black-through clear viewing section (d).

Hot days

The maximum temperature difference on the inner glazing (g4) for the warm, mainly clear day is 2.8°C, with the maximum temperature being in the viewing section and the minimum temperature being in the STPV section. For the hot cloudy day, the maximum temperature difference again drops to a 1.4°C difference, again with the maximum temperature occurring in the viewing section (Figure 5-25, Figure 5-26).

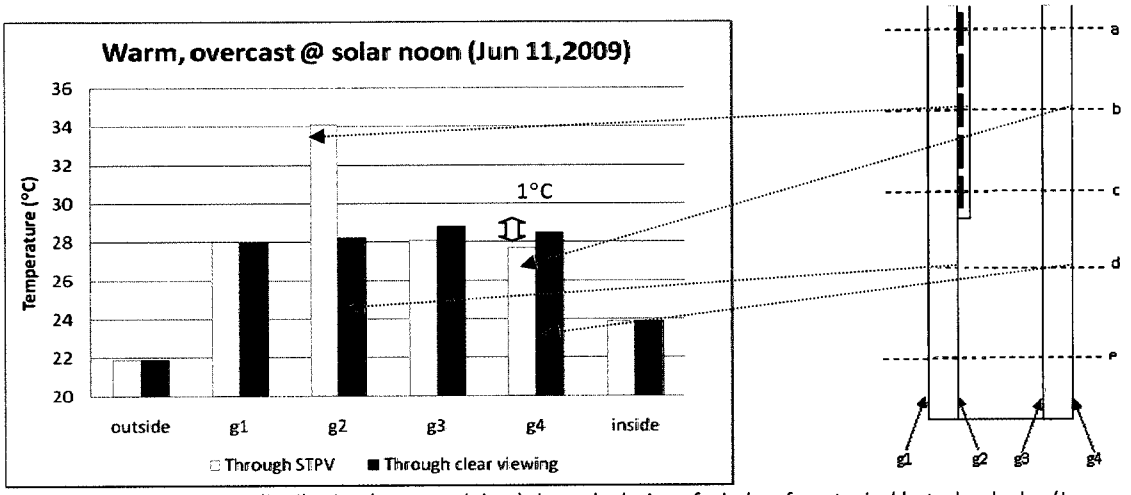

Figure 5-25: Temperature distribution (measured data) through glazing of window for a typical hot, cloudy day (Jun 11, 2009). Two cross sections are shown: grey-through STPV section (b), black-through clear viewing section (d).

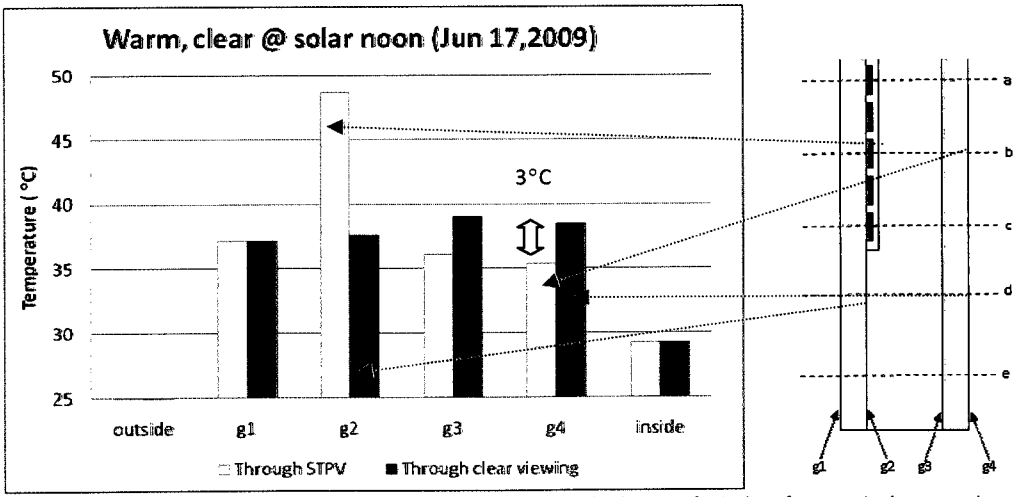

Figure 5-26: Temperature distribution (measured data) through glazing of window for a typical warm, clear day (Jun 17, 2009). Two cross sections are shown: grey-through STPV section (b), black-through clear viewing section (d).

For all four cases, the temperature difference between the viewing section and the STPV section is never more than 5°C, with the highest temperature always in the viewing section. The highest difference occurs on a cold clear day. These results demonstrate that the use of STPV over regular double glazing reduces the inner glazing temperature in all four major design days.

5.6.3.2 INFRARED CAMERA

Infrared photos were taken on both a clear (May 13, 2009) and overcast day (May 14, 2009). As there are no thermocouples behind the EVA, the interest of these photos was to give an idea of the temperatures of the EVA between the PV cells. It was also to verify the estimates of differences in temperature between the STPV and viewing sections. Normally an infrared camera is not used to measure temperature during the day due to solar radiation effects. Therefore the values will be used as relative temperatures and not absolute.

The temperature difference between the PV cells and the EVA is 0.1°C for an overcast day and 0.5°C on a clear day. Both of these measurements are smaller than the accuracy in the thermocouples. For our purposes we will use the same inner glazing temperatures for both the PV and the EVA. The differences between the viewing section temperatures and the STPV section is 4-5°C for the clear day, which is similar to the measured values with the thermocouples on a similar day. For the overcast day the differences were less than 1°C which is slightly less than those measured on a similar day with the thermocouples. The results are presented in Appendix IV.

5.6.3.3 PV CELL TEMPERATURE

For the four representative design days, the measured temperature of the PV is compared with the expression used for estimating PV cell temperature (Table 5-14). The PV cell temperature estimation is described in section 3.9.

Table 5-14: Comparison of measured PV cell temperature and estimated as used in simulations

	Cold		Hot	
	Mar 12, 2009	Apr 7, 2009	Jun 11,2009	Jun 17, 2009
Exterior temperature (To)	-7.5°C	2.0°C	21.9°C	26.6°C
Estimated PV cell temperature	32.1°C	7.6°C	32.2°C	42.7°C
Measured PV cell temperature	35.6°C	9.0°C	34.1°C	48°C
Difference	3.5°C	1.4°C	1.9°C	5.3°C

The measured values are not the actual PV cell temperature but rather the temperature behind the EVA which is behind the PV cell. The difference between the measured and estimated PV cell temperature is as high as 5°C for a clear warm day. If we use a power temperature coefficient of -.43%/K as used in the simulations, a difference of 5°C would cause a 2% in the power results.

5.6.3.4 ESTIMATED HEAT GAIN THROUGH WINDOW

To translate the temperature distribution in the windows into a useful heat gain value, the U-value and solar heat gains coefficient (SHGC) of the different section of the windows are calculated and used to estimate the instantaneous heat gain through the façade (see section 3.10).

Table 5-15: Estimated U-values and SHGC for the 3 sections of the experimental window, calculated at solar noon on representative design days

		PV		EVA		Clear	
		U	SHGC	U	SHGC	U	SHGC
Cold, clear-	Beam	1.78 W/m²K	0.040	1.78 W/m²K	0.813	1.70 W/m²K	.853
	Diffuse		0.037		0.414		.646
Cool, cloudy	Beam	1.01 W/m²K	0.018	1.01 W/m²K	.775	1.40 W/m²K	.817
	Diffuse		0.017		.409		.642
Hot, cloudy	Beam	1.38 W/m²K	0.069	1.38 W/m²K	.613	0.99 W/m²K	.643
	Diffuse		0.076		.424		.652
Warm, clear	Beam	1.65 W/m²K	.051	1.65 W/m²K	.603	1.18 W/m²K	.633
	Diffuse		.056		.419		.648

The U values vary greatly with changing outdoor conditions. The U values for the double glazed STPV section (through EVA and PV are the same) vary by as much as .77W/m²K and the U

values for the double glazed window section vary by as much as .71W/m²K (Table 5-15). The SHGC coefficients are calculated as a function of angle of incidence and are thus are calculated for both beam and diffuse components of radiation. The solar heat gain coefficients of the clear viewing section are the highest and the PV section the lowest (Figure 5-27).

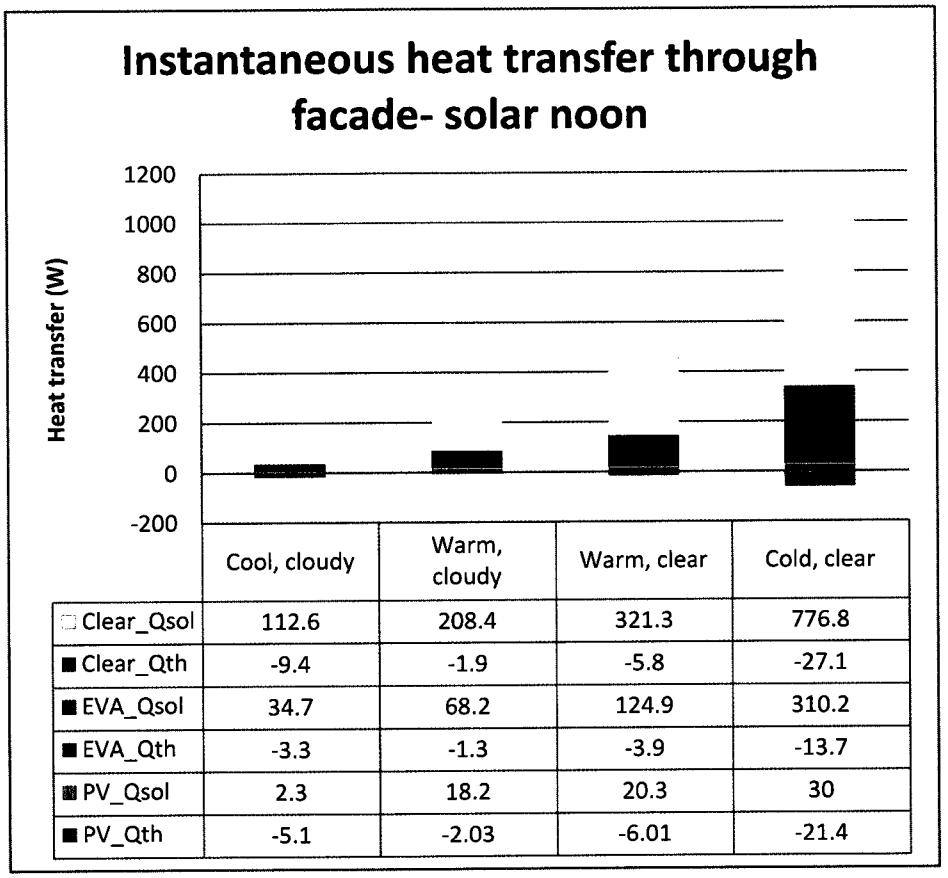

	Cool, cloudy	Warm, cloudy	Warm, clear	Cold, clear
Clear_Qsol	112.6	208.4	321.3	776.8
Clear_Qth	-9.4	-1.9	-5.8	-27.1
EVA_Qsol	34.7	68.2	124.9	310.2
EVA_Qth	-3.3	-1.3	-3.9	-13.7
PV_Qsol	2.3	18.2	20.3	30
PV_Qth	-5.1	-2.03	-6.01	-21.4

Figure 5-27: Heat gains through the different window sections. Qth=instantaneous energy flow due to indoor-outdoor temperature difference; Qsol=instantaneous energy flow due to solar radiation

The total energy through window (Q_{facade}) is equal to the heat transfer due to temperature difference between inside and outside (Q_{th}) + solar radiation transmitted through glazing + inward flow of solar radiation absorbed in glazing (Q_{sol}) (Athienitis & Santamouris 2002). The instantaneous heat gain from the façade will only give an indication of how the façade configurations will affect the heating and cooling loads and is based on the area of the window.

$$Q_{facade} = Q_{th} + Q_{sol} \tag{5.6.1}$$

$$Q_{facade} = U * A(t_{ext} - t_{int}) + SHGC * A * I_t \quad (5.6.2)$$

Where U is the calculated U factor of the window, A is the area of the window, t_{ext} and t_{int} are the exterior and interior temperatures, SHGC is the solar heat gain coefficient of the window and I_t is the incident solar radiation.

The highest heat gains through the window are on the clear days and the lowest on the overcast days and there is a significant difference between the two. The largest heat gains are always through the viewing section.

The experimental set-up was used to verify that all aspects of the simulation model were being calculated within an acceptable degree of error. It has been demonstrated in this section that the daylighting model provides accuracy to within 15% for diffuse light, such as for an overcast day or a clear day with a shade. The PV output model is accurate for the days measured to within 2%. The temperature distribution is used for discussion of heat gains only.

6 CONCLUSIONS AND RECOMMENDATIONS

6.1 CONCLUSIONS

This thesis demonstrated that semi-transparent photovoltaics can be used in commercial façades to improve the overall energy performance of the office space. The net electricity is taken into consideration, looking at both the workplane illuminance levels and the associated lighting loads as well as the electricity produced by the photovoltaics. A simulation of a typical small office with STPV in the upper section of a three-section façade was performed, to determine the ideal transmittance or PV area ratio of the semi-transparent photovoltaics which would give the maximum net electricity generation. In order that the results be general enough to be useful, several important design parameters were taken into consideration including changing façade orientation, site location, PV efficiency, lighting control strategies, and shading device transmittance. A comprehensive experimental study of an office with a custom-made two-section, double-glazed STPV-integrated window was used to verify the illuminance on the workplane, and to lead the discussion on the heat gains through the window.

An experimental study was performed using a custom-built STPV window integrated in an existing solar house in Montreal. The workplane illuminance for overcast and clear days was verified for 9 different workplane points. with a reasonable agreement. The principal assumptions made in the simulation that all reflections are perfectly diffuse and that the inside surface of the STPV and window act as perfectly diffuse luminous sources was evident in the results. Good agreement occurred for the overcast day (within 17%) with much larger errors for a clear day as even the direct daylight was modeled as being non-directional and distributing uniformly throughout the room. However it was demonstrated in the results that if the sunspot is treated as a luminous source and then distributed through the room the results match to within 14%. As the simulations include a shade on the viewing window section which blocks the direct solar radiation, this assumption is reasonable. The output of the PV was also

measured on a cold clear day in January with an difference from the measured to the simulated values of 2% for the time measured. Ideally, more measurements would have been taken for varying conditions.

Temperatures through the façade were also measured in the experiment and it was found that for the design days used (cold clear, cool overcast, warm clear, hot overcast) a temperature difference between the viewing section and the STPV section is never more than 5°C, with the highest temperature always in the viewing section. As office buildings tend to be cooling dominated the use of STPV over regular double glazing can potentially reduce the cooling loads.

There has been limited research on the development of guidelines for design/construction of glazed building façades with STPV. By providing an ideal PV area ratio in the semi-transparent PV section of the three-section façade, or by choosing thin film PV with an ideal efficiency/transmittance ratio, both the lighting loads and cooling loads may be kept to a minimum.

Based on the results of the simulations of this study, it can be concluded that:

- On an annual basis, the highest net electricity generation occurs with a 90% PV area ratio in the upper section, a 16% increase from the 100% PV area ratio case due to the significant increase in lighting load for 100% coverage.
- On a design day basis, a 100% PV area ratio in the upper section performs best for overcast cool and warm as well as clear cool days and in addition performs well in the winter but poorly in the summer. The 90% PV area ratio is ideal for a clear warm day and in general performs well throughout the year. The implications of these results are high when designing for peak load management.
- South facing façades have the highest annual net electricity generation with up to 60% higher net electricity generated than East or West facing façades. However, when faced

with South-West, South-East, West or East facing façades, a 90% PV area ratio is ideal for all orientations mentioned with little difference in results for South-West and South-East and much greater reductions for West and East. The hours in which lighting is required changes the results significantly, and can change the ideal from East to West.

- When changing PV efficiency from 6 to 22%, the ideal PV area ratio remains the same for all, at 90%. Evidently the values of the net electricity vary significantly from one to the other and the impact of changing from 90% to 100% PV area ratio for low efficiencies is much greater than for high efficiencies.

- Montreal, Vancouver, Iqaluit, Toronto and St. John's all have an ideal PV area ratio of 90% in the upper section. Of the cities explored, Montreal had the highest yearly PV output and mid-range lighting loads, thus making it the best candidate for STPV. Iqaluit, although having the highest lighting loads, had the second highest PV output. St. John's has the lowest PV output and mid lighting load requirements, making it the poorest candidate for STPV.

- For changing shade transmittances on the window viewing section, on an annual basis, there is little difference between 1%, 5% and 10% except for 100% PV coverage . On a design day basis and for a 90% PV area ratio, the only difference occurs for the clear warm day.

- Changing the lighting control strategy changes the net electricity results significantly. The active on/off control has an ideal PV area ratio of 80% instead of 90% and reduces the net electricity generation by 27% when compared with continuous dimming for a 90% PV area ratio and 77% for 100% PV area ratio. The passive control has an ideal PV area ratio at 100% but the PV can never cover the lighting loads required.

- The ideal PV area ratio is determined by several design variables and conditions. Lighting control strategy is a design variable which changes the PV area ratio

significantly while both shade transmittance and PV efficiency do not change the ideal PV area ratio. Of the site conditions, both location and orientation have little effect on the ideal PV area ratio.

However, there are several limitations of the work which need to be taken into consideration. The results are presented for a very specific three-section façade layout. Should a different layout be used, the results, and especially the ideal PV area ratio, would change. The study looked at only single offices with specific dimensions and layout. Again, should the space change dramatically, or its use change, the results may be very different.

6.2 Recommendations for future work

As there has been little work done in the area of evaluating the net electricity benefits of semi-transparent photovoltaics, the potential for future work is vast. It has been demonstrated in this thesis that the use of STPV with a 10% transmittance in the upper section of a 3-section façade can result in significant energy savings when compared with a normal double-glazed window or opaque PV spandrel in the same façade section. The recommendations for future work will be divided into 4-sections as follows: the addition of heating and cooling loads to the overall net energy balance, occupant comfort including glare protection, different applications of STPV from the vertical commercial façade and deviations from the strict three-section façade, and finally, the question of cost and comparing the different PV area ratios with a normal windows and opaque PV spandrel on a cost basis.

This thesis has focused on only daylighting and PV output without taking the heat transfer through the façade and its interaction with the space into consideration. It was shown through the experiments that the inner glazing temperature in the STPV was always lower than in the unobstructed viewing window section for the days examined. As most office buildings are cooling dominated, STPV thus provides an advantage over normal double glazed windows for this specific application. However, the measurements were only taken for a specific moment in

time and only for one PV area ratio. A complete transient heat transfer model would be necessary to give an idea of the potential cooling saving of the STPV.

Before commencing, a verification would be necessary of whether a 1-dimensional model is accurate enough or whether the 3-dimensional interactions between the cells and the rest of the window are large enough to merit a more complicated model. Furthermore, the heating and cooling seasons for a specific application, location and building would need to be explored in order to determine whether the increase or decrease in inner glazing temperatures result in beneficial or detrimental heat transfers.

At all times a minimum illuminance on the workplane was required but there was no attention paid to the maximum workplane illuminance or glare to the occupant. Further work should be done to explore whether the shade on the viewing section is sufficient for human comfort or whether other measures need to be taken.

Furthermore, the STPV section in the simulation model was treated as a diffuse surface with no direct light coming through the window. In reality this is not the case and sunspots on the workplane from the spaces between the cells may cause glare and discomfort. An exploration of the amount of direct light coming through this section and solutions to overcome the discomfit should be conducted. A ray-tracing model would be required to determine if a shade would be required over this section. If transparent thin-film photovoltaics were used instead of spaced cells, this problem could potentially be avoided.

Continuing in the subject of human comfort exploration, it would be interesting to look at existing STPV applications used in office façades and determine the level of satisfaction of those users and their level of visual and thermal comfort.

Vertical façades to be used in small offices was the only application of STPV explored in this thesis. STPV can be used in other commercial applications such as in awnings and in skylights, as well potentially in residential applications. In this thesis, the vertical façade normally

resulted in an ideal PV area ratio of 90% in the upper section of a three-section façade but this would not necessarily be the case for the other applications or façade layouts. Separate studies could be conducted for other applications and other façade layouts, much in the same way this one was conducted.

The net electricity was the only factor taken into consideration in this thesis. As the cost of PV is still fairly high and the cost of electricity in most parts of Canada still fairly low, including the overall cost in the equation could vary the ideal PV area ratio results greatly. This would be a challenging study to conduct as the cost of PV and electricity vary greatly from one location to another and from one year to another (and the case of electricity, sometimes from one hour to the next). However, in order to get STPV into the market, it is imperative that an extremely comprehensive study be conducted. This should consider the potential of STPV to offset peak loads, as a renewable resource which may include carbon offsetting or other incentives along with the electricity costs and reductions associated with its use.

REFERENCES

Armani, M., Parretta, A., Antonini, A., Butturi, M. & Stefancich, M. 2007, "Models for efficiency prediction of different PV module technology", *22nd European solar energy conference and exhibition.*

ASHRAE 2001, *ASHRAE handbook fundamentals,* American Society of Heating, Refrigerating, and Air-Conditioning Engineers, Inc., Altanta, USA.

Athienitis, A. & Santamouris, M. 2002, *Thermal analysis and design of passive solar buildings,* James & James, London.

Athienitis, A.K. & Tzempelikos, A. 2002, "A methodology for simulation of daylight room illuminance distribution and light dimming for a room with a controlled shading device", *Solar Energy,* vol. 72, no. 4, pp. 271.

Athienitis, A. 1999, *Building thermal analysis- Electronic MathCAD book,* 3rd edn, MathSoft Inc., Boston.

Begemann, S.H.A., Van den Beld, G.J. & Tenner, A.D. 1997, "Daylight, artificial light and people in an office environment, overview of visual and biological responses", *Industrial Ergonomics,* vol. 20, pp. 231.

Bessoudo, M. 2008, *Thermal comfort conditions near highly-glazed façades: An experimental and simulation study,* M.A.Sc. thesis, Concordia University, Montreal.

Boake, T.M. 2007, *Case studies in Canadian sustainable design.* Available: http://www.architecture.uwaterloo.ca/faculty_projects/terri/gallery.html [2009, 07/03].

Brandemuehl, M.J. & Beckman, W.A. 1980, "Transmission of diffuse radiation through CPC and flat plate collector glazings", *Solar Energy,* vol. 24, no. 5, pp. 511.

Bryan, H. & Clear, R. 1981, "Calculating daylight illuminance with a programmable hand calculator", *Journal of the Illumination Engineering Society,* vol. 10, no. 4, pp. 219.

Centennial Solar 2004, , *Centennial solar technical specifications.* Available: http://www.centennialsolar.com/en/technical.html [2009, 06/01] .

Chow, T.T., Fong, K.F., He, W., Lin, Z. & Chan, A.L.S. 2007, "Performance evaluation of a PV ventilated window applying to office building of Hong Kong", *Energy and Buildings,* vol. 39, pp. 643.

Cole, R., Cayuela, A., McCarry, B., Robinson, J., Tabatabaian, M. & Yen, D. 2007, "Centre for interactive research on sustainability: Integration of PV", *2nd Canadian solar buildings conference.*

Daystar Inc. 2006, *DS-100C I-V CURVE TRACER User Manual,* Las Cruces, NM.

De Boer, B.J. & Van Helden, W.G.J. 2001, "PV Mobi- PV modules optimised for building integration", *9th International conference on solar energy in high latitudes. NorthSun 2001.*

Duffie, J. & Beckman, W. 2006, *Solar engineering of thermal processes,* 3rd edn, John Wiley & Sons, Inc., New Jersey.

Environment Canada 2008, *National climate data and information archive.* Available: www.climate.weatheroffice.ec.gc.ca [2009, June 1] .

Franzetti, C., Fraisse, G. & Achard, G. 2004, "Influence of the coupling between daylight and artificial lighting on thermal loads in office buildings", *Energy and Buildings,* vol. 36, pp. 117.

Fung, T.Y.Y. & Yang, H. 2008, "Study on thermal performance of semi-transparent building-integrated photovoltaic glazings", *Energy and Buildings,* vol. 40, pp. 341.

Fung, Y.Y. 2006, *Energy performance of semi-transparent PV modules for applications in buildings,* PhD. Thesis, Hong Kong Polytechnic University.

German solar energy society 2005, *Planning and installing photovoltaic systems- A guide for installers, architects and engineers,* James & James, London.

Gonchar, J. 2006, *An evolving edifice that will improve with time.*

Heschong, L. 2002, "Daylighting and human performance", *ASHRAE Journal,* vol. 44, no. 8, pp. 65.

Hopkinson, R. 1954, "Reflected daylight", *Architectural Journal,* vol. 19.

I.E.A. 2002, *Potential for building integrated photovoltaics- Technical report.*

IESNA 2000, *IESNA lighting handbook,* Illuminating Engineering Society of North America, New York.

Kapsis, K. 2009, *Modeling, control & performance evaluation of bottom-up motorized shade,* M.A.Sc. Thesis, Concordia University, Montreal.

Kapsis, K., Tzempelikos, A., Athienitis, A. & Zmeureanu, R. 2009, "A control algorithm for bottom-up roller shade", *4th Canadian solar buildings conference.*

Kaufman, J. & Haynes, H. 1981, *IES lighting handbook,* , New York.

King, D.L., Boyson, W.E. & Kratochvil, J.E. 2004, *Photovoltaic array performance model,* Sandia National Laboratories, Albuquerque, NM.

Krauter, S.C.W. 2006, *Solar electric power generation - photovoltaic energy systems : modeling of optical and thermal performance, electrical yield, energy balance, effect on reduction of greenhouse gas emissions,* Springer, Berlin.

Lee, E.S., DiBartolomeo, D.L. & Selkowitz, S.E. 1998, "Thermal and daylighting performance of an automated venetian blind and lighting system in a full-scale private office", *Energy and Buildings,* vol. 29, no. 47.

Li, D., Lam, J. & Wong, S. 2005, "Daylighting and its effects on peak load determination", *Energy-The Int J.,* vol. 30, no. 10, pp. 1817.

Li, D.H.W., Lam, J.C. & Wong, S.L. 2002, "Daylighting and its implications to overall thermal transfer value (OTTV) determinations", *Energy,* vol. 27, pp. 991.

Li, D.H.W., Lam, T.N.T., Chan, W.W.H. & Mak, A.H.L. 2009, "Energy and cost analysis of semi-transparent photovoltaic in office buildings", *Applied Energy,* vol. 86, pp. 722.

Liu, B.Y.H. & Jordan, R.C. 1963, "The long-term average performance of flat-plate solar energy collectors", *Solar Energy,* vol. 7, pp. 53.

Luque, A. & Hegedus, S. 2003, *Handbook of photovoltaic science and engineering,* Wiley, West Sussex, UK.

Messenger, R. 2000, *Photovoltaic power systems,* CRC Press, Boca Raton, Fla.

Miyazaki, T., Akisawa, T. & Kashiwagi, T. 2005, "Energy Savings of office buildings by the use of semi-transparent solar cells for windows", *Renewable Energy,* vol. 30, pp. 281-304.

Murdoch, J.B. 2003, *Illuminating Engineering- from Edison's lamp to the LED,* 2nd edition, MacMillan Publishing Inc., New York.

NRTEE, 2009, *Geared for change: Energy efficiency in Canada's commercial building sector.* Prepared by the National round table on the environment and the economy and Sustainable development technology Canada, Ottawa, ON. Available: http://www.nrtee-trnee.com/eng/publications/commercial-buildings/contents-commercial-buildings.php [2009, April 15].

Notton, G., Cristofari, C., Mattei, M. & Poggi, P. 2005, "Modelling of a double-glass photovoltaic module using finite differences", *Applied Thermal Engineering,* vol. 25, pp. 2854.

NRCan, 2009, , *Energy use data handbook tables (Canada)* Prepared by Natural Resources Canada, Office of energy efficiency, Ottawa, ON. Available: http://oee.nrcan.gc.ca/corporate/statistics/neud/dpa/handbook_tables.cfm [2009, May 27].

NRCan, 2007, *Commercial and institutional consumption of energy survey. Summary report - June 2007,* Natural Resources Canada, Office of energy efficiency, Ottawa, ON.

NRCan, 2004, *Mainstreaming building-integrated photovoltaics in Canada.* Prepared by Natural Resources Canada, Varennes, QC and Royal Architectural Institute Canada, Ottawa, ON.

Pelland, S., McKenney, D., Poissant, Y., Morris, R., Lawrence, K., Campbell, K. & Papadopol, P. 2006, "The development of photovoltaic resource maps for Canada", *31st annual conference of the solar energy society of Canada.*

Perez, R., Ineichen, P., Seals, R., Michalsky, J. & Stewart, R. 1990, "Modeling daylight availability and irradiance components from direct and global irradiance", *Solar Energy,* vol. 44, no. 5, pp. 271.

Reed Construction data 2007, *Yellowknife's Greenstone Government of Canada building receives LEED Gold standard,* http://www.dailycommercialnews.com/article/id24198 [2009 , 06/18].

Reinhart, C.F. & Herkel, S. 2000, "The simulation of annual illuminance distributions- a state-of-the-art comparison of six Radiance-based methods", *Energy and Buildings,* vol. 32, no. 2, pp. 167.

Robinson, L.E. & Athienitis, A.K. 2009, "Design methodology for optimization of electricity generation and daylight utilization for façade with semi-transparent photovoltaics", *11th International Building Performance Simulation Association Conference and Exhibition.*

Robinson, L.E., Athienitis, A.K., Tzempelikos, A. 2008, "Development of a design methodology for integrating semi-transparent photovoltaics in building façades", *3rd Canadian solar buildings conference.*

Siegel, R. & Howell, J. 1982, "Thermal radiation heat transfer", *HPC Publication* .

Sylvania 2007, *Sylvania Lamps.* Available: http://www.sylvania-lamps.com/catalog/pdflib/lamps2pdf.php?id=314 [2009, 06/18] .

Takeoka, A., Kouzuma, S., Tanaka, H., Inoue, H., Murata, K., Morizane, M., Nakamura, N., Nishiwaki, H., Ohnishi, M., Nakano, S. & Kuwano, Y. 1993, "Development and application of see-through a-Si solar cells", *Solar energy materials and solar cells,* vol. 29, pp. 243.

Thevenard, D. & Haddad, K. 2006, "Ground reflectivity in the context of building energy simulation", *Energy and Buildings,* vol. 38, pp. 972.

Tregenza, P.R. & Waters, I.M. 1983, "Daylight Coefficients", *Lighting Research and Technology,* vol. 15, pp. 65.

Tsangrassoulis, A. & Bourdakis, V. 2003, "Comparison of radiosity and ray-tracing techniques with a practical design procedure for the prediction of daylight levels in atria", *Renewable Energy,* vol. 28, pp. 2157.

Tzempelikos, A. 2005, *A methodology for integrated daylighting and thermal analysis of buildings,* PhD. Thesis, Concordia University (Canada).

Tzempelikos, A. & Athienitis, A. 2007, "The impact of shading and control on building cooling and lighting demand", *Solar Energy,* vol. 81, pp. 369.

University of Illinois & Lawrence Berkeley National Laboratory 2008, *EnergyPlus engineering reference: The reference to EnergyPlus calculations,* U.S. Department of Energy.

University of Wisconsin 2006, A *TRaNsient Systems Simulation program.* Available: http://sel.me.wisc.edu/trnsys.htm [2009, 07/18]

Vartiainen, E. 2001, "Electricity benefits of daylighting and photovoltaics for various solar façade layouts in office buildings", *Energy and Buildings,* vol. 33, pp. 113.

Vartiainen, E. 2000, *Daylight modeling and optimization of solar façades,* PhD. Thesis, Helsinki University of Technology.

Vartiainen, E., Peippo, K. & Lund, P. 2000, "Daylight optimization of multifunctional solar façades", *Solar Energy,* vol. 68, no. 3, pp. 223.

Waldram, P. 1950, *A measuring diagram for daylight illumination,* Batsford Pub., London.

Wang, Y., Tian, W., Ren, J., Zhu, L. & Wang, Q. 2006, "Influence of a building's integrated-photovoltaics on heating and cooling loads", *Applied Energy,* vol. 83, pp. 989.

Ward, G.J. & Rubinstein, F.M. 1994, "A new technique for computer simulation of illuminated spaces", *Journal of the Illumination Engineering Society,* vol. 17, no. 1, pp. 777.

Whitaker, C.M., Wenger, H.J., Iliceto, A., Chimento, G. & Paletta, F. 1991, "Effects of irradiance and other factors on PV temperature coefficients", *Photovoltaic specialists conference, 22nd IEEE,* pp. 608.

Williams Engineering 2009, *Greenstone Building.* Available: http://www.williamsengineering.com/Project_Experience/view.php?ID=197 [2009, 06/12].

Wong, P.W., Shimoda, Y., Nonaka, M., Inoue, M. & Mizuno, M. 2008, "Semi-transparent PV: Thermal performance, power generation, daylight modelling and energy saving potential in a residential application", *Renewable Energy,* vol. 33, pp. 1024.

APPENDIX I

Select models used in numerical simulation

A- Solar Angles
B- Radiation Model
C- Transmittance, reflectance, and absorptance model

APPENDIX I A

Solar Angles

In order to calculate the radiation and illuminance incident on the inclined surface, several solar angles need to be defined.

Solar declination:

The solar declination (δ) is the angular distance of the sun north or south of the earth's equator and is based on the day of the year (n).

$$\delta = 23.45° \, sin\left[\frac{360}{365}(284 + n)\right] \tag{I.1}$$

Equation of time:

The equation of time (ET) converts clock time to solar time to compensate for the earth's axial tilt.

$$ET = 9.87 * sin\left[\frac{4\pi(n-81)}{364}\right] - 7.53 * cos\left[\frac{2\pi(n-81)}{364}\right] - 1.5 * sin\left[\frac{2\pi(n-81)}{364}\right] \tag{I.2}$$

Longitudinal time correction:

The longitudinal time zone correction (ΔT) corrects for the difference in the longitudinal location (Long) in the time zone compared to the standard time meridian (STM).

$$\Delta T = \frac{1hr}{15°}(STM - Long) \tag{I.3}$$

Apparent solar time:

Apparent solar time (AST) is the time describing the position of the sun relative to a specific location using the local time (t).

$$AST = t + ET + \Delta T \tag{I.4}$$

Hour angle:

The hour angle (H) describes the difference between the local solar time and solar noon.

$$H = \frac{15°}{hr}(AST - 12hr) \tag{I.5}$$

Solar altitude:

The solar altitude (α) is the angle of the sun the sky and is related to, among other things, the location's latitude (Lat).

$$sin \propto= (sinLat * sin\delta) + (cosLat * cos\delta * cosH) \quad (I.6)$$

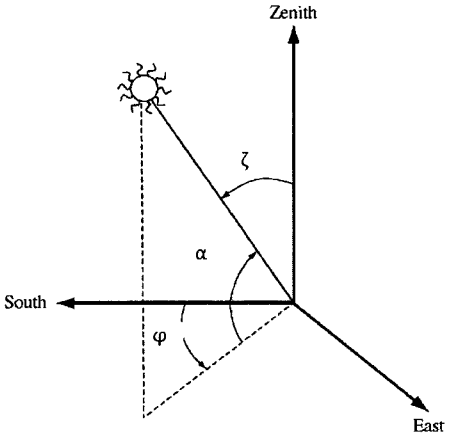

Figure I-1: Position of sun relative to fixed point on earth (Modified from (Luque, Hegedus 2003))

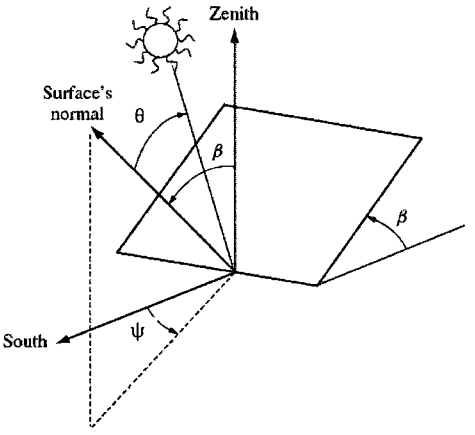

Figure I-2: Window surface position relative to sun (Modified from (Luque, Hegedus 2003))

Solar azimuth:

The solar azimuth (Φ) is the angle of the sun from due south.

$$cos\phi = \frac{(sin\alpha * sinLat) - sin\delta}{cos\alpha * cosLat} \quad (I.7)$$

Angle of incidence of sun on surface:

The angle of incidence of the sun on any surface (θ) is the angle between the sun and the surface with a tilt angle (β) and a surface azimuth (ψ) and a surface solar azimuth (γ).

$$cos\theta = \frac{(cos\alpha * cos|\gamma| * sin\beta) + (sin\alpha * cos\beta) + |(cos\alpha * cos\gamma * sin\beta) + (sin\alpha * cos\beta)|}{2} \quad (I.8)$$

Where $\gamma = \phi - \psi$

APPENDIX I B

Radiation model

The total solar radiation available incident on the surface is evaluated by adding the incident beam component, sky diffuse component and reflected component. The Perez all weather sky model (Perez et al. 1990) has been widely accepted as the most accurate model for treating diffuse radiation on an inclined surface. The model uses derived coefficients to control the horizon or zenith anisotropy which are calculated from horizon brightness, optical air mass, sky brightness and sky clearness. The beam normal (I_{bn}), diffuse horizontal (I_{dh}), beam horizontal radiation (I_{bh}) components as well as outdoor temperature (T_o), and dew point temperature (T_{dp}) are taken from a typical meteorological year (TMY2) derived from the 1961-90 National solar radiation database and converted by TRNSYS16 hourly weather observations.

Exterior radiation incident on inclined surface:

The total exterior radiation (I_t) incident on the surface is equal to the sum of the beam (I_b), diffuse (I_d) and ground reflected radiation (I_g).

$$I_t = I_b + I_d + I_g \tag{I.9}$$

The beam portion incident on the window (I_b) is a function of the angle of incidence of the sun on the window (θ) and the normal beam radiation (I_{bn}).

$$I_b = I_{bn} cos\theta \tag{I.10}$$

The diffuse radiation (I_d) on a tilted surface of angle (β) is estimated using the Perez all weather sky model (Perez et al. 1990) and uses derived coefficients F_1 and F_2- the circumsolar brightening coefficient and the horizon brightening coefficient.

$$I_d = I_{dh}\left[(1 - F_1)\left(\frac{1+cos\beta}{2}\right) + F_1\frac{a_p}{b_p} + F_2 sin\beta\right] \tag{I.11}$$

With the terms (a_p) and (b_p) defined as:

$$a_p = \max(0, cos\theta) \tag{I.12a}$$

$$b_p = \max(cos85°, sin\alpha) \tag{I.12b}$$

The circumsolar brightening coefficient (F_1) and the horizon brightening coefficient (F_2) are derived coefficients calculated from the derived irradiance coefficients relative air mass (m_{opt}), the sky brightness (Δ) and the sky clearness (ε).

$$F_1 = F_{11} + F_{12} * \Delta + F_{13}\frac{90°-\alpha}{180°} \tag{I.13}$$

$$F_2 = F_{21} + F_{22} * \Delta + F_{23}\frac{90°-\alpha}{180°} \tag{I.14}$$

$$m_{opt} = \frac{1}{sin\alpha + 0.15\left(\alpha\frac{\pi}{180°} + 3.885\right)^{-1.253}} \tag{I.15}$$

$$\Delta = m_{opt}\frac{I_{dh}}{I_{ex}} \tag{I.16}$$

$$\varepsilon = \frac{\frac{I_{dh}+I_{bn}}{I_{dh}} + 5.535*10^{-6}(90°-\alpha)^3}{1 + 5.535*10^{-6}(90°-\alpha)^3} \tag{I.17}$$

The ground reflected radiation (I_g) takes the portion of the horizontal diffuse (I_{dh}) and beam (I_{bh}) radiation which is reflected by the surrounding surfaces, or ground with an effective reflectance of (ρ_{grd}).

$$I_g = (I_{bh} + I_{dh})\rho_{grd}\left(\frac{1-cos\beta}{2}\right) \tag{I.18}$$

The ground reflectance is assumed to be 0.2 for no snow cover and 0.7 for ground snow cover (Liu & Jordan 1963).

Exterior illuminance incident on inclined surface:

The total exterior illuminance (E_t) incident on the surface is equal to the sum of the beam (E_b), diffuse (E_d) and ground reflected illuminance (E_g). The illuminance components are calculated using the Perez model (Perez et al. 1990) and the exterior radiation components.

$$E_t = E_b + E_d + E_g \tag{I.19}$$

The beam illuminance (E_b) incident on an inclined surface is calculated using the derived direct luminous efficacy coefficients (ab, bb, cb, db).

$$E_b = I_{bn}\left(ab + bb * WC + cb * e^{\left(5.73*(90°-\alpha)*\frac{\pi}{180°} - 5\right)} + db * \Delta\right) cos\theta \quad \text{(I.20)}$$

Where the precipitable water content (WC) is a function of the dew point temperature (T_{dp})

$$WC = e^{0.07T_{dp} - 0.075} \quad \text{(I.21)}$$

The diffuse illuminance (E_d) incident on an inclined surface is calculated the same way as the diffuse radiation.

$$E_d = E_{dh}\left[(1 - F_1)\left(\frac{1+cos\beta}{2}\right) + F_1\frac{a_p}{b_p} + F_2 sin\beta\right] \quad \text{(I.22)}$$

The horizontal diffuse illuminance (E_{dh}) is calculated similarly to the beam component but using diffuse luminous efficacy coefficients (ad, bd, cd, dd).

$$E_{dh} = I_{dh}(ad + bd * WC + cd * sin\alpha + dd * ln\,(\Delta + 10^{-10}) \quad \text{(I.23)}$$

The ground reflected illuminance (E_g) is calculated similarly to the ground reflected radiation.

$$E_g = (E_{bh} + E_{dh})\rho_{grd}\left(\frac{1-cos\beta}{2}\right) \quad \text{(I.24)}$$

APPENDIX I C

Transmittance, reflectance and absorptance model

For each layer, the visible and solar transmittance and reflectances are calculated for both beam and diffuse light. The beam components are calculated as a function of the angle of incidence of the sun on the surface (θ) while the diffuse components are assumed constant for all angles of incidence.

Single layer:

The transmittance, reflectance and absorption are functions of the incoming radiation, and the properties of the material- thickness (L), refractive index (ng) and extinction coefficient (k). The angle of refraction (θ') is calculated using Snell's law.

$$sin\theta' = \frac{sin\theta}{n_g} \tag{I.25}$$

The component reflectivity (r) is determined from the Fresnel expressions.

$$r = \frac{1}{2}\left[\left(\frac{\sin(\theta-\theta')}{\sin(\theta+\theta')}\right)^2 + \left(\frac{\tan(\theta-\theta')}{\tan(\theta+\theta')}\right)^2\right] \tag{I.26}$$

The fraction after attenuation (a):

$$a = e^{\left(-\frac{kL}{\sqrt{1-\left(\frac{sin\theta}{n_g}\right)^2}}\right)} \tag{I.27}$$

For each layer, the transmittances, reflectances and absorption (τ_{single}, ρ_{single}, α_{single}) will be calculated for both beam and diffuse components. These equations can equally be used for both solar and visible transmittances and reflectances.

$$\tau_{single} = \frac{(1-r^2)*a}{1-r^2-a^2} \tag{I.28}$$

$$\rho_{single} = r + \frac{r*(1-r^2)*a^2}{1-r^2-a^2} \tag{I.29}$$

$$\alpha_{single} = 1 - \tau_{single} - \rho_{single} \tag{I.30}$$

Multiple layers:

To calculate the effective transmittances through multiple glazing layers, Fresnel derived expressions are used which include both a parallel and perpendicular reflection component of radiation from one layer to the next.

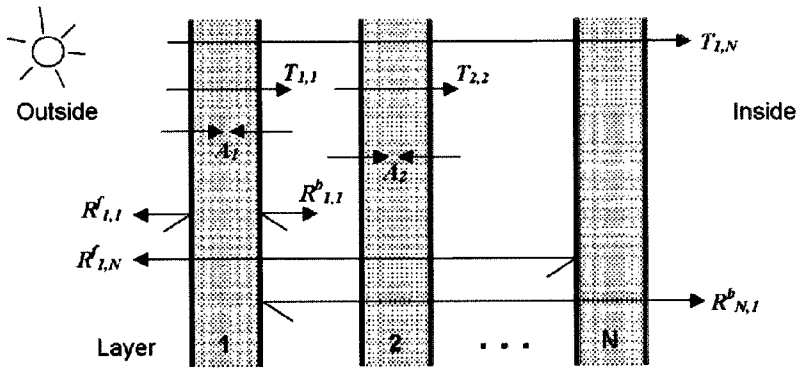

Figure I-3: Transmittance, reflectance and absorptance of radiation or illuminance within a multi-layer glazing system (University of Illinois & Lawrence Berkeley National Laboratory 2008)

The effective transmittance ($\tau_{i,j}$) is the transmittance through all layers of a multi-layer system from layers i to j is calculated using the effective reflectances of each layer.

$$\tau_{i,j} = \frac{\tau_{i,j-1} * \tau_{j,j}}{1-\rho_{j,j}{}^{f} * \rho_{j-1,i}{}^{b}} \tag{I.31}$$

The effective front reflectance is the reflectance ($\rho_{ij}{}^{f}$) from layers i to j and the effective back reflectance ($\rho_{ij}{}^{b}$) is the reflectance from layer j to i. For our window system $\rho_{ij}{}^{f}$ is the effective reflectance of the entire window system facing the exterior and $\rho_{ji}{}^{b}$ is facing into the room. Layer 1 is the outermost layer and layer N is the innermost layer. The effective front absorption ($\alpha_{j}{}^{f}$) is the absorption of j after having passed through the other layers.

$$\rho_{i,j}{}^{f} = \rho_{i,j-1}{}^{f} + \frac{(\tau_{i,j-1})^{2} * \rho_{j,j}{}^{f}}{1-\rho_{j,j}{}^{f} * \rho_{j-1,i}{}^{b}} \tag{I.32a}$$

$$\rho_{j,i}{}^{b} = \rho_{j,j}{}^{b} + \frac{(\tau_{j,j})^{2} * \rho_{j-1,i}{}^{b}}{1-\rho_{j-1,i}{}^{b} * \rho_{j,j}{}^{f}} \tag{I.32b}$$

$$\alpha_{j}{}^{f} = \frac{\tau_{1,j-1}(1-\tau_{j,j}-\rho_{j,j}{}^{f})}{1-\rho_{j,n}{}^{f} * \rho_{j-1,1}{}^{b}} + \frac{\tau_{1,j} * \rho_{j+1,n}{}^{f}(1-\tau_{j,j}-\rho_{j,j}{}^{f})}{1-\rho_{j,n}{}^{f} * \rho_{j-1,1}{}^{b}} \tag{I.33}$$

APPENDIX II

Simulation and window prototype inputs

A- Inputs used in simulation
B- Inputs for experimental verification using the window prototype

APPENDIX II A

Inputs used in simulation model

Daylighting model

Table II-1: Location information for cities used in the simulation model

Location	Montreal	St. John's	Iqaluit	Toronto	Vancouver	Ref.
Latitude	45°	47°	63°	43°	49°	
Longitude	74°	52°	68°	79°	123°	
Standard time meridian	75°	52.5°	75°	75°	120°	
Days with snow cover (ρ_{grd}=0.7)	1≤n≤90	1≤n≤90 335≤n≤365	1≤n≤90 274≤n≤365	1≤n≤59	-	1, 2

1. Liu, Jordan (1963)'s estimate of average ground reflectance is still widely used with the assumption that the reflectance is 0.2 when there is less than 2.5cm of snow on the ground and 0.7 otherwise (Thevenard, Haddad 2006).
2. (Environment Canada 2008) was used to determine the months in which there was historically at least 2.5cm of snow on the ground.

Table II-2: Small private office dimensions and properties. The room was based on an existing small private office in the EV building at Concordia University. Figure II-1 shows short forms used for dimension names.

Small private office			Reference
Height of room	HT	4m	
Length of room	LT	4m	
Width of room	WT	3m	
Height of window viewing section	HTV	1.5m	
Height of STPV section	HTPV	1.5m	
Height of spandrel below window	HTBOT	0.8m	
Width of window	WTW	2.8m	
Width of non-window section to left of window	WTL	0.1m	
Distance of workplane point from window	DW	2.0m	
Height of workplane point	WPH	0.8m	
Distance of workplane point to left wall	WPL	1.5m	
Distance of luminaires from ceiling	$h_{ceiling}$	0.2m	
Desired workplane illuminance	$E_{desired}$	400lx	1
Reflectance of walls	ρ_3 , ρ_6, ρ_7, ρ_8	0.6	2
Reflectance of floor	ρ_4	0.2	2
Reflectance of ceiling	ρ_5	0.8	2

1. A workplane illuminance of 400lx was chosen as a balance between the recommended illuminance for common visual tasks and below the maximum for use with video display terminals (VDT) (IESNA 2000)
2. IESNA (2000) gives recommended reflectance values for office surfaces.

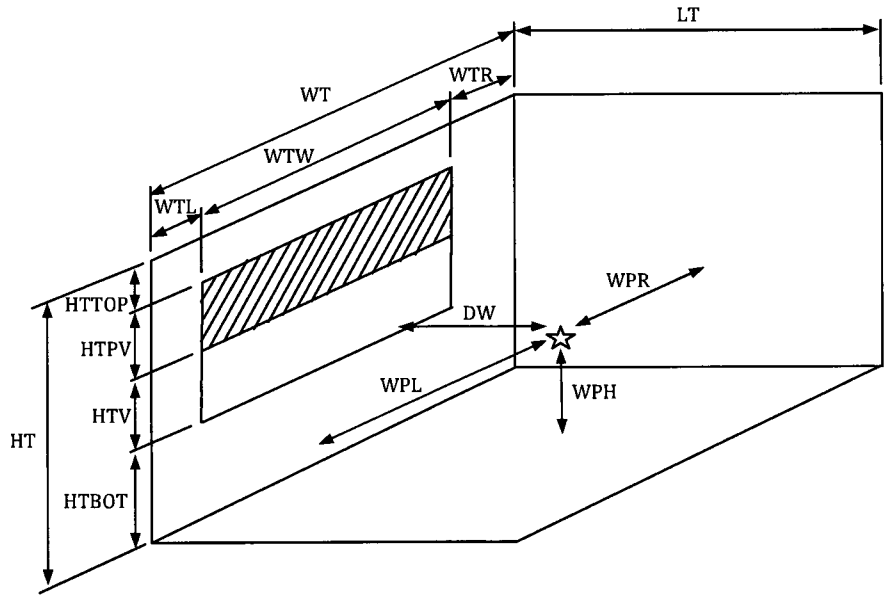

Figure II-1: Dimension short forms used in simulation model

Table II -3: Window visible properties used in simulation model

Window visible properties				Ref.
Front glazing	Thickness	L_{g1}	6mm	1
	Extinction coefficient	k_{g1}	26/m	1
	Index of refraction	n_{g_g1}	1.526	1
EVA	Thickness	L_{EVA}	0.5mm	2
	Extinction coefficient	k_{EVA}	25/m	2
	Index of refraction	n_{g_EVA}	1.45	2
Back Glazing	Thickness	L_{g2}	6mm	1
	Extinction coefficient	k_{g2}	6/m	1
	Index of refraction	n_{g_g2}	1.526	1
Blind	Transmittance	τ_{blind}	5%	3

1. Chow et al. (2007) used two extinction coefficients for normal window glass and low iron glass and the same values were used here.
2. These values were used in Krauter (2006).
3. Tzempelikos, Athienitis (2007) suggested that even though a blind transmittance of 20% satisfied daylighting and cooling requirements, that it would create glare problems and a blind transmittance of 5% would be more appropriate. Furthermore they suggested in a three-section façade to use a lower transmittance in the middle section and higher transmittance in the upper section with an average approaching 20%.

Inputs to artificial lighting model

Table II-4: The lamp used in the artificial lighting model for the simulations

Sylvania F032W/31K 830 -Warm white deluxe 3 lamp 32-W, T-8 rapid-start fluorescent system with electronic ballast			Ref.
Lamp Watts	P_{tube}	32W	1
Initial lumens	Lm_{tube}	2900lm	1
Minimum fractional electrical lighting power input when using dimmers	f_{P_min}	0.08	2
Minimum fractional electrical lighting power output when using dimmers	f_{L_min}	0.01	2
Efficiency	EFF	0.727	2
Lighting loss factor	LLF	0.8	2
Special allowance factor	F_{sa}	0.97***	3

1. A Sylvania F032W/ 31K 830 Warm white deluxe 3 lamp 32-W, T-8 rapid-start fluorescent system with electronic ballast was chosen for the simulation (Sylvania 2007)
2. IESNA (2000) gives values for the fractional power input and output for the lamp used.
3. The special allowance factor for this type of lamp was taken from ASHRAE (2001).

Inputs to PV model

Table II -5: The PV module used in the simulations

Centennial Solar transparent crystalline solar module- CS140VG (based on CS 140)			Ref.
Rated power	P_{MPP}	140W	1
Voltage at maximum power	V_{MPP}	17.89V	1
Current at maximum power	I_{MPP}	7.82A	1
Open circuit voltage	V_{OC}	22.01V	1
Short circuit current	I_{SC}	8.37A	1
Module efficiency	η	14.11%	1
Nominal operating cell temperature	NOCT	45°C	1
Power temperature coefficient	η_{power_temp}	-.43%/°K	1

1. The PV module used was a Centennial Solar transparent crystalline module CS140VG (Centennial Solar 2004).

APPENDIX II B

Inputs for experimental verification using the window prototype

Daylighting model

Table II-6: Dimensions and properties of room used in experimental verification

Small private office			Ref.
Height of room	HT	2.3m	
Length of room	LT	2.95m	
Width of room	WT	3.25m	
Height of window viewing section	HTV	0.42m	
Height of STPV section	HTPV	0.52m	
Height of spandrel below window	HTBOT	1.0m	
Width of window	WTW	2.4m	
Width of non-window section to left of window	WTL	0.2m	
Width of non-window section to right of window	WTR	0.65m	
Distance of workplane point from window	DW	0.25-2.75m	
Height of workplane point	WPH	0.8m	
Distance of workplane point to left wall	WPL	0.55m/1.625m/ 2.175m	
Reflectance of walls	ρ_3 , ρ_6, ρ_7, ρ_8	0.86	
Reflectance of floor	ρ_4	0.28	
Reflectance of ceiling	ρ_5	0.85	

Window visible and solar properties- See Appendix III.

Table II-7: Thermal properties of window used in experimental verification

Window thermal properties				Ref.
Front glazing	Thickness	t_{g1}	6mm	
	Thermal conductivity	k_{g1}	0.78 (W/m*K)	1
	Emissivity-facing into cavity	ε_{g1}	0.9	
EVA	Thickness	t_{EVA}	2mm	2
	Thermal conductivity	k_{EVA}	0.116 (W/m*K)	1
PV	Thickness	t_{PV}	0.1mm	2
	Thermal conductivity	k_{PV}	168 (W/m*K)	1
Back Glazing	Thickness	t_{g2}	6mm	
	Thermal conductivity	k_{g2}	0.78 (W/m*K)	1
	Emissivity- facing into cavity	ε_{g2}	0.1	

1. Wong et al. (2008)
2. Approximated from verbal communication with Sam Myles, Centennial Solar

PV model

See section 5.6.2

APPENDIX III

Transmittance of window prototype

A- Diffuse transmittance of individual layers

B- Direct transmittance of individual layers

C- Diffuse and direct transmittance of entire window

D- Solar absorptance of individual layers

APPENDIX III A

Diffuse transmittance of individual layers

The diffuse transmittance of the individual layers are measured values. See section 5.4.1 for description of measurement method and tabular results. There are several limitations of these measurements, the most notable being that the measurements were taken indoors and thus the solar radiation was already spectrally modified before reaching the glazings and the are possible reflections from the façade behind which we were taking the measurements.

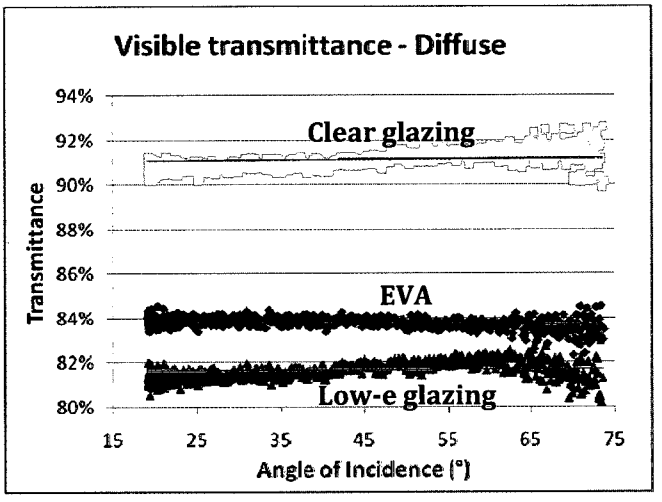

Figure III-1: Visible transmittance of each individual layer-overcast day (Jan.7 2009).

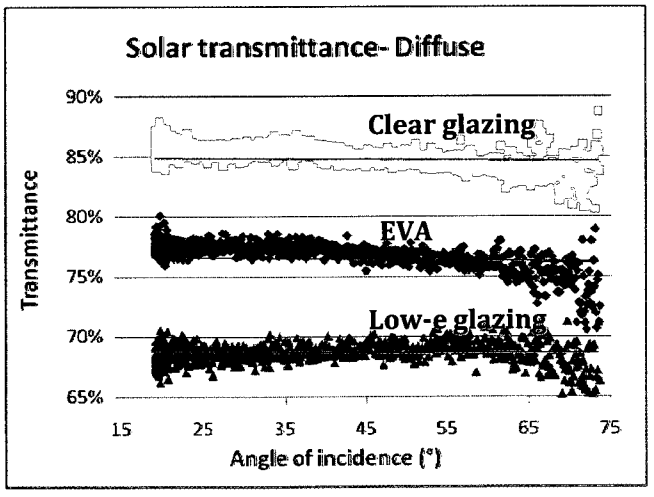

Figure III-2: Solar transmittance of each individual layer- overcast (Jan.7 2009)

APPENDIX III B

Direct transmittance of individual layers

The direct transmittance of the individual layers are approximated using measured results from overcast and clear days. See section 5.4.1 for description of measurement method and tabular results. Again, these measurements were taken indoors. The direct transmittance is the transmittance on the clear day, with the diffuse portion removed.

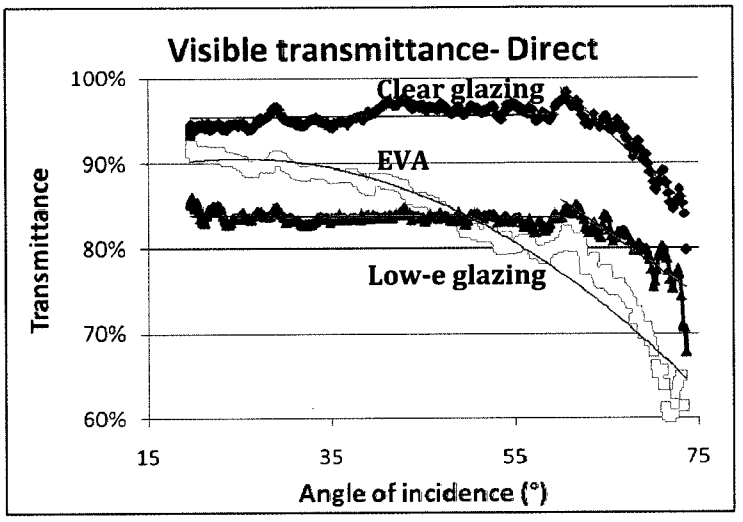

Figure III-3: Visible transmittance of each individual layer- direct. Total transmittance from clear day (Jan 10 2009) less diffuse transmittance from overcast day (Jan.7 2009)

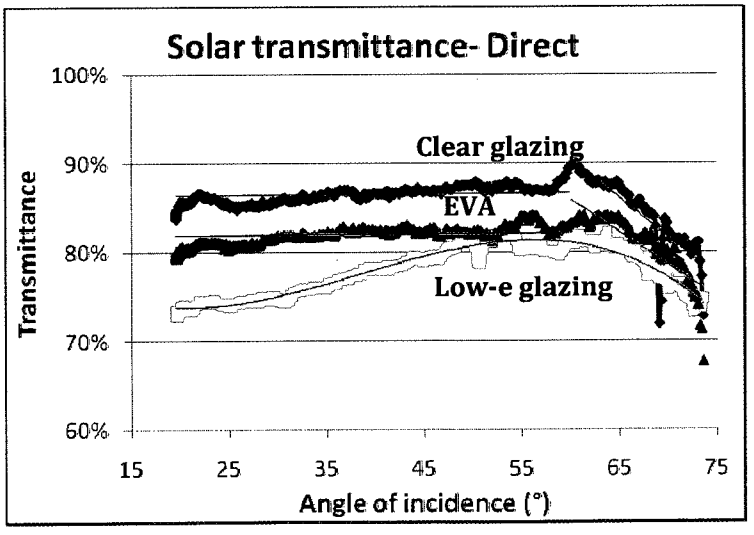

Figure III- 4: Solar transmittance of each individual layer- direct. Total transmittance from clear day (Jan 10 2009) less diffuse transmittance from overcast day (Jan.7 2009)

APPENDIX III C

Diffuse and direct transmittance of entire window

The direct transmittance of entire window is calculated using the Fresnel equations and an estimate of the index of refraction and extinction coefficient of the individual layers. These estimates were chosen as they most closely matched the transmittance as a function of angle of incidence curves. The diffuse transmittance is taken from the entire direct window calculations at angle of 60 degrees. See section 5.4.2 for description of measurement method and tabular results. Note that this is a combination of measured values for the single glazing transmittances and calculated values using the Fresnel equations for the double glazing transmittances.

There are several limitations as can be seen from the results. Measured values of the entire glazing system were taken but not used due to inconsistencies in the results. The installed window is shaded by buildings and trees, and the EVA is shaded by the cells themselves. Thus the extinction coefficient and refractive index were estimated for each layer and the Fresnel equations employed to get an overall effective transmittance. However, these equations are not very accurate for an advanced multi-layer glazing system and other means should have been used. This was however out of the scope of the project but should be taken into consideration for all future work..

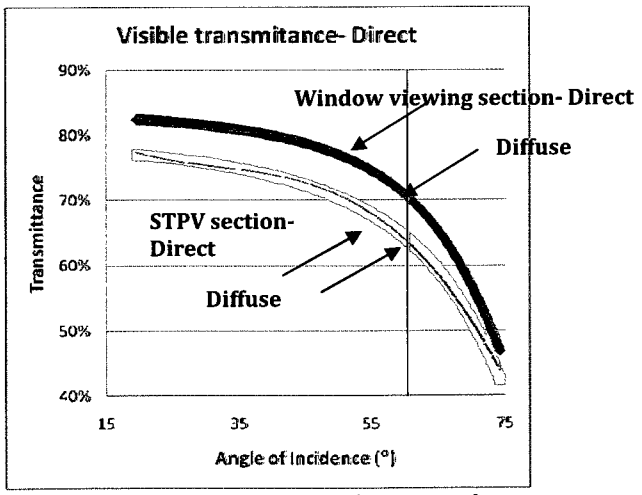

Figure III-5: Visible transmittance of entire window

Table III-1: Estimated visible properties of individual layers used in Fresnel calculations for entire window transmittances

Estimated visible properties	Front glazing	EVA + front glazing	Back glazing
Extinction coefficient	5	15.4	21.7
Index of refraction	1.15	1.1	1.3

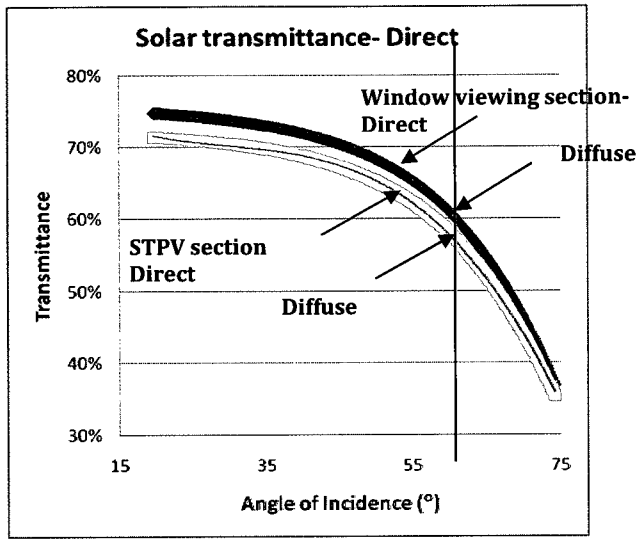

Figure III-6: Solar transmittance of entire window

Table III-2: Estimated visible properties of individual layers used in Fresnel calculations for entire window transmittances

Estimated solar properties	Front glazing	EVA + front glazing	Back glazing
Extinction coefficient	13.3	7.7	21.7
Index of refraction	1.4	1.7	1.2

APPENDIX III D

Solar absorption of individual layers of entire window

The solar absorptances of each individual layer were calculated for the 3 separate sections of the window- the window viewing section, and both the PV and EVA in the STPV section. These were calculated using the Fresnel equations and the calculated transmittances.

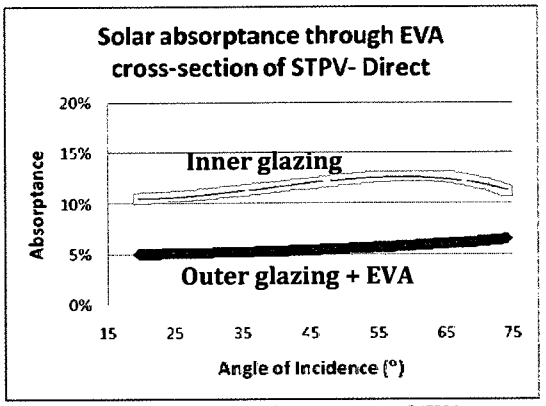

Figure III-7: Direct solar absorptance of EVA+ outer glazing and inner glazing in the EVA cross section of STPV

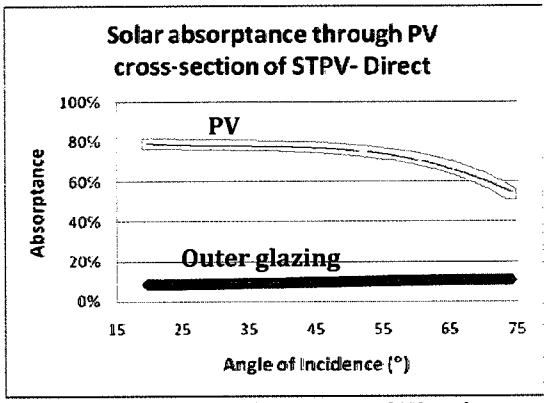

Figure III-8: Direct solar absorptance of PV and outer glazing in the PV cross section of STPV

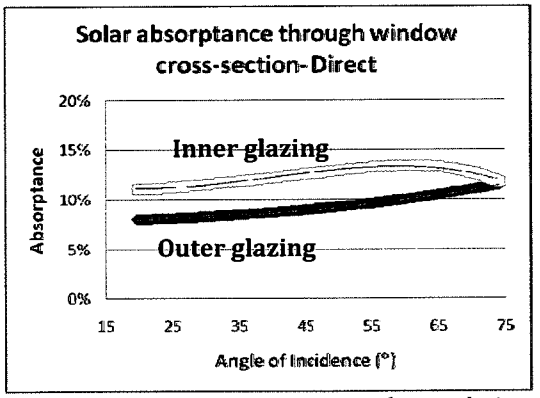

Figure III-9: Direct solar absorptance of outer glazing and inner glazing in the EVA cross section of the window viewing section

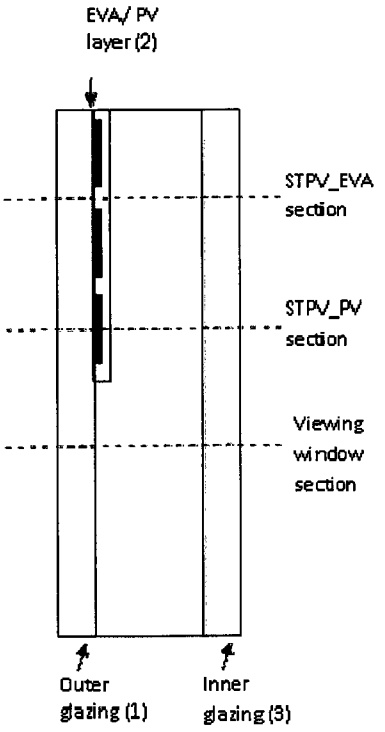

APPENDIX IV

Temperature distribution in window prototype

A- Infrared camera results
B- Thermocouple placement in window layers
C- Channel organisation in data acquisition system and VEE program

APPENDIX IV A

Infrared camera results

Infrared photos were taken of the temperature distribution of the inner glazing using a ThermaCAM S60 infrared camera (Flir Systems) on both an overcast (May 14, 2009) and a clear day (May 13, 2009). As there are no thermocouples behind the EVA, the interest of these photos was to give an idea of the temperatures of the EVA between the PV cells. It was also to verify the estimates of differences in temperature between the STPV and viewing sections.

Overcast day

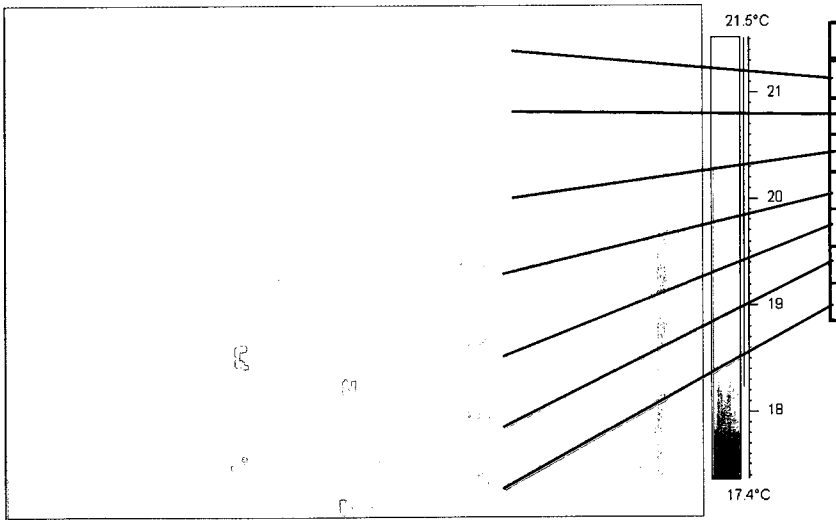

Figure IV-1: Infrared photo of West window on overcast day (May 14, 2009) at solar noon (13:00). Note- figure in center is reflection of photographer

Point	Temp	
SP01	19.3°C	EVA
SP02	19.2°C	PV
SP03	19.0°C	PV
SP04	18.9°C	EVA
SP05	18.8°C	View
SP06	18.7°C	View
SP07	18.6°C	View

Table IV-1: Temperatures taken with infrared camera- overcast day

Clear day

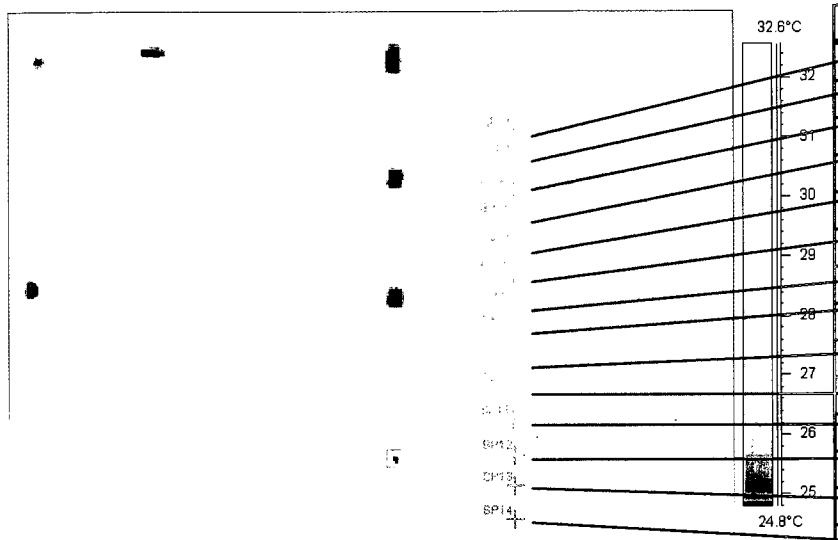

Point	Temp	
SP01	27.2°C	PV
SP02	27.4°C	EVA
SP03	27.0°C	PV
SP04	27.2°C	EVA
SP05	26.7°C	PV
SP06	27.0°C	EVA
SP07	26.9°C	PV
SP08	27.1°C	EVA
SP09	27.2°C	PV
SP10	28.3°C	EVA
SP11	29.7°C	View
SP12	30.4°C	View
SP13	30.6°C	View
SP14	31.0°C	View

Figure IV-2: Infrared photo of window on clear day (May 13, 2009) at solar noon (13:00). Note figure in center is reflection of photographer.

Table IV-2: Temperatures taken with infrared camera-clear day

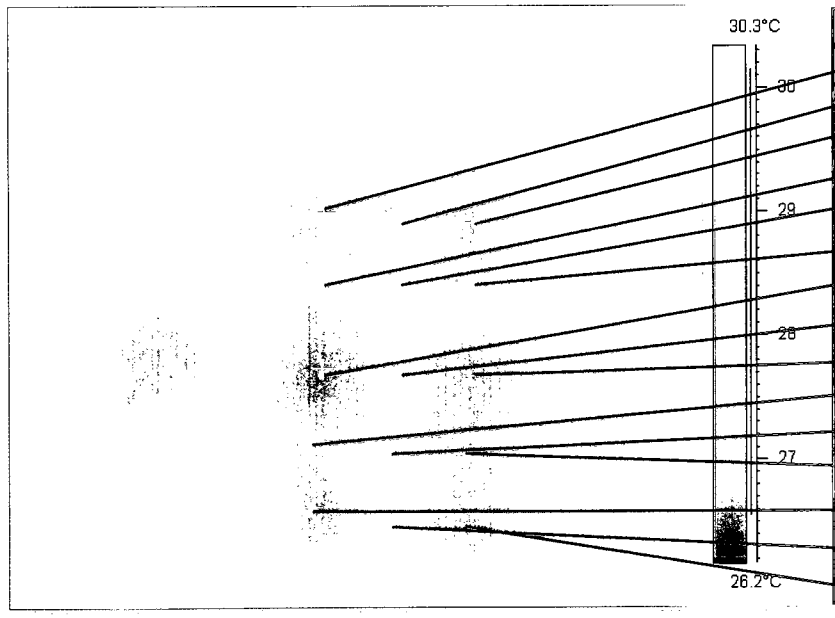

Point	Temp	
SP01	27.0°C	PV
SP06	27.5°C	EVA
SP11	26.9°C	PV
SP02	27.1°C	EVA
SP07	27.5°C	EVA
SP12	27.1°C	EVA
SP03	26.8°C	PV
SP08	27.3°C	EVA
SP13	26.5°C	PV
SP04	27.0°C	EVA
SP09	27.3°C	EVA
SP14	26.9°C	EVA
SP05	26.9°C	PV
SP10	27.4°C	EVA
SP15	26.8°C	PV

Figure IV-3: Close-up infrared photo of PV cells and EVA of on clear day (May 13, 2009) at solar noon (13:00). Note- figure in center is reflection of photographer.

Table IV-3: Temperatures taken with infrared camera-clear day-close up

APPENDIX IV B

Thermocouple placement in window

Thermocouples on exterior of exterior glazing (g1), room and outdoor

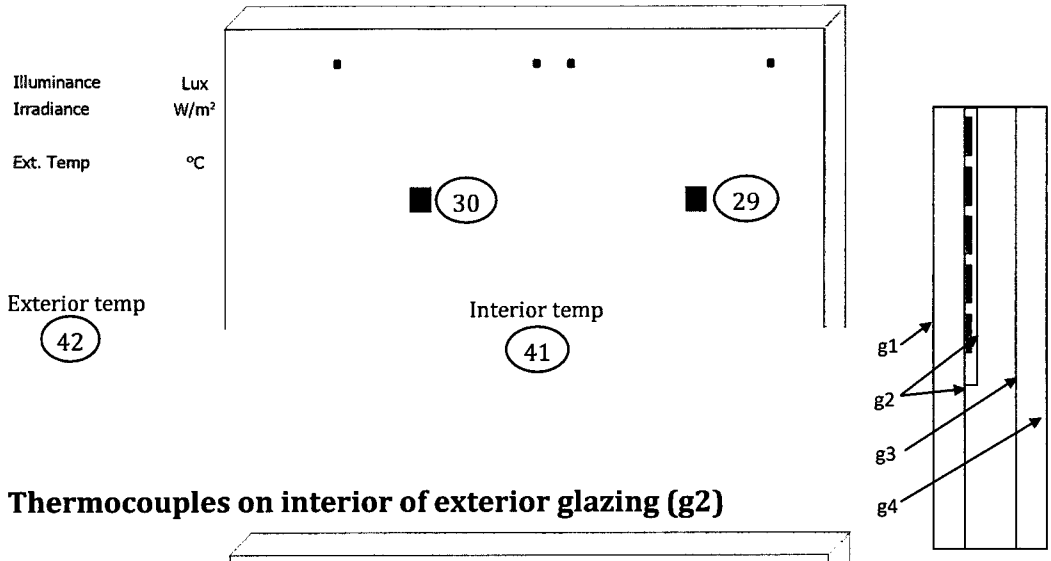

Thermocouples on interior of exterior glazing (g2)

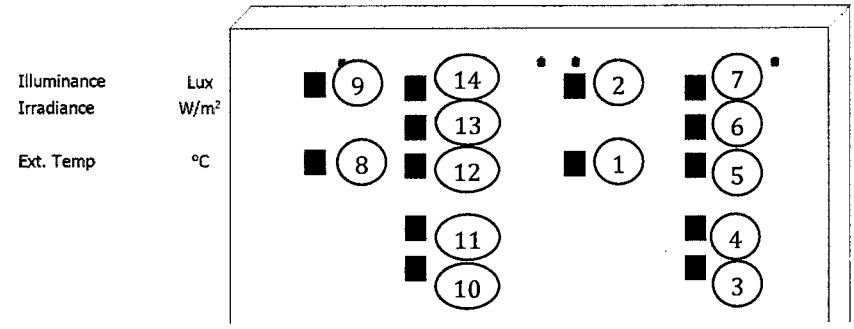

Thermocouples exterior of interior glazing (g3)

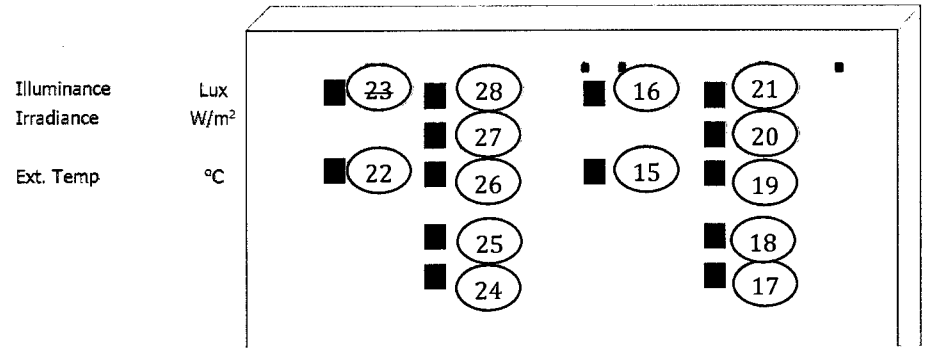

Thermocouples on interior of interior glazing (g4)

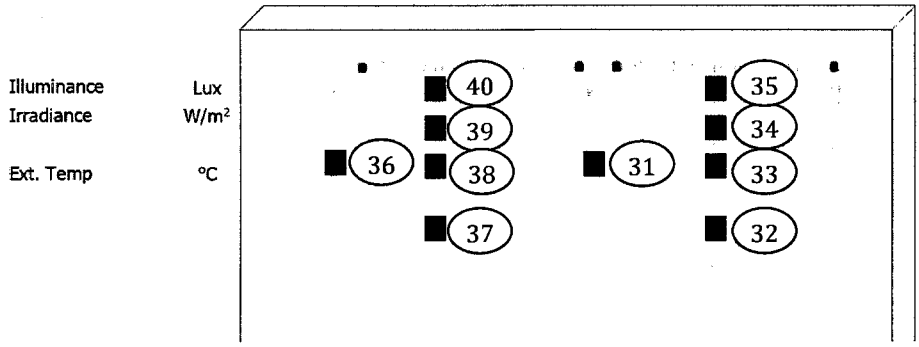

Interior workplane photometers, reference photometers/ pyranometers, PV output

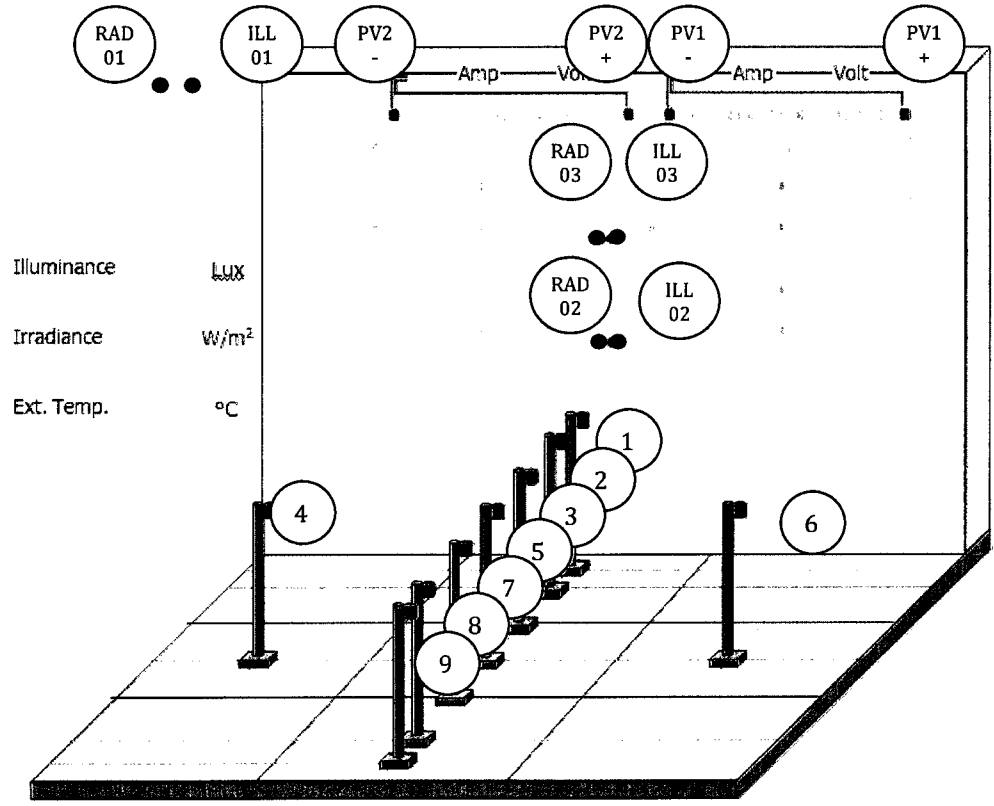

APPENDIX IV C

Channel organisation in data acquisition system and VEE program

PV outputs

File column file	# in Appendix IV B	Channel	VEE
PV1_PV_voltage_Imp	PV1	217	B0
PV2_PV_voltage_Imp	PV2	218	B1
PV1_PV_voltage_Vmp	PV1	219	B2
PV2_PV_voltage_Vmp	PV2	220	B3

Reference photometers/ pyranometers

File column name	# in Appendix IV B	Channel	VEE
RefRd1_ext_rad_ext	ILL01	301	B4
RefRd2_int_rad_clr	RAD01	302	B5
RefRd3_int_rad_EVA	ILL02	303	B6
Refll1_ext_ill_ext	RAD02	304	B7
Refll2_int_ill_clr	ILL03	305	B8
Refll3_int_ill_EVA	RAD03	306	B9

Interior workplane photometers

File column name	# in Appendix IV B	Channel	VEE
P01_wkpl_frnt_left	1	307	B10
P02_wkpl_frnt_midl	2	308	B11
P03_wkpl_frnt_rght	3	309	B12
P04_wkpl_cntr_left	4	310	B13
P05_wkpl_cntr_midl	5	311	B14
P06_wkpl_cntr_rght	6	312	B15
P07_wkpl_back_left	7	313	B16
P08_wkpl_back_midl	8	314	B17
P09_wkpl_back_rght	9	315	B18

Thermocouples on exterior of exterior glazing (g1), room, outdoor

File column name	# in Appendix IV B	Channel	VEE
T29_g1_pv1_cen_b/m	29	316	C0
T30_g1_pv2_cen_b/m	30	317	C1
T41_center_of_room	41	318	C2
T42_exterior_tempe	42	319	C3

Thermocouples on interior of exterior glazing (g2)

File column name	# in Appendix IV B	Channel	VEE
T01_g2_pv1_edg_bot	1	101	A0
T02_g2_pv1_edg_top	2	102	A1
T03_g2_pv1_cen_bot	3	103	A2
T04_g2_pv1_cen_b/m	4	104	A3
T05_g2_pv1_cen_mid	5	105	A4
T06_g2_pv1_cen_m/t	6	106	A5
T07_g2_pv1_cen_top	7	107	A6
T08_g2_pv2_edg_bot	8	108	A7
T09_g2_pv2_edg_bot	9	109	A8
T10_g2_pv2_cen_bot	10	110	A9
T11_g2_pv2_cen_b/m	11	111	A10
T12_g2_pv2_cen_mid	12	112	A11
T13_g2_pv2_cen_m/t	13	113	A12
T14_g2_pv2_cen_top	14	114	A13

Thermocouples exterior of interior glazing (g3)

File column name	# in Appendix IV B	Channel	VEE
T15_g3_pv1_edg_bot	15	115	A14
T16_g3_pv1_edg_top	16	116	A15
T17_g3_pv1_cen_bot	17	117	A16
T18_g3_pv1_cen_b/m	18	118	A17
T19_g3_pv1_cen_mid	19	119	A18
T20_g3_pv1_cen_m/t	20	120	A19
T21_g3_pv1_cen_top	21	201	A20
T22_g3_pv2_edg_bot	22	202	A21
~~T23_g3_pv2_edg_top~~	~~23~~		
T24_g3_pv2_cen_bot	24	204	A23
T25_g3_pv2_cen_b/m	25	205	A24
T26_g3_pv2_cen_mid	26	206	A25
T27_g3_pv2_cen_m/t	27	207	A26
T28_g3_pv2_cen_top	28	208	A27

Thermocouples on interior of interior glazing (g4)

	# in Appendix IV B	Channel	VEE
T31_g4_pv1_edg_bot	31	209	A28
T32_g4_pv1_cen_b/m	32	210	A29
T33_g4_pv1_cen_mid	33	211	A30
T34_g4_pv1_cen_m/t	34	212	A31
T35_g4_pv1_cen_top	35	213	A32
T36_g4_pv2_edg_bot	36	214	A33
T37_g4_pv2_cen_b/m	37	215	A34
T38_g4_pv2_cen_mid	38	216	A35
T39_g4_pv2_cen_m/t	39	203	A22
T40_g4_pv2_cen_top	40	320	C4

Notes

Symbols	
PV1	PV panel with uniform cells –on the right side (West)
PV2	PV panel with different cells –on the left side (East)
g1	Glazing side 1- exterior of exterior glazing
g2	Glazing side 2- interior of exterior glazing
g3	Glazing side 3- exterior of interior glazing
g4	Glazing side 4- interior of interior glazing
edg	Horizontal placement of thermocouples - placed closest to the frame edge
cen	Horizontal placement of thermocouples - placed in center of glazing (farthest from frame)
bot	Vertical placement of thermocouples – placed closest to bottom frame
b/m	Vertical placement of thermocouples – placed between bottom and middle
mid	Vertical placement of thermocouples – placed in middle
m/t	Vertical placement of thermocouples – placed between middle and top
top	Vertical placement of thermocouples – placed closest to top frame

APPENDIX V

Design day conditions

APPENDIX V

Design day conditions

All data is taken from the typical meteorological year (TMY2) data and used for the design day calculations. See section 3.6 for more information.

Feb. 8 (Cold, overcast)

Beam horizontal radiation:

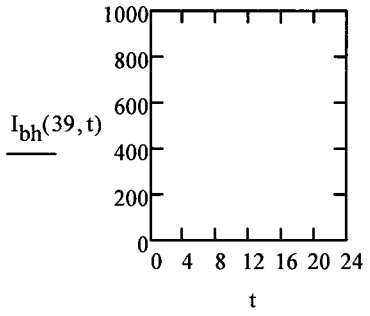

Diffuse horizontal radiation:

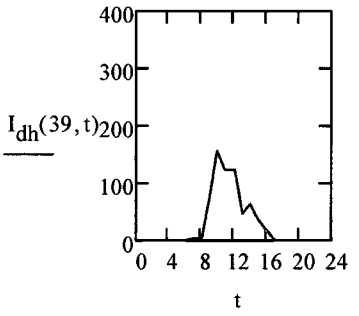

Outdoor temperature:

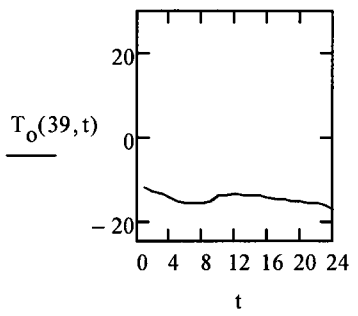

Radiation incident on surface:

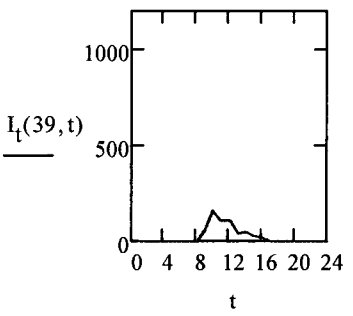

Illuminance incident on surface:

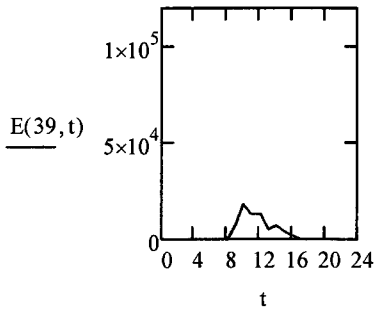

Illuminance inside viewing section:

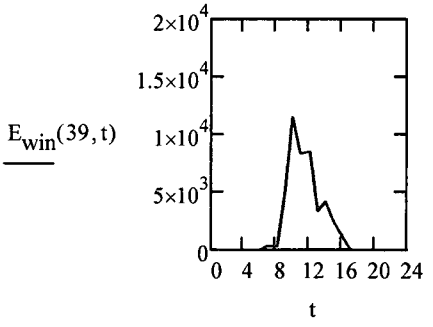

Feb. 12 (Cold, clear)

Beam horizontal radiation:

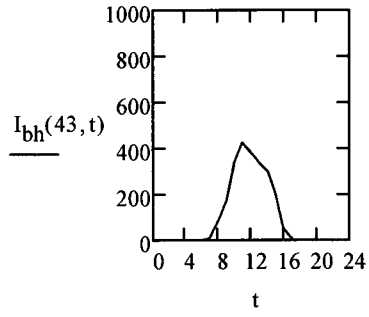

Diffuse horizontal radiation:

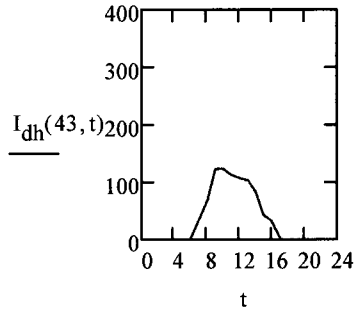

Outdoor temperature:

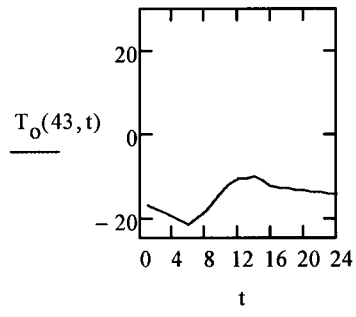

Radiation incident on surface:

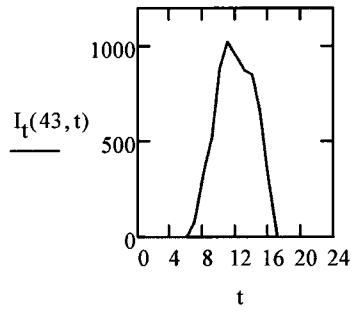

Illuminance incident on surface:

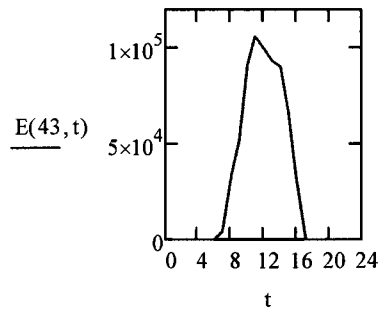

Illuminance inside window viewing surface:

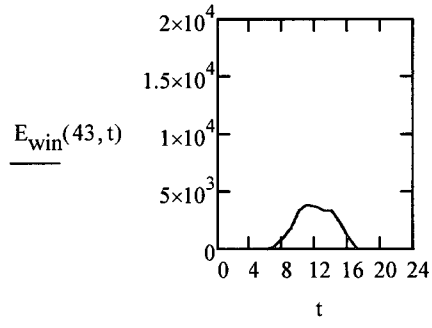

Jun. 28 (Warm, overcast)

Beam horizontal radiation:

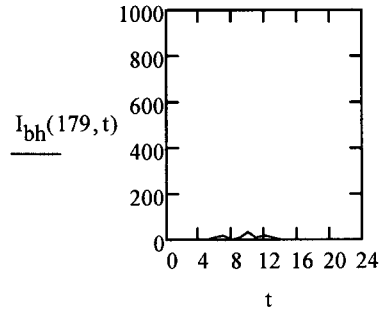

Diffuse horizontal radiation:

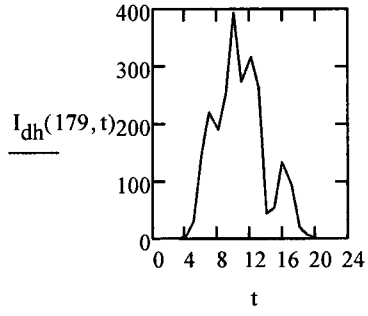

Outdoor temperature:

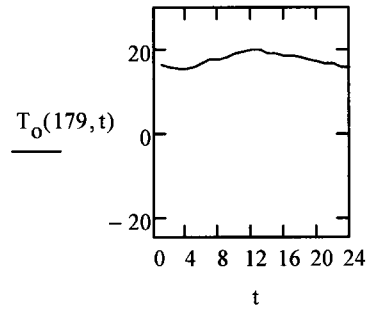

Radiation incident on surface:

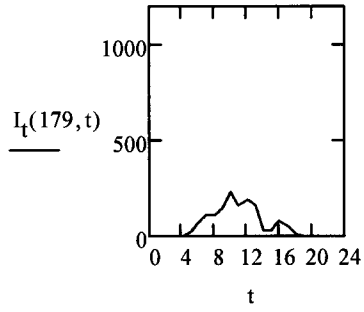

Illuminance incident on surface:

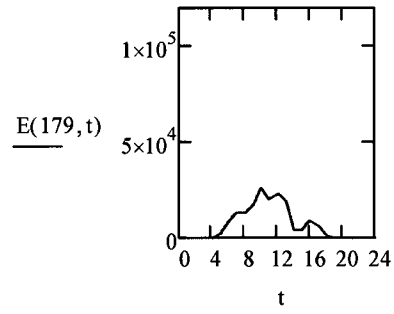

Illuminance inside window viewing surface:

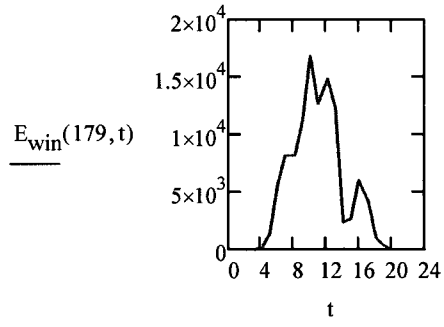

Jun. 30 (Warm, clear)

Beam horizontal radiation:

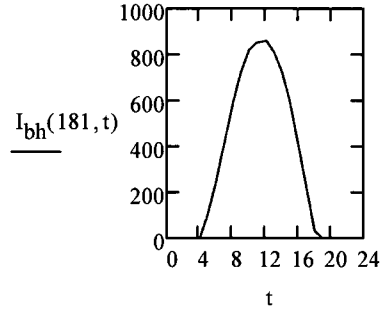

Diffuse horizontal radiation:

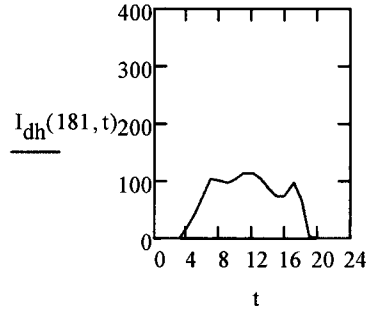

Outdoor temperature:

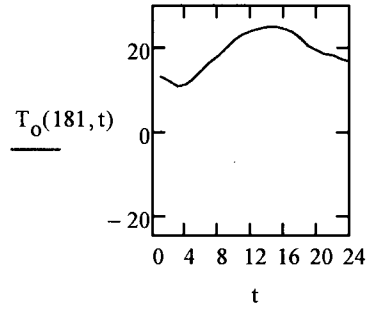

Radiation incident on surface:

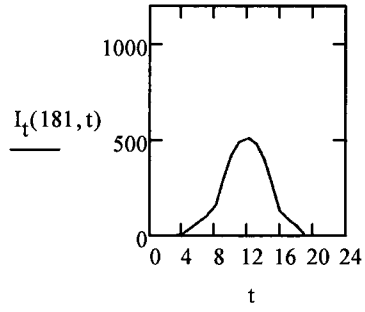

Illuminance incident on surface:

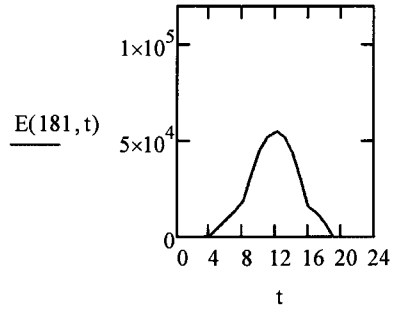

Illuminance inside window viewing surface:

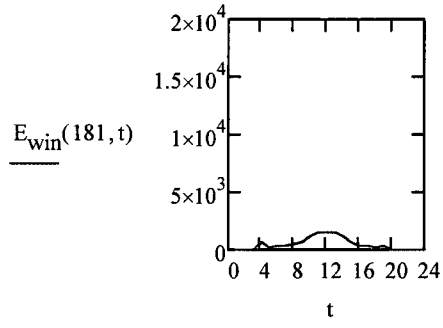

APPENDIX VI

MathCAD simulation model

A- Model inputs
B- Weather data
C- Solar geometry
D- Exterior solar radiation incident on inclined surface
E- Exterior illuminance incident on inclined surface
F- Visible transmittance of glazings
G- View factors
H- Configuration factors
I- Workplane illuminance
J- Artificial lighting load
K- PV power output

APPENDIX VI A

Inputs:

Time information:

Day to evaluate:

$n := 1, 2.. 365$

Time to evaluate :

$t := 1, 2.. 24$

Office hours (time lights on):

$t_{oh} := 8.. 17$

Location information:

Latitude:

$Lat := 45 \cdot deg$

Longitude:

$Long := 74 \cdot deg$

Standard time meridien:

$STM := 75 \cdot deg$

Ground reflectance:

$$\rho_{grd}(n) := \begin{cases} 0.7 & \text{if } 1 \le n < 90 \\ 0.2 & \text{otherwise} \end{cases}$$

Rho=0.7 for snow cover, 0.2 for no snow

Window information:

Surface azimuth

$\psi := 0 \cdot deg$ 0deg = South, West of S would be +ve, East would be -ve

$\beta := 90 \cdot deg$ Tilt angle. 90deg = vertical, 0deg = horizontal

PV information:

$\eta_{STC} := 0.141$ Efficiency of PV at standard test conditions

$A_{PV} := 0, 0.1.. 1$ Area ratio of PV cells in upper STPV section

$\rho_{PV\_back} := 0.9$ The reflectance of the back side of the PV cells

$\eta_{power\_temp} := -.004$ Power temperature coefficient

$NOCT := 46$ Nominal operating cell temperature

Room information:

$HT := 4 \cdot m$	Height of room
$LT := 4 \cdot m$	Length of room
$WT := 3 \cdot m$	Width of room
$HTV := 1.5 \cdot m$	Window height of viewing section
$HTPV := 1.5 \cdot m$	Window height of PV section
$HTBOT := 0.8 \cdot m$	Opaque section below window
$HTTOP := 0.2 \cdot m$	Opaque section above window
$WTW := 2.8 \cdot m$	Width of the window
$WTR := .1 \cdot m$	Width of opaque to right of window
$WTL := .1 \cdot m$	Width of opaque to left of window
$DW := \frac{LT}{2} = 2\,m$	Distance of workplane point from window
$WPH := 0.8 \cdot m$	Workplane height
$WPL := \frac{WT}{2}$	Distance from workplane point to left wall
$WPR := WT - WPL = 1.5\,m$	Distance from workplane point to right wall

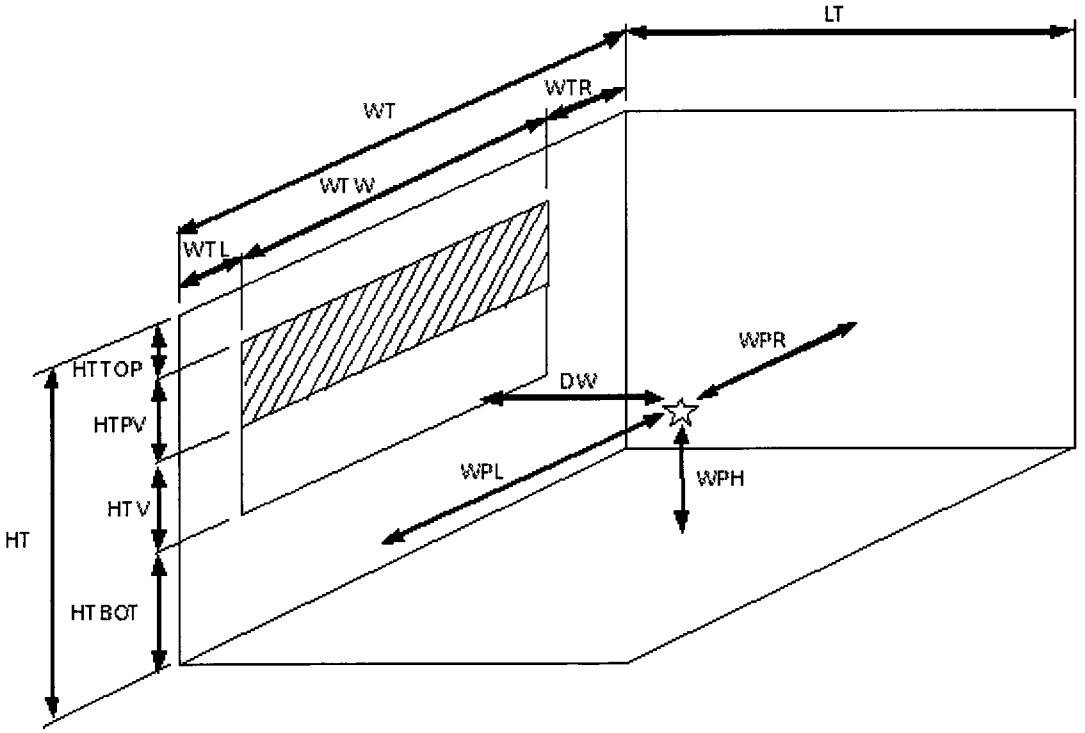

Surface reflectances:

ρ 1 & ρ 2 are calculated in section on transmittances & reflectances of glazings

Surface 1: STPV window (upper section)

Surface 2: Viewing window (middle section)

$\rho_3 := 0.6$ Surface 3: Front wall (with windows)

$\rho_4 := 0.2$ Surface 4: Floor

$\rho_5 := 0.8$ Surface 5: Ceiling

$\rho_6 := 0.6$ Surface 6: Back wall

$\rho_7 := 0.6$ Surface 7: Right wall

$\rho_8 := 0.6$ Surface 8: Left wall

Window & blind properties:

Clear front glazing

$L_{g1} := 6 \cdot mm$ Thickness

$k_{g1} := \frac{6}{m}$ Extinction coefficient

$n_{g\_g1} := 1.526$ Index of refraction

$kL_{g1} := k_{g1} \cdot L_{g1}$

EVA layer between PV spacings

$L_{EVA} := .5 \cdot mm$ Thickness

$k_{EVA} := \frac{25}{m}$ Extinction coefficient

$n_{g\_EVA} := 1.45$ Index of refraction

$kL_{EVA} := k_{EVA} \cdot L_{EVA}$

Clear back glazing

$L_{g2} := 6 \cdot mm$ Thickness

$k_{g2} := \frac{26}{m}$ Extinction coefficient

$n_{g\_g2} := 1.526$ Index of refraction

$kL_{g2} := k_{g1} \cdot L_{g1}$

Blind :

$\tau_{blind\_STPV} := 1$	Blind transmittance on STPV section = 1 if there is no blind
$\tau_{blind\_window} := 0.05$	Blind transmittance on viewing section

Luminaires:

$E_{desired} := 400 \cdot lx$	Desired workplane illuminance
$h_{ceiling} := 0.2 \cdot m$	Distance of luminaires to ceiling
$EFF := 0.727$	Efficiency of luminaire
$Lm_{tube} := 2900 \cdot lm$	Initial lumens of each tube
$P_{tube} := 32 \cdot watt$	Power of each tube
$N_{tubes} := 3$	Number of tubes in the luminaire
$LLF := 0.8$	Light loss factor
$f_{Lmin} := 0.01$	Minimum fractional electrical lighting power output when using dimmers
$f_{pmin} := 0.08$	Minimum fractional electrical lighting power input when using dimmers
$F_{sa} := 0.97$	Special allowance factor of luminaire fixture

APPENDIX VI B

Analytical weather data

A typical meteorological year (TMY2) derived from the 1961-1990 National Solar Radiation Data Base is used, converted by **TRNSYS16** hourly weather observations.

Beam horizontal radiation:

$I_{bh} :=$

	0
0	0
1	0
2	...

Beam normal radiation:

$I_{bn} :=$

	0
0	0
1	0
2	...

Diffuse horizontal radiation:

$I_{dh} :=$

	0
0	0
1	0
2	...

Outdoor temperature:

$T_o :=$

	0
0	0
1	0
2	...

Dew point temperature:

$T_{dp} :=$

	0
0	0
1	0
2	...

There are 23 zeroes at beginning of file in order to get day number and time number index correct. In TRNSYS, 0 is used for start of n and t and 1 is used here.

Packing functions:

The packing functions are used in order to sort the data into days so that you can input your day number and time number rather than just an hour number. This was written by Dr. Tzempelikos

$p := 24 \qquad q := 365$

$$\text{Pack}(I_{bh}, p, q) := \left| \begin{array}{l} \text{for } j \in 1..q \\ \quad \text{for } i \in 1..p \\ \quad\quad MM_{i,j} \leftarrow I_{bh_{i+p\cdot j}} \quad \text{if } i + p\cdot j < \text{rows}(I_{bh}) \\ MM \end{array} \right.$$

$$\text{Pack}(I_{dh}, p, q) := \left| \begin{array}{l} \text{for } j \in 1..q \\ \quad \text{for } i \in 1..p \\ \quad\quad NN_{i,j} \leftarrow I_{dh_{i+p\cdot j}} \quad \text{if } i + p\cdot j < \text{rows}(I_{dh}) \\ NN \end{array} \right.$$

$$\text{Pack}(I_{bn}, p, q) := \left| \begin{array}{l} \text{for } j \in 1..q \\ \quad \text{for } i \in 1..p \\ \quad\quad KK_{i,j} \leftarrow I_{bn_{i+p\cdot j}} \quad \text{if } i + p\cdot j < \text{rows}(I_{bn}) \\ KK \end{array} \right.$$

$$\text{Pack}(T_o, p, q) := \left| \begin{array}{l} \text{for } j \in 1..q \\ \quad \text{for } i \in 1..p \\ \quad\quad LL_{i,j} \leftarrow T_{o_{i+p\cdot j}} \text{ if } i + p\cdot j < \text{rows}(T_o) \\ LL \end{array} \right.$$

$$\text{Pack}(T_{dp}, p, q) := \left| \begin{array}{l} \text{for } j \in 1..q \\ \quad \text{for } i \in 1..p \\ \quad\quad QQ_{i,j} \leftarrow T_{dp_{i+p\cdot j}} \text{ if } i + p\cdot j < \text{rows}(T_{dp}) \\ QQ \end{array} \right.$$

$MM := \text{Pack}(I_{bh}, p, q)$ $\quad NN := \text{Pack}(I_{dh}, p, q)$ $\quad KK := \text{Pack}(I_{bn}, p, q)$

$LL := \text{Pack}(T_o, p, q)$ $\quad QQ := \text{Pack}(T_{dp}, p, q)$

$I_{bh}(n,t) := (MM^T)_{n,t} \cdot \frac{W}{m^2}$ $\quad I_{dh}(n,t) := (NN^T)_{n,t} \cdot \frac{W}{m^2}$ $\quad I_{bn}(n,t) := (KK^T)_{n,t} \cdot \frac{W}{m^2}$

$T_o(n,t) := (LL^T)_{n,t}$ $\quad T_{dp}(n,t) := (QQ^T)_{n,t}$

Weather data for entire year at 12:00 standard time

Beam horizontal radiation:

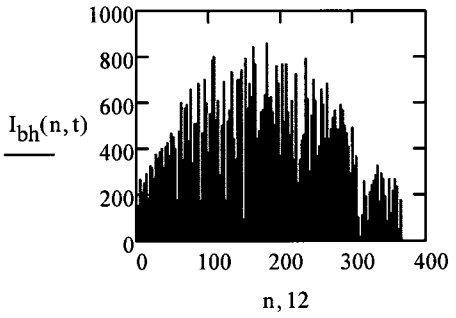

Beam normal radiation:

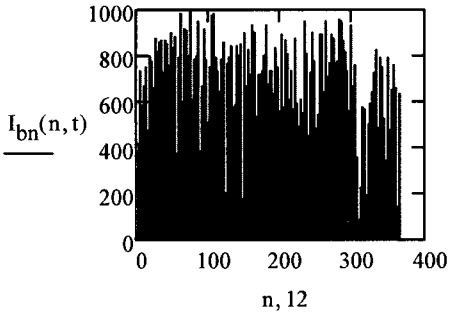

Diffuse horizontal radiation:

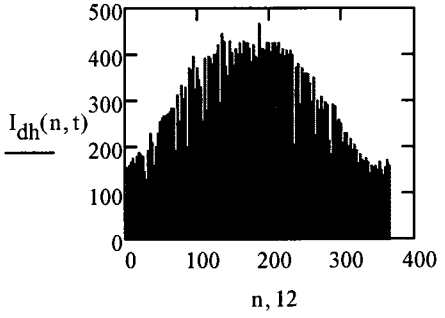

Outdoor temperature:

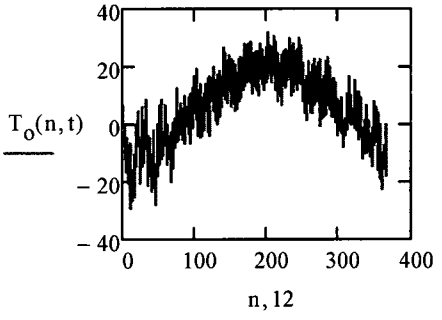

APPENDIX VI C

Solar geometry of window surface

Solar declination:

$$\delta(n) := 23.45\,deg \cdot \sin\left[\frac{360}{365}(284 + n)\cdot deg\right]$$

Equation of time:

$$ET(n) := 9.87\,min \cdot \sin\left[\frac{4\cdot\pi\cdot(n-81)}{364}\right] - 7.53\,min \cdot \cos\left[\frac{2\cdot\pi\cdot(n-81)}{364}\right] - 1.5\,min \cdot \sin\left[\frac{2\cdot\pi\cdot(n-81)}{364}\right]$$

Longitudinal Time Correction:

$$\Delta T := \frac{1\cdot hr}{15\cdot deg}\cdot(STM - Long)$$

Apparent Solar Time:

$$AST(n,t) := (t)\cdot hr + ET(n) + \Delta T$$

Hour angle:

$$H(n,t) := \frac{15}{hr}\cdot deg\cdot(AST(n,t) - 12\cdot hr)$$

Solar altitude:

$$\alpha(n,t) := \begin{cases} \asin\left[\begin{matrix}\sin(Lat)\cdot\sin(\delta(n)) \ldots \\ +(\cos(Lat))\cdot\cos(\delta(n))\cdot\cos(H(n,t))\end{matrix}\right] & \text{if } \asin\left[\begin{matrix}\sin(Lat)\cdot\sin(\delta(n)) \ldots \\ +(\cos(Lat))\cdot\cos(\delta(n))\cdot\cos(H(n,t))\end{matrix}\right] > 2\cdot deg \\ 0 \quad \text{otherwise} \end{cases}$$

Solar azimuth:

$$\phi(n,t) := \acos\left(\frac{\sin(\alpha(n,t))\cdot\sin(Lat) - \sin(\delta(n))}{\cos(\alpha(n,t))\cdot\cos(Lat)}\right)\cdot\frac{H(n,t)}{|H(n,t)|}$$

Surface solar azimuth:

$$\gamma(n,t) := \phi(n,t) - \psi$$

Angle of incidence:

$$\theta(n,t) := \acos\left[\frac{1}{2}\cdot\left[\begin{matrix}(\cos(\alpha(n,t))\cdot\cos(|\gamma(n,t)|)\cdot\sin(\beta) + \sin(\alpha(n,t))\cdot\cos(\beta)) \ldots \\ +|(\cos(\alpha(n,t))\cdot\cos(|\gamma(n,t)|)\cdot\sin(\beta) + \sin(\alpha(n,t))\cdot\cos(\beta))|\end{matrix}\right]\right]$$

Zenith Angle:

$$\zeta(n,t) := 90\cdot deg - \alpha(n,t)$$

APPENDIX VI D

Perez Irradiance model for exterior solar radiation incident on window

Extraterrestrial solar radiation (outside the atmosphere):

$$I_{sc} := 1367 \cdot \frac{W}{m^2}$$ Solar constant

$$I_{ex}(n) := I_{sc} \cdot \left(1 + 0.033 \cdot \cos\left(\frac{360 \cdot n}{365} \cdot deg\right)\right)$$ Normal extraterrestrial solar radiation

Incident beam radiation on an inclined surface:

$$I_b(n,t) := \left(I_{bn}(n,t) \cdot \cos(\theta(n,t))\right)$$

Horizon brightness coefficients:

$$a_P(n,t) := \max(0, \cos(\theta(n,t)))$$

$$b_P(n,t) := \max(\cos(85 \cdot deg), \sin(\alpha(n,t)))$$

Relative optical air mass:

$$m_{opt}(n,t) := \frac{1}{\sin(\alpha(n,t)) + 0.15 \cdot \left(\alpha(n,t) \cdot \frac{\pi}{180 \cdot deg} + 3.885\right)^{-1.253}}$$

Sky brightness:

$$\Delta(n,t) := m_{opt}(n,t) \cdot \frac{I_{dh}(n,t)}{I_{ex}(n)}$$

Sky clearness:

$$\varepsilon(n,t) := \begin{cases} \dfrac{\dfrac{I_{dh}(n,t) + I_{bn}(n,t)}{I_{dh}(n,t)} + 5.535\,10^{-6} \cdot (90 \cdot deg - \alpha(n,t))^3}{1 + 5.535\,10^{-6} \cdot (90 \cdot deg - \alpha(n,t))^3} & \text{if } I_{dh}(n,t) > 0 \cdot \dfrac{W}{m^2} \\ 0 \text{ otherwise} \end{cases}$$

Statistically derived irradiance coefficients for Perez model:

$$f_{11}(n,t) := \begin{cases} -0.008 \text{ if } \varepsilon(n,t) \le 1.065 \\ 0.130 \text{ if } 1.065 < \varepsilon(n,t) \le 1.23 \\ 0.330 \text{ if } 1.23 < \varepsilon(n,t) \le 1.5 \\ 0.568 \text{ if } 1.5 < \varepsilon(n,t) \le 1.95 \\ 0.873 \text{ if } 1.95 < \varepsilon(n,t) \le 2.8 \\ 1.132 \text{ if } 2.8 < \varepsilon(n,t) \le 4.5 \\ 1.060 \text{ if } 4.5 < \varepsilon(n,t) \le 6.2 \\ 0.678 \text{ otherwise} \end{cases}$$

$$f_{12}(n,t) := \begin{cases} 0.588 \text{ if } \varepsilon(n,t) \le 1.065 \\ 0.683 \text{ if } 1.065 < \varepsilon(n,t) \le 1.23 \\ 0.487 \text{ if } 1.23 < \varepsilon(n,t) \le 1.5 \\ 0.187 \text{ if } 1.5 < \varepsilon(n,t) \le 1.95 \\ -0.392 \text{ if } 1.95 < \varepsilon(n,t) \le 2.8 \\ -1.237 \text{ if } 2.8 < \varepsilon(n,t) \le 4.5 \\ -1.600 \text{ if } 4.5 < \varepsilon(n,t) \le 6.2 \\ -0.327 \text{ otherwise} \end{cases}$$

$$f_{13}(n,t) := \begin{cases} -0.062 \text{ if } \varepsilon(n,t) \le 1.065 \\ -0.151 \text{ if } 1.065 < \varepsilon(n,t) \le 1.23 \\ -0.221 \text{ if } 1.23 < \varepsilon(n,t) \le 1.5 \\ -0.295 \text{ if } 1.5 < \varepsilon(n,t) \le 1.95 \\ -0.362 \text{ if } 1.95 < \varepsilon(n,t) \le 2.8 \\ -0.412 \text{ if } 2.8 < \varepsilon(n,t) \le 4.5 \\ -0.359 \text{ if } 4.5 < \varepsilon(n,t) \le 6.2 \\ -0.25 \text{ otherwise} \end{cases} \qquad f_{21}(n,t) := \begin{cases} -0.060 \text{ if } \varepsilon(n,t) \le 1.065 \\ -0.019 \text{ if } 1.065 < \varepsilon(n,t) \le 1.23 \\ 0.055 \text{ if } 1.23 < \varepsilon(n,t) \le 1.5 \\ 0.109 \text{ if } 1.5 < \varepsilon(n,t) \le 1.95 \\ 0.226 \text{ if } 1.95 < \varepsilon(n,t) \le 2.8 \\ 0.288 \text{ if } 2.8 < \varepsilon(n,t) \le 4.5 \\ 0.264 \text{ if } 4.5 < \varepsilon(n,t) \le 6.2 \\ 0.156 \text{ otherwise} \end{cases}$$

$$f_{22}(n,t) := \begin{cases} 0.072 \text{ if } \varepsilon(n,t) \le 1.065 \\ 0.066 \text{ if } 1.065 < \varepsilon(n,t) \le 1.23 \\ -0.064 \text{ if } 1.23 < \varepsilon(n,t) \le 1.5 \\ -0.152 \text{ if } 1.5 < \varepsilon(n,t) \le 1.95 \\ -0.462 \text{ if } 1.95 < \varepsilon(n,t) \le 2.8 \\ -0.823 \text{ if } 2.8 < \varepsilon(n,t) \le 4.5 \\ -1.127 \text{ if } 4.5 < \varepsilon(n,t) \le 6.2 \\ -1.377 \text{ otherwise} \end{cases} \qquad f_{23}(n,t) := \begin{cases} -0.022 \text{ if } \varepsilon(n,t) \le 1.065 \\ -0.029 \text{ if } 1.065 < \varepsilon(n,t) \le 1.23 \\ -0.026 \text{ if } 1.23 < \varepsilon(n,t) \le 1.5 \\ -0.014 \text{ if } 1.5 < \varepsilon(n,t) \le 1.95 \\ -0.001 \text{ if } 1.95 < \varepsilon(n,t) \le 2.8 \\ 0.056 \text{ if } 2.8 < \varepsilon(n,t) \le 4.5 \\ 0.131 \text{ if } 4.5 < \varepsilon(n,t) \le 6.2 \\ 0.251 \text{ otherwise} \end{cases}$$

Brightness coefficients:

$$F_1(n,t) := \max\left[0, f_{11}(n,t) + f_{12}(n,t)\cdot\Delta(n,t) + \pi\cdot\frac{(90\cdot\text{deg} - \alpha(n,t))}{180\cdot\text{deg}}\cdot f_{13}(n,t)\right]$$

$$F_2(n,t) := \max\left[0, f_{21}(n,t) + f_{22}(n,t)\cdot\Delta(n,t) + \pi\cdot\frac{(90\cdot\text{deg} - \alpha(n,t))}{180\cdot\text{deg}}\cdot f_{23}(n,t)\right]$$

Total diffuse radiation on a tilted surface:

$$I_d(n,t) := \left(I_{dh}(n,t)\right)\cdot\left[\left(1 - F_1(n,t)\right)\cdot\left(\frac{1 + \cos(\beta)}{2}\right) + F_1(n,t)\cdot\frac{a_P(n,t)}{b_P(n,t)} + F_2(n,t)\cdot\sin(\beta)\right]$$

Ground-reflected radiation on a tilted surface:

$$I_g(n,t) := \left(I_{bh}(n,t) + I_{dh}(n,t)\right)\cdot\rho_{grd}(n)\cdot\frac{1 - \cos(\beta)}{2}$$

The total incident solar radiation on a tilted surface is equal to:

$$I_t(n,t) := I_b(n,t) + I_d(n,t) + I_g(n,t)$$

This model is based on Perez et al. 1990 and the MathCAD simulation file was written by Dr. Tzempelikos

APPENDIX VI E

Perez Illuminance model for exterior illuminance incident on window

Luminous efficacy coefficients:

Direct luminous efficacy:

$$ab(n,t) := \begin{cases} 57.20 & \text{if } \varepsilon(n,t) \le 1.065 \\ 98.99 & \text{if } 1.065 < \varepsilon(n,t) \le 1.23 \\ 109.83 & \text{if } 1.23 < \varepsilon(n,t) \le 1.5 \\ 110.34 & \text{if } 1.5 < \varepsilon(n,t) \le 1.95 \\ 106.36 & \text{if } 1.95 < \varepsilon(n,t) \le 2.8 \\ 107.19 & \text{if } 2.8 < \varepsilon(n,t) \le 4.5 \\ 105.75 & \text{if } 4.5 < \varepsilon(n,t) \le 6.2 \\ 101.18 & \text{otherwise} \end{cases}$$

$$bb(n,t) := \begin{cases} -4.55 & \text{if } \varepsilon(n,t) \le 1.065 \\ -3.46 & \text{if } 1.065 < \varepsilon(n,t) \le 1.23 \\ -4.90 & \text{if } 1.23 < \varepsilon(n,t) \le 1.5 \\ -5.84 & \text{if } 1.5 < \varepsilon(n,t) \le 1.95 \\ -3.97 & \text{if } 1.95 < \varepsilon(n,t) \le 2.8 \\ -1.25 & \text{if } 2.8 < \varepsilon(n,t) \le 4.5 \\ 0.77 & \text{if } 4.5 < \varepsilon(n,t) \le 6.2 \\ 1.58 & \text{otherwise} \end{cases}$$

$$cb(n,t) := \begin{cases} -2.98 & \text{if } \varepsilon(n,t) \le 1.065 \\ -1.21 & \text{if } 1.065 < \varepsilon(n,t) \le 1.23 \\ -1.71 & \text{if } 1.23 < \varepsilon(n,t) \le 1.5 \\ -1.99 & \text{if } 1.5 < \varepsilon(n,t) \le 1.95 \\ -1.75 & \text{if } 1.95 < \varepsilon(n,t) \le 2.8 \\ -1.51 & \text{if } 2.8 < \varepsilon(n,t) \le 4.5 \\ -1.26 & \text{if } 4.5 < \varepsilon(n,t) \le 6.2 \\ -1.10 & \text{otherwise} \end{cases}$$

$$db(n,t) := \begin{cases} 117.12 & \text{if } \varepsilon(n,t) \le 1.065 \\ 12.38 & \text{if } 1.065 < \varepsilon(n,t) \le 1.23 \\ -8.81 & \text{if } 1.23 < \varepsilon(n,t) \le 1.5 \\ -4.56 & \text{if } 1.5 < \varepsilon(n,t) \le 1.95 \\ -6.16 & \text{if } 1.95 < \varepsilon(n,t) \le 2.8 \\ -26.73 & \text{if } 2.8 < \varepsilon(n,t) \le 4.5 \\ -34.44 & \text{if } 4.5 < \varepsilon(n,t) \le 6.2 \\ -8.29 & \text{otherwise} \end{cases}$$

Diffuse luminous efficacy:

$$ad(n,t) := \begin{cases} 97.24 & \text{if } \varepsilon(n,t) \le 1.065 \\ 107.22 & \text{if } 1.065 < \varepsilon(n,t) \le 1.23 \\ 104.97 & \text{if } 1.23 < \varepsilon(n,t) \le 1.5 \\ 102.39 & \text{if } 1.5 < \varepsilon(n,t) \le 1.95 \\ 100.71 & \text{if } 1.95 < \varepsilon(n,t) \le 2.8 \\ 106.42 & \text{if } 2.8 < \varepsilon(n,t) \le 4.5 \\ 141.88 & \text{if } 4.5 < \varepsilon(n,t) \le 6.2 \\ 152.23 & \text{otherwise} \end{cases}$$

$$bd(n,t) := \begin{cases} -0.46 & \text{if } \varepsilon(n,t) \le 1.065 \\ 1.15 & \text{if } 1.065 < \varepsilon(n,t) \le 1.23 \\ 2.96 & \text{if } 1.23 < \varepsilon(n,t) \le 1.5 \\ 5.59 & \text{if } 1.5 < \varepsilon(n,t) \le 1.95 \\ 5.94 & \text{if } 1.95 < \varepsilon(n,t) \le 2.8 \\ 3.83 & \text{if } 2.8 < \varepsilon(n,t) \le 4.5 \\ 1.90 & \text{if } 4.5 < \varepsilon(n,t) \le 6.2 \\ 0.35 & \text{otherwise} \end{cases}$$

$$cd(n,t) := \begin{cases} 12.00 \text{ if } \varepsilon(n,t) \le 1.065 \\ 0.59 \text{ if } 1.065 < \varepsilon(n,t) \le 1.23 \\ -5.53 \text{ if } 1.23 < \varepsilon(n,t) \le 1.5 \\ -13.95 \text{ if } 1.5 < \varepsilon(n,t) \le 1.95 \\ -22.75 \text{ if } 1.95 < \varepsilon(n,t) \le 2.8 \\ -36.15 \text{ if } 2.8 < \varepsilon(n,t) \le 4.5 \\ -53.24 \text{ if } 4.5 < \varepsilon(n,t) \le 6.2 \\ -45.27 \text{ otherwise} \end{cases} \qquad dd(n,t) := \begin{cases} -8.91 \text{ if } \varepsilon(n,t) \le 1.065 \\ -3.95 \text{ if } 1.065 < \varepsilon(n,t) \le 1.23 \\ -8.77 \text{ if } 1.23 < \varepsilon(n,t) \le 1.5 \\ -13.90 \text{ if } 1.5 < \varepsilon(n,t) \le 1.95 \\ -23.74 \text{ if } 1.95 < \varepsilon(n,t) \le 2.8 \\ -28.83 \text{ if } 2.8 < \varepsilon(n,t) \le 4.5 \\ -14.03 \text{ if } 4.5 < \varepsilon(n,t) \le 6.2 \\ -7.98 \text{ otherwise} \end{cases}$$

Precipitable water content:

$$WC(n,t) := e^{0.07 \cdot T_{dp}(n,t) - 0.075}$$

Diffuse horizontal illuminance:

$$E_{dh}(n,t) := I_{dh}(n,t) \cdot \left(\begin{array}{l} ad(n,t) + bd(n,t) \cdot WC(n,t) + cd(n,t) \cdot \sin(\alpha(n,t)) \ldots \\ + dd(n,t) \cdot \ln\left(\Delta(n,t) + 10^{-10}\right) \end{array} \right) \cdot lx \cdot \frac{m^2}{W}$$

Direct normal illuminance:

$$E_{bn}(n,t) := \max\left[0, I_{bn}(n,t) \cdot \left[\begin{array}{l} ab(n,t) + bb(n,t) \cdot WC(n,t) \ldots \\ + cb(n,t) \cdot e^{5.73 \cdot (90 \cdot deg - \alpha(n,t)) \cdot \frac{\pi}{180 \cdot deg} - 5} + db(n,t) \cdot \Delta(n,t) \end{array} \right] \cdot lx \cdot \frac{m^2}{W}\right]$$

Direct horizontal illuminance:

$$E_{bh}(n,t) := E_{bn}(n,t) \cdot \sin(\alpha(n,t))$$

Hourly average beam illuminance on a tilted surface:

$$E_b(n,t) := \left(E_{bn}(n,t) \cdot \cos(\theta(n,t))\right)$$

Sky diffuse illuminance on a tilted surface is calculated by:

$$E_d(n,t) := E_{dh}(n,t) \cdot \left[\left(1 - F_1(n,t)\right) \cdot \left(\frac{1 + \cos(\beta)}{2} \right) + F_1(n,t) \cdot \frac{a_p(n,t)}{b_p(n,t)} + F_2(n,t) \cdot \sin(\beta) \right]$$

Ground-reflected illuminance on a tilted surface:

$$E_g(n,t) := \left(E_{bh}(n,t) + E_{dh}(n,t)\right) \cdot \rho_{grd}(n) \cdot \frac{1 - \cos(\beta)}{2}$$

The total incident illuminance on a tilted surface is equal to:

$$E(n,t) := E_b(n,t) + E_d(n,t) + E_g(n,t)$$

This model is based on Perez et al. 1990 and the MathCAD simulation file was written by Dr. Tzempelikos

APPENDIX VI F

Effective visible transmittance and reflectance of double glazed window sections

The transmittances of both double glazing sections are calculated using the fresnel equations. The beam and diffuse transmittances of each individual layer are calculated using Snell's law.

The diffuse transmittance is caluclated from expression used in (Brandemuehl, Beckman 1980)

$$\theta_d := 59.68 - .1388\beta + 0.001497\beta^2 = 59.466$$

As we desire the workplane illuminance to be a certain level during office hours, this needs only be calculated for t.oh (office hours)

Beam transmittance and reflectance of front glazing (g1):

Angle of refraction and component reflectivity:

$$\theta'_{b\_g1}(n,t_{oh}) := \operatorname{asin}\left(\frac{\sin(\theta(n,t_{oh}))}{n_{g\_g1}}\right) \qquad a_{b\_g1}(n,t_{oh}) := \exp\left[-\frac{kL_{g1}}{\sqrt{1-\left(\frac{\sin(\theta(n,t_{oh}))}{n_{g\_g1}}\right)^2}}\right]$$

$$r_{b\_g1}(n,t_{oh}) := \frac{1}{2}\cdot\left[\left(\frac{\sin(\theta(n,t_{oh}) - \theta'_{b\_g1}(n,t_{oh}))}{\sin(\theta(n,t_{oh}) + \theta'_{b\_g1}(n,t_{oh}))}\right)^2 + \left(\frac{\tan(\theta(n,t_{oh}) - \theta'_{b\_g1}(n,t_{oh}))}{\tan(\theta(n,t_{oh}) + \theta'_{b\_g1}(n,t_{oh}))}\right)^2\right]$$

Transmittance:

$$\tau_{b\_g1}(n,t_{oh}) := \frac{(1 - r_{b\_g1}(n,t_{oh}))^2 \cdot a_{b\_g1}(n,t_{oh})}{1 - (r_{b\_g1}(n,t_{oh}))^2 \cdot (a_{b\_g1}(n,t_{oh}))^2}$$

Reflectance:

$$\rho_{b\_g1}(n,t_{oh}) := r_{b\_g1}(n,t_{oh}) + \frac{r_{b\_g1}(n,t_{oh}) \cdot (1 - r_{b\_g1}(n,t_{oh}))^2 \cdot (a_{b\_g1}(n,t_{oh}))^2}{1 - (r_{b\_g1}(n,t_{oh}))^2 \cdot (a_{b\_g1}(n,t_{oh}))^2}$$

Diffuse transmittance and reflectance of front glazing (g1):

$$\theta'_{d\_g1} := \operatorname{asin}\left(\frac{\sin(\theta_d)}{n_{g\_g1}}\right) \qquad a_{d\_g1} := \exp\left[-\frac{kL_{g1}}{\sqrt{1-\left(\frac{\sin(\theta_d)}{n_{g\_g1}}\right)^2}}\right]$$

$$r_{d\_g1} := \frac{1}{2}\cdot\left[\left(\frac{\sin(\theta_d - \theta'_{d\_g1})}{\sin(\theta_d + \theta'_{d\_g1})}\right)^2 + \left(\frac{\tan(\theta_d - \theta'_{d\_g1})}{\tan(\theta_d + \theta'_{d\_g1})}\right)^2\right]$$

Transmittance:

$$\tau_{d\_g1} := \frac{\left(1 - r_{d\_g1}\right)^2 \cdot a_{d\_g1}}{1 - \left(r_{d\_g1}\right)^2 \cdot \left(a_{d\_g1}\right)^2}$$

Reflectance:

$$\rho_{d\_g1} := r_{d\_g1} + \frac{r_{d\_g1} \cdot \left(1 - r_{d\_g1}\right)^2 \cdot \left(a_{d\_g1}\right)^2}{1 - \left(r_{d\_g1}\right)^2 \cdot \left(a_{d\_g1}\right)^2}$$

Beam transmittance and reflectance of back glazing (g2):

Angle of refraction and component reflectivity:

$$\theta'_{b\_g2}(n, t_{oh}) := \operatorname{asin}\left(\frac{\sin\left(\theta(n, t_{oh})\right)}{n_{g\_g2}}\right) \qquad a_{b\_g2}(n, t_{oh}) := \exp\left[-\frac{kL_{g2}}{\sqrt{1 - \left(\frac{\sin\left(\theta(n, t_{oh})\right)}{n_{g\_g2}}\right)^2}}\right]$$

$$r_{b\_g2}(n, t_{oh}) := \frac{1}{2} \cdot \left[\left(\frac{\sin\left(\theta(n, t_{oh}) - \theta'_{b\_g2}(n, t_{oh})\right)}{\sin\left(\theta(n, t_{oh}) + \theta'_{b\_g2}(n, t_{oh})\right)}\right)^2 + \left(\frac{\tan\left(\theta(n, t_{oh}) - \theta'_{b\_g2}(n, t_{oh})\right)}{\tan\left(\theta(n, t_{oh}) + \theta'_{b\_g2}(n, t_{oh})\right)}\right)^2\right]$$

Transmittance:

$$\tau_{b\_g2}(n, t_{oh}) := \frac{\left(1 - r_{b\_g2}(n, t_{oh})\right)^2 \cdot a_{b\_g2}(n, t_{oh})}{1 - \left(r_{b\_g2}(n, t_{oh})\right)^2 \cdot \left(a_{b\_g2}(n, t_{oh})\right)^2}$$

Reflectance:

$$\rho_{b\_g2}(n, t_{oh}) := r_{b\_g2}(n, t_{oh}) + \frac{r_{b\_g2}(n, t_{oh}) \cdot \left(1 - r_{b\_g2}(n, t_{oh})\right)^2 \cdot \left(a_{b\_g2}(n, t_{oh})\right)^2}{1 - \left(r_{b\_g2}(n, t_{oh})\right)^2 \cdot \left(a_{b\_g2}(n, t_{oh})\right)^2}$$

Diffuse transmittance and reflectance of back glazing (g2):

$$\theta'_{d\_g2} := \operatorname{asin}\left(\frac{\sin\left(\theta_d\right)}{n_{g\_g2}}\right) \qquad a_{d\_g2} := \exp\left[-\frac{kL_{g2}}{\sqrt{1 - \left(\frac{\sin\left(\theta_d\right)}{n_{g\_g2}}\right)^2}}\right]$$

$$r_{d\_g2} := \frac{1}{2} \cdot \left[\left(\frac{\sin\left(\theta_d - \theta'_{d\_g2}\right)}{\sin\left(\theta_d + \theta'_{d\_g2}\right)}\right)^2 + \left(\frac{\tan\left(\theta_d - \theta'_{d\_g2}\right)}{\tan\left(\theta_d + \theta'_{d\_g2}\right)}\right)^2\right]$$

Transmittance:

$$\tau_{d\_g2} := \frac{\left(1 - r_{d\_g2}\right)^2 \cdot a_{d\_g2}}{1 - \left(r_{d\_g2}\right)^2 \cdot \left(a_{d\_g2}\right)^2}$$

Reflectance:

$$\rho_{d\_g2} := r_{d\_g2} + \frac{r_{d\_g2}\cdot\left(1 - r_{d\_g2}\right)^2\cdot\left(a_{d\_g2}\right)^2}{1 - \left(r_{d\_g2}\right)^2\cdot\left(a_{d\_g2}\right)^2}$$

Beam transmittance and reflectance of EVA:

The 'EVA' layer is considered as the EVA and front glazing as 1

Angle of refraction and component reflectivity:

$$\theta'_{b\_EVA}(n,t_{oh}) := \operatorname{asin}\left(\frac{\sin(\theta(n,t_{oh}))}{n_{g\_EVA}}\right) \qquad a_{b\_EVA}(n,t_{oh}) := \exp\left[-\frac{kL_{EVA}}{\sqrt{1-\left(\frac{\sin(\theta(n,t_{oh}))}{n_{g\_EVA}}\right)^2}}\right]$$

$$r_{b\_EVA}(n,t_{oh}) := \frac{1}{2}\cdot\left[\left(\frac{\sin(\theta(n,t_{oh}) - \theta'_{b\_EVA}(n,t_{oh}))}{\sin(\theta(n,t_{oh}) + \theta'_{b\_EVA}(n,t_{oh}))}\right)^2 + \left(\frac{\tan(\theta(n,t_{oh}) - \theta'_{b\_EVA}(n,t_{oh}))}{\tan(\theta(n,t_{oh}) + \theta'_{b\_EVA}(n,t_{oh}))}\right)^2\right]$$

Transmittance:

$$\tau_{b\_EVA}(n,t_{oh}) := \frac{\left(1 - r_{b\_EVA}(n,t_{oh})\right)^2\cdot a_{b\_EVA}(n,t_{oh})}{1 - \left(r_{b\_EVA}(n,t_{oh})\right)^2\cdot\left(a_{b\_EVA}(n,t_{oh})\right)^2}$$

Reflectance:

$$\rho_{b\_EVA}(n,t_{oh}) := r_{b\_EVA}(n,t_{oh}) + \frac{r_{b\_EVA}(n,t_{oh})\cdot\left(1 - r_{b\_EVA}(n,t_{oh})\right)^2\cdot\left(a_{b\_EVA}(n,t_{oh})\right)^2}{1 - \left(r_{b\_EVA}(n,t_{oh})\right)^2\cdot\left(a_{b\_EVA}(n,t_{oh})\right)^2}$$

Diffuse transmittance and reflectance of EVA:

$$\theta'_{d\_EVA} := \operatorname{asin}\left(\frac{\sin(\theta_d)}{n_{g\_EVA}}\right) \qquad a_{d\_EVA} := \exp\left[-\frac{kL_{EVA}}{\sqrt{1-\left(\frac{\sin(\theta_d)}{n_{g\_EVA}}\right)^2}}\right]$$

$$r_{d\_EVA} := \frac{1}{2}\cdot\left[\left(\frac{\sin(\theta_d - \theta'_{d\_EVA})}{\sin(\theta_d + \theta'_{d\_EVA})}\right)^2 + \left(\frac{\tan(\theta_d - \theta'_{d\_EVA})}{\tan(\theta_d + \theta'_{d\_EVA})}\right)^2\right]$$

Transmittance:

$$\tau_{d\_EVA} := \frac{\left(1 - r_{d\_EVA}\right)^2\cdot a_{d\_EVA}}{1 - \left(r_{d\_EVA}\right)^2\cdot\left(a_{d\_EVA}\right)^2}$$

Reflectance:

$$\rho_{d\_EVA} := r_{d\_EVA} + \frac{r_{d\_EVA}\cdot\left(1 - r_{d\_EVA}\right)^2\cdot\left(a_{d\_EVA}\right)^2}{1 - \left(r_{d\_EVA}\right)^2\cdot\left(a_{d\_EVA}\right)^2}$$

Double glazing:

Effective beam transmittance and reflectance of EVA in the STPV section (EVA & glazing (EVA) + back glazing (g2)) into room:

$$\tau_{b\_STPV\_EVA}(n,t_{oh}) := \frac{\tau_{b\_EVA}(n,t_{oh})\cdot\tau_{b\_g2}(n,t_{oh})}{1-\rho_{b\_EVA}(n,t_{oh})\cdot\rho_{b\_g2}(n,t_{oh})}$$

$$\rho_{b\_STPV\_EVA}(n,t_{oh}) := \rho_{b\_g2}(n,t_{oh}) + \frac{(\tau_{b\_g2}(n,t_{oh}))^2\cdot\rho_{b\_EVA}(n,t_{oh})}{1-\rho_{b\_EVA}(n,t_{oh})\cdot\rho_{b\_g2}(n,t_{oh})}$$

Effective diffuse transmittance and reflectance of EVA in the STPV section (EVA & glazing (EVA) + back glazing (g2)) into room:

$$\tau_{d\_STPV\_EVA} := \frac{\tau_{d\_EVA}\cdot\tau_{d\_g2}}{1-\rho_{d\_EVA}\cdot\rho_{d\_g2}}$$

$$\rho_{d\_STPV\_EVA} := \rho_{d\_g2}\cdot\frac{(\tau_{d\_g2})^2\cdot\rho_{d\_EVA}}{1-\rho_{d\_EVA}\cdot\rho_{d\_g2}}$$

Effective beam reflectance of PV in STPV section (PV + back glazing (g2)) into room:

$$\tau_{b\_STPV\_PV}(n,t_{oh}) := 0$$ The PV cells are opaque

$$\rho_{b\_STPV\_PV}(n,t_{oh}) := \rho_{b\_g2}(n,t_{oh}) + \frac{(\tau_{b\_g2}(n,t_{oh}))^2\cdot\rho_{PV\_back}}{1-\rho_{PV\_back}\cdot\rho_{b\_g2}(n,t_{oh})}$$

Effective diffuse reflectance of PV in STPV section (PV + back glazing (g2)) into room:

$$\tau_{d\_STPV\_PV} := 0$$ The PV cells are opaque

$$\rho_{d\_STPV\_PV} := \rho_{d\_g2} + \frac{(\tau_{d\_g2})^2\cdot\rho_{PV\_back}}{1-\rho_{PV\_back}\cdot\rho_{d\_g2}}$$

Reflectance and transmittance of STPV section:

Simplified estimation calculated as an area weighted sum of the effective EVA and PV reflectances and transmittances. A.pv = PV area ratio from 0 to 1

$$\tau_{b\_STPV}(n,t_{oh},A_{PV}) := \tau_{b\_STPV\_EVA}(n,t_{oh})\cdot(1-A_{PV}) + \tau_{b\_STPV\_PV}(n,t_{oh})\cdot A_{PV}$$

$$\tau_{d\_STPV}(A_{PV}) := \tau_{d\_STPV\_EVA}\cdot(1-A_{PV}) + \tau_{d\_STPV\_PV}A_{PV}$$

$$\rho_{b\_STPV}(n,t_{oh},A_{PV}) := \rho_{b\_STPV\_EVA}(n,t_{oh})\cdot(1-A_{PV}) + \rho_{b\_STPV\_PV}(n,t_{oh})\cdot A_{PV}$$

$$\rho_{d\_STPV}(A_{PV}) := \rho_{d\_STPV\_EVA}\cdot(1-A_{PV}) + \rho_{d\_STPV\_PV}A_{PV}$$

Effective beam transmittance and reflectance of window viewing section (front glazing (g1) + back glazing (g2)) into room:

$$\tau_{b\_win}(n,t_{oh}) := \frac{\tau_{b\_g1}(n,t_{oh})\cdot\tau_{b\_g2}(n,t_{oh})}{1-\rho_{b\_g1}(n,t_{oh})\cdot\rho_{b\_g2}(n,t_{oh})}$$

$$\rho_{b\_win}(n,t_{oh}) := \rho_{b\_g2}(n,t_{oh})\cdot\frac{(\tau_{b\_g2}(n,t_{oh}))^2\cdot\rho_{b\_g1}(n,t_{oh})}{1-\rho_{b\_g1}(n,t_{oh})\cdot\rho_{b\_g2}(n,t_{oh})}$$

Effective diffuse transmittance and reflectance of window viewing section (front glazing (g1) + back glazing (g2)) into room:

$$\tau_{d\_win} := \frac{\tau_{d\_g1}\cdot\tau_{d\_g2}}{1-\rho_{d\_g1}\cdot\rho_{d\_g2}}$$

$$\rho_{d\_win} := \rho_{d\_g2}\cdot\frac{(\tau_{d\_g2})^2\cdot\rho_{d\_g1}}{1-\rho_{d\_g1}\cdot\rho_{d\_g2}}$$

Blind model

The blind automatically goes down when the outdoor normal beam irradiance reaches 100 W/m2

$$\tau_{b\_win\_blind}(n,t_{oh}) := \begin{cases} \tau_{b\_win}(n,t_{oh}) & \text{if } I_{bn}(n,t_{oh}) \le 100\frac{W}{m^2} \\ \tau_{b\_win}(n,t_{oh})\cdot\tau_{blind\_window} & \text{otherwise} \end{cases}$$

$$\tau_{d\_win\_blind}(n,t_{oh}) := \begin{cases} \tau_{d\_win} & \text{if } I_{bn}(n,t_{oh}) \le 100\frac{W}{m^2} \\ \tau_{d\_win}\cdot\tau_{blind\_window} & \text{otherwise} \end{cases}$$

$$\tau_{b\_STPV\_blind}(n,t_{oh},A_{PV}) := \begin{cases} \tau_{b\_STPV}(n,t_{oh},A_{PV}) & \text{if } I_{bn}(n,t_{oh}) \le 100\frac{W}{m^2} \\ \tau_{b\_STPV}(n,t_{oh},A_{PV})\cdot\tau_{blind\_STPV} & \text{otherwise} \end{cases}$$

$$\tau_{d\_STPV\_blind}(n,t_{oh},A_{PV}) := \begin{cases} \tau_{d\_STPV}(A_{PV}) & \text{if } I_{bn}(n,t_{oh}) \le 100\frac{W}{m^2} \\ \tau_{d\_STPV}(A_{PV})\cdot\tau_{blind\_STPV} & \text{otherwise} \end{cases}$$

APPENDIX VI G

View factors (form factors) of the room

View factors relate each surface to each other and are used in the radiosity method when determining the workplane illuminance

Total number of interior surfaces: 8

Surface 1: STPV window (upper section)
Surface 2: Viewing window (middle section)
Surface 3: Front wall (with windows)
Surface 4: Floor
Surface 5: Ceiling
Surface 6: Back wall
Surface 7: Right wall
Surface 8: Left wall

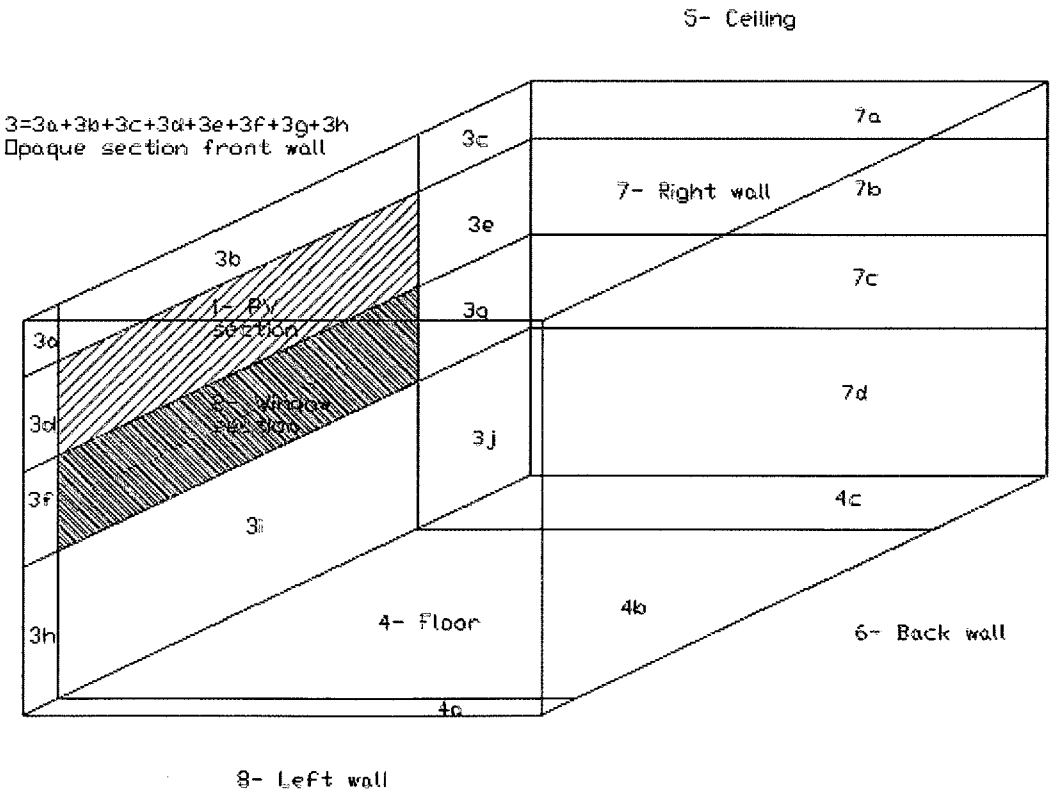

Areas of surfaces:

$A_1 := WTW \cdot HTPV = 4.2m^2$ STPV window (upper section)

$A_2 := WTW \cdot HTV = 4.2m^2$ Viewing window (middle section)

$A_{3a} := WTL \cdot HTTOP = 0.02m^2$ $A_{3b} := WTW \cdot HTTOP = 0.56m^2$ Front wall (with windows)

$A_{3c} := WTR \cdot HTTOP = 0.02m^2$ $A_{3d} := WTL \cdot HTPV = 0.15m^2$

$A_{3e} := WTR \cdot HTPV = 0.15m^2$ $A_{3f} := WTL \cdot HTV = 0.15m^2$

$A_{3g} := WTR \cdot HTV = 0.15m^2$ $A_{3h} := WTL \cdot HTBOT = 0.08m^2$

$A_{3i} := WTW \cdot HTBOT = 2.24m^2$ $A_{3j} := WTR \cdot HTBOT = 0.08m^2$

$A_3 := A_{3a} + A_{3b} + A_{3c} + A_{3d} + A_{3e} + A_{3f} + A_{3g} + A_{3h} + A_{3i} + A_{3j} = 3.6m^2$

$A_4 := LT \cdot WT = 12m^2$ Floor

$A_{4a} := LT \cdot WTL = 0.4m^2$ $A_{4b} := LT \cdot WTW = 11.2m^2$ $A_{4c} := LT \cdot WTR = 0.4m^2$

$A_5 := A_4 = 12m^2$ Ceiling

$A_{5a} := A_{4a}$ $A_{5b} := A_{4b}$ $A_{5c} := A_{4c}$

$A_6 := WT \cdot HT = 12m^2$ Back wall

$A_7 := LT \cdot HT = 16m^2$ Right wall

$A_{7a} := LT \cdot HTTOP = 0.8m^2$ $A_{7b} := LT \cdot HTPV = 6m^2$

$A_{7c} := LT \cdot HTV = 6m^2$ $A_{7d} := LT \cdot HTBOT = 3.2m^2$

$A_8 := A_7 = 16m^2$ Left wall

$A_{8a} := A_{7a}$ $A_{8b} := A_{7b}$ $A_{8c} := A_{7c}$ $A_{8d} := A_{7d}$

View factors for three dimensional geometries

2 parallel planes of equal area:

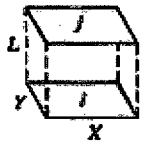

$$f(s,tt) := \frac{2}{\pi \cdot s \cdot tt}\left[\frac{1}{2}\ln\left[\frac{\left(1+s^2\right)\cdot\left(1+tt^2\right)}{1+s^2+tt^2}\right] + tt\cdot\sqrt{1+s^2}\cdot\operatorname{atan}\left(\frac{tt}{\sqrt{1+s^2}}\right) \ldots \right.$$
$$\left. + s\cdot\sqrt{1+tt^2}\cdot\operatorname{atan}\left(\frac{s}{\sqrt{1+tt^2}}\right) - tt\cdot\operatorname{atan}(tt) - s\cdot\operatorname{atan}(s)\right]$$

2 perpendicular planes, with common edge:

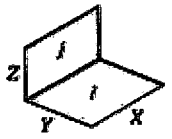

$$g(W,H) := \frac{1}{\pi \cdot W}\cdot\left[W\cdot\operatorname{atan}\left(\frac{1}{W}\right) + H\cdot\operatorname{atan}\left(\frac{1}{H}\right) - \left(H^2+W^2\right)^{\frac{1}{2}}\cdot\operatorname{atan}\left[\frac{1}{\left(H^2+W^2\right)^{\frac{1}{2}}}\right] \ldots\right.$$
$$\left. + \frac{1}{4}\cdot\ln\left[\frac{\left(1+W^2\right)\cdot\left(1+H^2\right)}{1+W^2+H^2}\cdot\left[W^2\cdot\frac{\left(1+W^2+H^2\right)}{\left(1+W^2\right)\cdot\left(W^2+H^2\right)}\right]^{W^2}\cdot\left[H^2\cdot\frac{\left(1+H^2+W^2\right)}{\left(1+H^2\right)\cdot\left(H^2+W^2\right)}\right]^{H^2}\right]\right]$$

View factors between single surface:

$F_{11} := 0$ $F_{22} := 0$ $F_{33} := 0$ $F_{44} := 0$ $F_{55} := 0$

$F_{66} := 0$ $F_{77} := 0$ $F_{88} := 0$ $F_{12} := 0$ $F_{13} := 0$

$F_{21} := 0$ $F_{23} := 0$ $F_{31} := 0$ $F_{32} := 0$

None of the surfaces 'see' themselves or others on the same plane

View factors between floor and ceiling (4 , 5):

$tt := \frac{LT}{HT}$ $s := \frac{WT}{HT}$ $F_{45} := f(s, tt) = 0.163$ $F_{54} := F_{45} = 0.163$

View factors between right wall and left wall (7, 8):

$tt := \frac{LT}{WT}$ $s := \frac{HT}{WT}$ $F_{78} := f(s, tt) = 0.283$ $F_{87} := F_{78} = 0.283$

View factors between floor/ceiling and back wall (4/5, 6):

$W := \frac{LT}{WT}$ $H := \frac{HT}{WT}$ $F_{46} := g(W, H) = 0.179$ $F_{56} := F_{46} = 0.179$

$F_{64} := F_{46} \cdot \frac{A_4}{A_6} = 0.179$ $F_{65} := F_{56} \cdot \frac{A_5}{A_6} = 0.179$

View factors between floor/ceiling and right/left wall (4/5, 7/8):

$W := \frac{WT}{LT}$ $H := \frac{HT}{LT}$ $F_{47} := g(W, H) = 0.239$ $F_{74} := F_{47} \cdot \frac{A_4}{A_7} = 0.179$

$F_{48} := F_{47}$ $F_{57} := F_{47}$ $F_{58} := F_{48}$

$F_{84} := F_{48} \cdot \frac{A_4}{A_8} = 0.179$ $F_{75} := F_{57} \cdot \frac{A_5}{A_7} = 0.179$ $F_{85} := F_{58} \cdot \frac{A_5}{A_8} = 0.179$

View factors between back wall and right/left wall (6, 7/8):

$W := \frac{WT}{HT}$ $H := \frac{LT}{HT}$ $F_{67} := g(W, H) = 0.239$ $F_{68} := F_{67} = 0.239$

$F_{76} := F_{67} \cdot \frac{A_6}{A_7} = 0.179$ $F_{86} := F_{68} \cdot \frac{A_6}{A_8} = 0.179$

View factors between PV section and floor (1, 4):

Using perpendicular planes and principle of superposition:

$H := \frac{HTPV + HTV + HTBOT}{WTW}$ $W := \frac{LT}{WTW}$ $F_{4b\_123i} := g(W,H) = 0.172$

$H := \frac{HTV + HTBOT}{WTW}$ $W := \frac{LT}{WTW}$ $F_{4b\_23i} := g(W,H) = 0.141$

$H := \frac{HTPV + HTV + HTBOT}{WTL + WTW}$ $W := \frac{LT}{WTL + WTW}$ $F_{4a4b\_3d3f3h123i} := g(W,H) = 0.174$

$H := \frac{HTV + HTBOT}{WTL + WTW}$ $W := \frac{LT}{WTL + WTW}$ $F_{4a4b\_3f3h23i} := g(W,H) = 0.143$

$H := \frac{HTPV + HTV + HTBOT}{WTL}$ $W := \frac{LT}{WTL}$ $F_{4a\_3d3f3h} := g(W,H) = 0.019$

$H := \frac{HTV + HTBOT}{WTL}$ $W := \frac{LT}{WTL}$ $F_{4a\_3f3h} := g(W,H) = 0.018$

$H := \frac{HTPV + HTV + HTBOT}{WTR + WTW}$ $W := \frac{LT}{WTR + WTW}$ $F_{4b4c\_3e3g3j123i} := g(W,H) = 0.174$

$H := \frac{HTV + HTBOT}{WTR + WTW}$ $W := \frac{LT}{WTR + WTW}$ $F_{4b4c\_3g3j23i} := g(W,H) = 0.143$

$H := \frac{HTPV + HTV + HTBOT}{WTR}$ $W := \frac{LT}{WTR}$ $F_{4c\_3e3g3j} := g(W,H) = 0.019$

$H := \frac{HTV + HTBOT}{WTR}$ $W := \frac{LT}{WTR}$ $F_{4c\_3g3j} := g(W,H) = 0.018$

$F_{4b\_1} := F_{4b\_123i} - F_{4b\_23i} = 0.031$ $F_{1\_4b} := F_{4b\_1} \cdot \frac{A_{4b}}{A_1} = 0.081$

$$F_{4a\_123i} := \frac{F_{4a4b\_3d3f3h123i}(A_{4a} + A_{4b}) - F_{4b\_123i}(A_{4b}) - F_{4a\_3d3f3h} \cdot (A_{4a})}{2 \cdot A_{4a}} = 0.113$$

$$F_{4a\_23i} := \frac{F_{4a4b\_3f3h23i}(A_{4a} + A_{4b}) - F_{4a\_3f3h} \cdot (A_{4a}) - F_{4b\_23i} \cdot (A_{4b})}{2 \cdot A_{4a}} = 0.087$$

$$F_{4c\_123i} := \frac{F_{4b4c\_3e3g3j123i}(A_{4b} + A_{4c}) - F_{4b\_123i}(A_{4b}) - F_{4c\_3e3g3j} \cdot (A_{4c})}{2 \cdot A_{4c}} = 0.113$$

$$F_{4c\_23i} := \frac{F_{4b4c\_3g3j23i}(A_{4b} + A_{4c}) - F_{4c\_3g3j} \cdot (A_{4c}) - F_{4b\_23i} \cdot (A_{4b})}{2 \cdot A_{4c}} = 0.087$$

$F_{4a\_1} := F_{4a\_123i} - F_{4a\_23i} = 0.026$ $F_{4c\_1} := F_{4c\_123i} - F_{4c\_23i} = 0.026$

$F_{1\_4a} := F_{4a\_1} \cdot \frac{A_{4a}}{A_1} = 2.484 \times 10^{-3}$ $F_{1\_4c} := F_{4c\_1} \cdot \frac{A_{4c}}{A_1} = 2.484 \times 10^{-3}$

$F_{14} := F_{1\_4a} + F_{1\_4b} + F_{1\_4c} = 0.086$ $F_{41} := F_{14} \cdot \frac{A_1}{A_4} = 0.03$

View factor from Window section to floor (2, 4):

$H := \frac{HTBOT}{WTW}$ $W := \frac{LT}{WTW}$ $F_{4b\_3i} := g(W,H) = 0.073$

$H := \frac{HTBOT}{WTL + WTW}$ $W := \frac{LT}{WTL + WTW}$ $F_{4a4b\_3h3i} := g(W,H) = 0.073$

$H := \frac{HTBOT}{WTL}$ $W := \frac{LT}{WTL}$ $F_{4a\_3h} := g(W,H) = 0.014$

$H := \frac{HTBOT}{WTR + WTW}$ $W := \frac{LT}{WTR + WTW}$ $F_{4b4c\_3i3j} := g(W,H) = 0.073$

$H := \frac{HTBOT}{WTR}$ $W := \frac{LT}{WTR}$ $F_{4c\_3j} := g(W,H) = 0.014$

$F_{4b\_2} := F_{4b\_23i} - F_{4b\_3i} = 0.068$

$$F_{4a\_3i} := \frac{F_{4a4b\_3h3i}\cdot(A_{4a} + A_{4b}) - F_{4a\_3h}\cdot(A_{4a}) - F_{4b\_3i}\cdot(A_{4b})}{2\cdot A_{4a}} = 0.037$$

$F_{4a\_2} := F_{4a\_23i} - F_{4a\_3i} = 0.05$

$$F_{4c\_3i} := \frac{F_{4b4c\_3i3j}(A_{4b} + A_{4c}) - F_{4c\_3j}\cdot(A_{4c}) - F_{4b\_3i}\cdot(A_{4b})}{2\cdot A_{4c}} = 0.037$$

$F_{4c\_2} := F_{4c\_23i} - F_{4c\_3i} = 0.05$

$F_{2\_4a} := F_{4a\_2}\cdot\frac{A_{4a}}{A_2} = 4.785\times 10^{-3}$ $F_{2\_4b} := F_{4b\_2}\cdot\frac{A_{4b}}{A_2} = 0.182$ $F_{2\_4c} := F_{4c\_2}\cdot\frac{A_{4c}}{A_2} = 4.785\times 10^{-3}$

$F_{24} := F_{2\_4a} + F_{2\_4b} + F_{2\_4c} = 0.192$ $F_{42} := F_{24}\cdot\frac{A_2}{A_4} = 0.067$

View factor from front wall section to floor (3, 4):

$H := \frac{HT}{WTL + WTW + WTR}$ $W := \frac{LT}{WTL + WTW + WTR}$ $F_{4\_123} := g(W,H) = 0.179$

$F_{43} := F_{4\_123} - F_{41} - F_{42} = 0.082$ $F_{34} := F_{43}\cdot\frac{A_4}{A_3} = 0.274$

View factors between window section and ceiling (2, 5):

$H := \frac{HTV + HTPV + HTTOP}{WTW}$ $W := \frac{LT}{WTW}$ $F_{5b\_213b} := g(W,H) = 0.162$

$H := \frac{HTPV + HTTOP}{WTW}$ $W := \frac{LT}{WTW}$ $F_{5b\_13b} := g(W,H) = 0.121$

$H := \frac{HTV + HTPV + HTTOP}{WTL + WTW}$ $W := \frac{LT}{WTL + WTW}$ $F_{5a5b\_3f3d3a213b} := g(W,H) = 0.164$

$H := \frac{HTPV + HTTOP}{WTL + WTW}$ $W := \frac{LT}{WTL + WTW}$ $F_{5a5b\_3d3a13b} := g(W,H) = 0.122$

$H := \frac{HTV + HTPV + HTTOP}{WTL}$ $W := \frac{LT}{WTL}$ $F_{5a\_3f3d3a} := g(W,H) = 0.019$

$H := \frac{HTPV + HTTOP}{WTL}$ $W := \frac{LT}{WTL}$ $F_{5a\_3d3a} := g(W,H) = 0.017$

$H := \frac{HTV + HTPV + HTTOP}{WTR + WTW}$ $W := \frac{LT}{WTR + WTW}$ $F_{5b5c\_3g3e3c213b} := g(W,H) = 0.164$

$H := \frac{HTPV + HTTOP}{WTR + WTW}$ $W := \frac{LT}{WTR + WTW}$ $F_{5b5c\_3e3c13b} := g(W,H) = 0.122$

$H := \frac{HTV + HTPV + HTTOP}{WTR}$ $W := \frac{LT}{WTR}$ $F_{5c\_3g3e3c} := g(W,H) = 0.019$

$H := \frac{HTPV + HTTOP}{WTR}$ $W := \frac{LT}{WTR}$ $F_{5c\_3e3c} := g(W,H) = 0.017$

$F_{5b\_2} := F_{5b\_213b} - F_{5b\_13b} = 0.042$

$$F_{5a\_213b} := \frac{F_{5a5b\_3f3d3a213b}\cdot(A_{5a} + A_{5b}) - F_{5b\_213b}\cdot(A_{5b}) - F_{5a\_3f3d3a}\cdot(A_{5a})}{2\cdot A_{5a}} = 0.104$$

$$F_{5a\_13b} := \frac{F_{5a5b\_3d3a13b}\cdot(A_{5a} + A_{5b}) - F_{5a\_3d3a}\cdot(A_{5a}) - F_{5b\_13b}\cdot(A_{5b})}{2\cdot A_{5a}} = 0.07$$

$F_{5a\_2} := F_{5a\_213b} - F_{5a\_13b} = 0.034$

$$F_{5c\_213b} := \frac{F_{5b5c\_3g3e3c213b}\cdot(A_{5b} + A_{5c}) - F_{5b\_213b}\cdot(A_{5b}) - F_{5c\_3g3e3c}\cdot(A_{5c})}{2\cdot A_{5c}} = 0.104$$

$$F_{5c\_13b} := \frac{F_{5b5c\_3e3c13b}\cdot(A_{5b} + A_{5c}) - F_{5c\_3e3c}\cdot(A_{5c}) - F_{5b\_13b}\cdot(A_{5b})}{2\cdot A_{5c}} = 0.07$$

$F_{5c\_2} := F_{5c\_213b} - F_{5c\_13b} = 0.034$

$F_{2\_5a} := F_{5a\_2}\cdot\frac{A_{5a}}{A_2} = 3.245\times 10^{-3}$ $F_{2\_5b} := F_{5b\_2}\cdot\frac{A_{5b}}{A_2} = 0.111$ $F_{2\_5c} := F_{5c\_2}\cdot\frac{A_{5c}}{A_2} = 3.245\times 10^{-3}$

$F_{25} := F_{2\_5a} + F_{2\_5b} + F_{2\_5c} = 0.118$ $F_{52} := F_{25}\cdot\frac{A_2}{A_5} = 0.041$

View factor from PV section to ceiling (1, 5):

$H := \frac{HTTOP}{WTW}$ $W := \frac{LT}{WTW}$ $F_{5b\_3b} := g(W,H) = 0.023$

$H := \frac{HTTOP}{WTL + WTW}$ $W := \frac{LT}{WTL + WTW}$ $F_{5a5b\_3a3b} := g(W,H) = 0.023$

$H := \frac{HTTOP}{WTL}$ $W := \frac{LT}{WTL}$ $F_{5a\_3a} := g(W,H) = 8.8\times 10^{-3}$

$H := \frac{HTTOP}{WTR + WTW}$ $W := \frac{LT}{WTR + WTW}$ $F_{5b5c\_3b3c} := g(W,H) = 0.023$

$H := \frac{HTTOP}{WTR}$ $W := \frac{LT}{WTR}$ $F_{5c\_3c} := g(W,H) = 8.8\times 10^{-3}$

$F_{5b\_1} := F_{5b\_13b} - F_{5b\_3b} = 0.098$

$F_{5a\_3b} := \frac{F_{5a5b\_3a3b}\cdot(A_{5a} + A_{5b}) - F_{5a\_3a}\cdot(A_{5a}) - F_{5b\_3b}\cdot(A_{5b})}{2\cdot A_{5a}} = 7.698\times 10^{-3}$

$F_{5a\_1} := F_{5a\_13b} - F_{5a\_3b} = 0.063$

$F_{5c\_3b} := \frac{F_{5b5c\_3b3c}\cdot(A_{5b} + A_{5c}) - F_{5c\_3c}\cdot(A_{5c}) - F_{5b\_3b}\cdot(A_{5b})}{2\cdot A_{5c}} = 7.698\times 10^{-3}$

$F_{5c\_1} := F_{5c\_13b} - F_{5c\_3b} = 0.063$

$F_{1\_5a} := F_{5a\_1}\cdot\frac{A_{5a}}{A_1} = 5.973\times 10^{-3}$ $F_{1\_5b} := F_{5b\_1}\cdot\frac{A_{5b}}{A_1} = 0.261$ $F_{1\_5c} := F_{5c\_1}\cdot\frac{A_{5c}}{A_1} = 5.973\times 10^{-3}$

$F_{15} := F_{1\_5a} + F_{1\_5b} + F_{1\_5c} = 0.273$ $F_{51} := F_{15}\cdot\frac{A_1}{A_5} = 0.096$

View factor from front wall section to floor (3, 5):

$H := \frac{HT}{WTL + WTW + WTR}$ $W := \frac{LT}{WTL + WTW + WTR}$ $F_{5\_123} := g(W,H) = 0.179$

$F_{53} := F_{5\_123} - F_{51} - F_{52} = 0.043$ $F_{35} := F_{53}\cdot\frac{A_5}{A_3} = 0.142$

View factor between PV section and right wall (1, 7)

$H := \frac{WTW + WTR}{HTPV}$ $W := \frac{LT}{HTPV}$ $F_{7b\_13e} := g(W,H) = 0.118$

$H := \frac{WTR}{HTPV}$ $W := \frac{LT}{HTPV}$ $F_{7b\_3e} := g(W,H) = 0.011$

$H := \frac{WTW + WTR}{HTPV + HTTOP}$ $W := \frac{LT}{HTPV + HTTOP}$ $F_{7a7b\_13e3b3c} := g(W,H) = 0.125$

$H := \frac{WTR}{HTPV + HTTOP}$ $W := \frac{LT}{HTPV + HTTOP}$ $F_{7a7b\_3e3c} := g(W,H) = 0.011$

$H := \frac{WTW + WTR}{HTTOP}$ $W := \frac{LT}{HTTOP}$ $F_{7a\_3b3c} := g(W,H) = 0.032$

$H := \frac{WTR}{HTTOP}$ $W := \frac{LT}{HTTOP}$ $F_{7a\_3c} := g(W,H) = 8.095 \times 10^{-3}$

$H := \frac{WTW + WTR}{HTPV + HTV + HTBOT}$ $W := \frac{LT}{HTPV + HTV + HTBOT}$ $F_{7b7c7d\_123i3e3g3j} := g(W,H) = 0.174$

$H := \frac{WTR}{HTPV + HTV + HTBOT}$ $W := \frac{LT}{HTPV + HTV + HTBOT}$ $F_{7b7c7d\_3e3g3j} := g(W,H) = 0.012$

$H := \frac{WTW + WTR}{HTV + HTBOT}$ $W := \frac{LT}{HTV + HTBOT}$ $F_{7c7d\_23i3g3j} := g(W,H) = 0.144$

$H := \frac{WTR}{HTV + HTBOT}$ $W := \frac{LT}{HTV + HTBOT}$ $F_{7c7d\_3g3j} := g(W,H) = 0.012$

$$F_{7a\_13e} := \frac{F_{7a7b\_13e3b3c} \cdot (A_{7a} + A_{7b}) - F_{7b\_13e} \cdot (A_{7b}) - F_{7a\_3b3c} \cdot (A_{7a})}{2 \cdot A_{7a}} = 0.076$$

$$F_{7a\_3e} := \frac{F_{7a7b\_3e3c} \cdot (A_{7a} + A_{7b}) - F_{7a\_3c} \cdot (A_{7a}) - F_{7b\_3e} \cdot (A_{7b})}{2 \cdot A_{7a}} = 2.059 \times 10^{-3}$$

$F_{7a\_1} := F_{7a\_13e} - F_{7a\_3e} = 0.074$ $F_{7b\_1} := F_{7b\_13e} - F_{7b\_3e} = 0.106$

$$F_{7c7d\_13e} := \frac{F_{7b7c7d\_123i3e3g3j}(A_{7b} + A_{7c} + A_{7d}) - F_{7b\_13e} \cdot (A_{7b}) - F_{7c7d\_23i3g3j}(A_{7c} + A_{7d})}{2 \cdot (A_{7c} + A_{7d})}$$

$$F_{7c7d\_3e} := \frac{F_{7b7c7d\_3e3g3j} \cdot (A_{7b} + A_{7c} + A_{7d}) - F_{7c7d\_3g3j} \cdot (A_{7c} + A_{7d}) - F_{7b\_3e} \cdot (A_{7b})}{2 \cdot (A_{7c} + A_{7d})}$$

$F_{7c7d\_1} := F_{7c7d\_13e} - F_{7c7d\_3e} = 0.033$ $F_{7c7d\_13e} = 0.033$ $F_{7c7d\_3e} = 3.055 \times 10^{-4}$

$F_{1\_7a} := F_{7a\_1} \cdot \frac{A_{7a}}{A_1} = 0.014$ $F_{1\_7b} := F_{7b\_1} \cdot \frac{A_{7b}}{A_1} = 0.152$ $F_{1\_7c7d} := F_{7c7d\_1} \cdot \frac{(A_{7c} + A_{7d})}{A_1} = 0.072$

$F_{17} := F_{1\_7a} + F_{1\_7b} + F_{1\_7c7d} = 0.238$ $F_{71} := F_{17} \cdot \frac{A_1}{A_7} = 0.062$

View factor between window section and right wall (2, 7)

$H := \frac{WTW + WTR}{HTV}$ $W := \frac{LT}{HTV}$ $F_{7c\_23g} := g(W,H) = 0.118$

$H := \frac{WTR}{HTV}$ $W := \frac{LT}{HTV}$ $F_{7c\_3g} := g(W,H) = 0.011$

$H := \frac{WTW + WTR}{HTBOT}$ $W := \frac{LT}{HTBOT}$ $F_{7d\_3i3j} := g(W,H) = 0.082$

$H := \frac{WTR}{HTBOT}$ $W := \frac{LT}{HTBOT}$ $F_{7d\_3j} := g(W,H) = 0.011$

$H := \frac{WTW + WTR}{HTV + HTPV + HTTOP}$ $W := \frac{LT}{HTV + HTPV + HTTOP}$

$F_{7c7b7a\_213b3g3e3c} := g(W,H) = 0.164$

$H := \frac{WTR}{HTV + HTPV + HTTOP}$ $W := \frac{LT}{HTV + HTPV + HTTOP}$

$F_{7c7b7a\_3g3e3c} := g(W,H) = 0.012$

$$F_{7d\_23g} := \frac{F_{7c7d\_23i3g3j}\cdot(A_{7c} + A_{7d}) - F_{7c\_23g}\cdot(A_{7c}) - F_{7d\_3i3j}\cdot(A_{7d})}{2\cdot A_{7d}} = 0.056$$

$$F_{7d\_3g} := \frac{F_{7c7d\_3g3j}\cdot(A_{7c} + A_{7d}) - F_{7d\_3j}\cdot(A_{7d}) - F_{7c\_3g}\cdot(A_{7c})}{2\cdot A_{7d}} = 7.672\times 10^{-4}$$

$F_{7d\_2} := F_{7d\_23g} - F_{7d\_3g} = 0.055$ $F_{7c\_2} := F_{7c\_23g} - F_{7c\_3g} = 0.106$

$$F_{7a7b\_23g} := \frac{F_{7c7b7a\_213b3g3e3c}\cdot(A_{7c} + A_{7b} + A_{7a}) - F_{7c\_23g}\cdot(A_{7c}) - F_{7a7b\_13e3b3c}\cdot(A_{7a} + A_{7b})}{2\cdot(A_{7a} + A_{7b})}$$

$$F_{7a7b\_3g} := \frac{F_{7c7b7a\_3g3e3c}\cdot(A_{7c} + A_{7b} + A_{7a}) - F_{7a7b\_3e3c}\cdot(A_{7a} + A_{7b}) - F_{7c\_3g}\cdot(A_{7c})}{2\cdot(A_{7a} + A_{7b})} = 4.026\times 10^{-4}$$

$F_{7a7b\_2} := F_{7a7b\_23g} - F_{7a7b\_3g} = 0.039$ $F_{7a7b\_23g} = 0.04$

$F_{2\_7a7b} := F_{7a7b\_2}\cdot\frac{(A_{7a} + A_{7b})}{A_2} = 0.064$ $F_{2\_7c} := F_{7c\_2}\cdot\frac{A_{7c}}{A_2} = 0.152$ $F_{2\_7d} := F_{7d\_2}\cdot\frac{A_{7d}}{A_2} = 0.042$

$F_{27} := F_{2\_7a7b} + F_{2\_7c} + F_{2\_7d} = 0.258$ $F_{72} := F_{27}\frac{A_2}{A_7} = 0.068$

View factor between PV section and left wall (1, 8):

$H := \frac{WTW + WTL}{HTPV}$ $W := \frac{LT}{HTPV}$ $F_{8b\_13d} := g(W,H) = 0.118$

$H := \frac{WTL}{HTPV}$ $W := \frac{LT}{HTPV}$ $F_{8b\_3d} := g(W,H) = 0.011$

$H := \frac{WTW + WTL}{HTPV + HTTOP}$ $W := \frac{LT}{HTPV + HTTOP}$ $F_{8a8b\_13d3b3a} := g(W,H) = 0.125$

$H := \frac{WTL}{HTPV + HTTOP}$ $W := \frac{LT}{HTPV + HTTOP}$ $F_{8a8b\_3d3a} := g(W,H) = 0.011$

$H := \frac{WTW + WTL}{HTTOP}$ $W := \frac{LT}{HTTOP}$ $F_{8a\_3a3b} := g(W,H) = 0.032$

$H := \frac{WTL}{HTTOP}$ $W := \frac{LT}{HTTOP}$ $F_{8a\_3a} := g(W,H) = 8.095 \times 10^{-3}$

$H := \frac{WTW + WTL}{HTPV + HTV + HTBOT}$ $W := \frac{LT}{HTPV + HTV + HTBOT}$

$F_{8b8c8d\_123i3d3f3h} := g(W,H) = 0.174$

$H := \frac{WTL}{HTPV + HTV + HTBOT}$ $W := \frac{LT}{HTPV + HTV + HTBOT}$ $F_{8b8c8d\_3d3f3h} := g(W,H) = 0.012$

$H := \frac{WTW + WTL}{HTV + HTBOT}$ $W := \frac{LT}{HTV + HTBOT}$ $F_{8c8d\_23i3f3h} := g(W,H) = 0.144$

$H := \frac{WTL}{HTV + HTBOT}$ $W := \frac{LT}{HTV + HTBOT}$ $F_{8c8d\_3f3h} := g(W,H) = 0.012$

$F_{8b\_1} := F_{8b\_13d} - F_{8b\_3d} = 0.106$

$$F_{8a\_13d} := \frac{F_{8a8b\_13d3b3a} \cdot (A_{8a} + A_{8b}) - F_{8b\_13d} \cdot (A_{8b}) - F_{8a\_3a3b} \cdot (A_{8a})}{2 \cdot A_{8a}} = 0.076$$

$$F_{8a\_3d} := \frac{F_{8a8b\_3d3a} \cdot (A_{8a} + A_{8b}) - F_{8a\_3a} \cdot (A_{8a}) - F_{8b\_3d} \cdot (A_{8b})}{2 \cdot A_{8a}} = 2.059 \times 10^{-3}$$

$F_{8a\_1} := F_{8a\_13d} - F_{8a\_3d} = 0.074$

$$F_{8c8d\_13d} := \frac{F_{8b8c8d\_123i3d3f3h} (A_{8b} + A_{8c} + A_{8d}) - F_{8b\_13d} \cdot (A_{8b}) - F_{8c8d\_23i3f3h} (A_{8c} + A_{8d})}{2 \cdot (A_{8c} + A_{8d})}$$

$$F_{8c8d\_3d} := \frac{F_{8b8c8d\_3d3f3h} \cdot (A_{8b} + A_{8c} + A_{8d}) - F_{8c8d\_3f3h} \cdot (A_{8c} + A_{8d}) - F_{8b\_3d} \cdot (A_{8b})}{2 \cdot (A_{8c} + A_{8d})}$$

$F_{8c8d\_13d} = 0.033$ $F_{8c8d\_3d} = 3.055 \times 10^{-4}$ $F_{8c8d\_1} := F_{8c8d\_13d} - F_{8c8d\_3d} = 0.033$

$$F_{1\_8a} := F_{8a\_1}\cdot\frac{A_{8a}}{A_1} = 0.014 \qquad F_{1\_8b} := F_{8b\_1}\cdot\frac{A_{8b}}{A_1} = 0.152 \qquad F_{1\_8c8d} := F_{8c8d\_1}\cdot\frac{(A_{8c}+A_{8d})}{A_1} = 0.072$$

$$F_{18} := F_{1\_8a} + F_{1\_8b} + F_{1\_8c8d} = 0.238$$

$$F_{81} := F_{18}\cdot\frac{A_1}{A_8} = 0.062$$

View factor between window section and left wall (2, 8)

$$H := \frac{WTW + WTL}{HTV} \qquad W := \frac{LT}{HTV} \qquad F_{8c\_23f} := g(W,H) = 0.118$$

$$H := \frac{WTL}{HTV} \qquad W := \frac{LT}{HTV} \qquad F_{8c\_3f} := g(W,H) = 0.011$$

$$H := \frac{WTW + WTL}{HTBOT} \qquad W := \frac{LT}{HTBOT} \qquad F_{8d\_3h3i} := g(W,H) = 0.082$$

$$H := \frac{WTL}{HTBOT} \qquad W := \frac{LT}{HTBOT} \qquad F_{8d\_3h} := g(W,H) = 0.011$$

$$H := \frac{WTW + WTL}{HTV + HTPV + HTTOP} \qquad W := \frac{LT}{HTV + HTPV + HTTOP} \qquad F_{8c8b8a\_213b3f3d3a} := g(W,H) = 0.164$$

$$H := \frac{WTL}{HTV + HTPV + HTTOP} \qquad W := \frac{LT}{HTV + HTPV + HTTOP} \qquad F_{8c8b8a\_3f3d3a} := g(W,H) = 0.012$$

$$F_{8d\_23f} := \frac{F_{8c8d\_23i3f3h}\cdot(A_{8c}+A_{8d}) - F_{8c\_23f}\cdot(A_{8c}) - F_{8d\_3h3i}\cdot(A_{8d})}{2\cdot A_{8d}} = 0.056$$

$$F_{8d\_3f} := \frac{F_{8c8d\_3f3h}\cdot(A_{8c}+A_{8d}) - F_{8d\_3h}\cdot(A_{8d}) - F_{8c\_3f}\cdot(A_{8c})}{2\cdot A_{8d}} = 7.672\times 10^{-4}$$

$$F_{8d\_2} := F_{8d\_23f} - F_{8d\_3f} = 0.055 \qquad F_{8c\_2} := F_{8c\_23f} - F_{8c\_3f} = 0.106$$

$$F_{8a8b\_23f} := \frac{F_{8c8b8a\_213b3f3d3a}\cdot(A_{8c}+A_{8b}+A_{8a}) - F_{8c\_23f}\cdot(A_{8c}) - F_{8a8b\_13d3b3a}\cdot(A_{8a}+A_{8b})}{2\cdot(A_{8a}+A_{8b})}$$

$$F_{8a8b\_3f} := \frac{F_{8c8b8a\_3f3d3a}\cdot(A_{8c}+A_{8b}+A_{8a}) - F_{8a8b\_3d3a}\cdot(A_{8a}+A_{8b}) - F_{8c\_3f}\cdot(A_{8c})}{2\cdot(A_{8a}+A_{8b})}$$

$$F_{8a8b\_23f} = 0.04 \qquad F_{8a8b\_3f} = 4.026\times 10^{-4}$$

$$F_{8a8b\_2} := F_{8a8b\_23f} - F_{8a8b\_3f} = 0.039 \qquad F_{2\_8a8b} := F_{8a8b\_2}\cdot\frac{(A_{8a}+A_{8b})}{A_2} = 0.064$$

$$F_{2\_8c} := F_{8c\_2}\cdot\frac{A_{8c}}{A_2} = 0.152 \qquad F_{2\_8d} := F_{8d\_2}\cdot\frac{A_{8d}}{A_2} = 0.042$$

$$F_{28} := F_{2\_8a8b} + F_{2\_8c} + F_{2\_8d} = 0.258 \qquad F_{82} := F_{28}\cdot\frac{A_2}{A_8} = 0.068$$

View factor between front wall section and right wall (3, 7)

$$F_{73} := 1 - F_{71} - F_{72} - F_{74} - F_{75} - F_{76} - F_{77} - F_{78} = 0.049$$

$$F_{37} := F_{73} \cdot \frac{A_7}{A_3} = 0.219$$

View factor between front wall section and left wall (3, 8)

$$F_{83} := 1 - F_{81} - F_{82} - F_{84} - F_{85} - F_{86} - F_{87} - F_{88} = 0.049$$

$$F_{38} := F_{83} \cdot \frac{A_8}{A_3} = 0.219$$

View factor from PV section to back wall (1, 6):

$$F_{16} := 1 - F_{11} - F_{12} - F_{13} - F_{14} - F_{15} - F_{17} - F_{18} = 0.164$$

$$F_{61} := F_{16} \cdot \frac{A_1}{A_6} = 0.058$$

View factor from window section to back wall (2, 6):

$$F_{26} := 1 - F_{21} - F_{22} - F_{23} - F_{24} - F_{25} - F_{27} - F_{28} = 0.175$$

$$F_{62} := F_{26} \cdot \frac{A_2}{A_6} = 0.061$$

View factor from opaque section to back wall (3, 6):

$$F_{36} := 1 - F_{31} - F_{32} - F_{33} - F_{34} - F_{35} - F_{37} - F_{38} = 0.147$$

$$F_{63} := F_{36} \cdot \frac{A_3}{A_6} = 0.044$$

Check that the form factors add to 1

$$F_{11} + F_{12} + F_{13} + F_{14} + F_{15} + F_{16} + F_{17} + F_{18} = 1$$
$$F_{21} + F_{22} + F_{23} + F_{24} + F_{25} + F_{26} + F_{27} + F_{28} = 1$$
$$F_{31} + F_{32} + F_{33} + F_{34} + F_{35} + F_{36} + F_{37} + F_{38} = 1$$
$$F_{41} + F_{42} + F_{43} + F_{44} + F_{45} + F_{46} + F_{47} + F_{48} = 1$$
$$F_{51} + F_{52} + F_{53} + F_{54} + F_{55} + F_{56} + F_{57} + F_{58} = 1$$
$$F_{61} + F_{62} + F_{63} + F_{64} + F_{65} + F_{66} + F_{67} + F_{68} = 1$$
$$F_{71} + F_{72} + F_{73} + F_{74} + F_{75} + F_{76} + F_{77} + F_{78} = 1$$
$$F_{81} + F_{82} + F_{83} + F_{84} + F_{85} + F_{86} + F_{87} + F_{88} = 1$$

$$F := \begin{pmatrix} F_{11} & F_{12} & F_{13} & F_{14} & F_{15} & F_{16} & F_{17} & F_{18} \\ F_{21} & F_{22} & F_{23} & F_{24} & F_{25} & F_{26} & F_{27} & F_{28} \\ F_{31} & F_{32} & F_{33} & F_{34} & F_{35} & F_{36} & F_{37} & F_{38} \\ F_{41} & F_{42} & F_{43} & F_{44} & F_{45} & F_{46} & F_{47} & F_{48} \\ F_{51} & F_{52} & F_{53} & F_{54} & F_{55} & F_{56} & F_{57} & F_{58} \\ F_{61} & F_{62} & F_{63} & F_{64} & F_{65} & F_{66} & F_{67} & F_{68} \\ F_{71} & F_{72} & F_{73} & F_{74} & F_{75} & F_{76} & F_{77} & F_{78} \\ F_{81} & F_{82} & F_{83} & F_{84} & F_{85} & F_{86} & F_{87} & F_{88} \end{pmatrix}$$

$$F = \begin{pmatrix} 0 & 0 & 0 & 0.086 & 0.273 & 0.164 & 0.238 & 0.238 \\ 0 & 0 & 0 & 0.192 & 0.118 & 0.175 & 0.258 & 0.258 \\ 0 & 0 & 0 & 0.274 & 0.142 & 0.147 & 0.219 & 0.219 \\ 0.03 & 0.067 & 0.082 & 0 & 0.163 & 0.179 & 0.239 & 0.239 \\ 0.096 & 0.041 & 0.043 & 0.163 & 0 & 0.179 & 0.239 & 0.239 \\ 0.058 & 0.061 & 0.044 & 0.179 & 0.179 & 0 & 0.239 & 0.239 \\ 0.062 & 0.068 & 0.049 & 0.179 & 0.179 & 0.179 & 0 & 0.283 \\ 0.062 & 0.068 & 0.049 & 0.179 & 0.179 & 0.179 & 0.283 & 0 \end{pmatrix}$$

APPENDIX VI H

Configuration factors relating room surfaces to workplane point

Configuration factors relate each surface to the workplane point and are required to calculate the workplane illuminance using the radiosity method

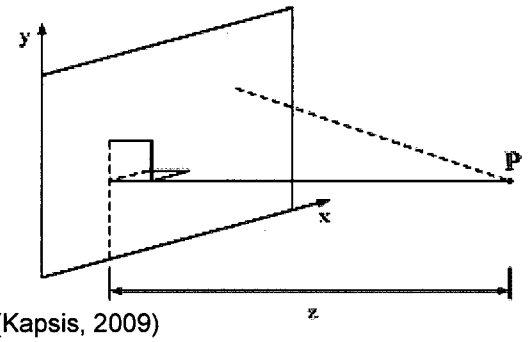

(Kapsis, 2009)

For perpendicular planes

$$f(x,y,z) := \frac{1}{2\cdot\pi}\cdot\left(\operatorname{atan}\left(\frac{x}{z}\right) - \frac{z}{\sqrt{y^2+z^2}}\cdot\operatorname{atan}\left(\frac{x}{\sqrt{y^2+z^2}}\right)\right)$$

For parallel planes

$$g(x,y,z) := \frac{1}{2\cdot\pi}\cdot\left[\left(\frac{y}{\sqrt{y^2+z^2}}\right)\cdot\operatorname{atan}\left(\frac{x}{\sqrt{y^2+z^2}}\right) + \frac{x}{\sqrt{x^2+z^2}}\cdot\operatorname{atan}\left(\frac{y}{\sqrt{x^2+z^2}}\right)\right]$$

Configuration factor between PV section of window and workplane point (surface 1)

$x := WPL - WTL$ $\quad y := HTBOT + HTPV + HTV - WPH = 3\,m$ $\quad z := DW$

$f_{1_1} := f(x,y,z)$ $\quad f_{1_1} = 0.065$

$x := WPR - WTR$ $\quad y := HTBOT + HTPV + HTV - WPH$ $\quad z := DW$

$f_{1_2} := f(x,y,z)$ $\quad f_{1_2} = 0.065$

$x := WPL - WTL$ $\quad y := HTBOT + HTPV - WPH$ $\quad z := DW$

$f_{1_3} := f(x,y,z)$ $\quad f_{1_3} = 0.032$

$x := WPR - WTR$ $\quad y := HTBOT + HTPV - WPH$ $\quad z := DW$

$f_{1_4} := f(x,y,z)$ $\quad f_{1_4} = 0.032$

$f1 := \left(f1_1 - f1_3\right) + \left(f1_2 - f1_4\right)$ $f1 = 0.065$

Configuration factor between viewing section of window and workplane point (surface 2)

$x := WPL - WTL$ $y := HTBOT + HTV - WPH$ $z := DW$

$f2_1 := f(x,y,z)$ $f2_1 = 0.032$

$x := WPR - WTR$ $y := HTBOT + HTV - WPH$ $z := DW$

$f2_2 := f(x,y,z)$ $f2_2 = 0.032$

$x := WPL - WTL$ $y := HTBOT - WPH$ $z := DW$

$f2_3 := f(x,y,z)$ $f2_3 = 0$

$x := WPR - WTR$ $y := HTBOT - WPH$ $z := DW$

$f2_4 := f(x,y,z)$ $f2_4 = 0$

$f2 := \left(f2_1 - f2_3\right) + \left(f2_2 - f2_4\right)$ $f2 = 0.064$

Configuration factor between floor and workplane point (surface 4)

$f4 := 0$

Configuration factor between ceiling and workplane point (Surface 5)

$x := DW$ $y := WPL$ $z := HT - WPH$ $g5_1 := g(x,y,z)$ $g5_1 = 0.067$

$x := DW$ $y := WPR$ $z := HT - WPH$ $g5_2 := g(x,y,z)$ $g5_2 = 0.067$

$x := LT - DW$ $y := WPL$ $z := HT - WPH$ $g5_3 := g(x,y,z)$ $g5_3 = 0.067$

$x := LT - DW$ $y := WPR$ $z := HT - WPH$ $g5_4 := g(x,y,z)$ $g5_4 = 0.067$

$f5 := \left(g5_1 + g5_2 + g5_3 + g5_4\right)$ $f5 = 0.267$

Configuration factor between back wall and workplane point (surface 6)

$x := WPL$ $y := HT - WPH$ $z := LT - DW$ $f6_1 := f(x,y,z)$ $f6_1 = 0.071$

$x := WPR$ $y := HT - WPH$ $z := LT - DW$ $f6_2 := f(x,y,z)$ $f6_2 = 0.071$

$f6 := \left(f6_1 + f6_2\right)$ $f6 = 0.141$

Configuration factor between right and left wall and workplane point (Surfaces 7, 8)

$x := DW$ $y := HT - WPH$ $z := WPR$ $f_{7_1} := f(x,y,z)$ $f_{7_1} = 0.113$

$x := LT - DW$ $y := HT - WPH$ $z := WPR$ $f_{7_2} := f(x,y,z)$ $f_{7_2} = 0.113$

$f7 := f_{7_1} + f_{7_2}$ $f7 = 0.226$

$x := DW$ $y := HT - WPH$ $z := WPL$ $f_{8_1} := f(x,y,z)$ $f_{8_1} = 0.113$

$x := LT - DW$ $y := HT - WPH$ $z := WPL$ $f_{8_2} := f(x,y,z)$ $f_{8_2} = 0.113$

$f8 := f_{8_1} + f_{8_2}$ $f8 = 0.226$

Configuration factor between front wall and workplane point (surface 3)

$f3 := 1 - f1 - f2 - f4 - f5 - f6 - f7 - f8 = 0.012$

$$f := \begin{pmatrix} f1 \\ f2 \\ f3 \\ f4 \\ f5 \\ f6 \\ f7 \\ f8 \end{pmatrix} = \begin{pmatrix} 0.065 \\ 0.064 \\ 0.012 \\ 0 \\ 0.267 \\ 0.141 \\ 0.226 \\ 0.226 \end{pmatrix}$$

The configuration factors between the workplane point and all the interior surfaces

APPENDIX VI I

Workplane illuminance

Illuminances through STPV and window viewing sections

Blind is employed only when normal beam irradiance is more than 100W/m2
Illuminance in STPV section is dependant on the PV area ratio

Effective illuminance of STPV section

$$E_{b\_STPV}(n,t_{oh},A_{PV}) := E_b(n,t_{oh})\cdot\tau_{b\_STPV\_blind}(n,t_{oh},A_{PV})$$

$$E_{d\_STPV}(n,t_{oh},A_{PV}) := E_d(n,t_{oh})\cdot\tau_{d\_STPV\_blind}(n,t_{oh},A_{PV})$$

$$E_{g\_STPV}(n,t_{oh},A_{PV}) := E_g(n,t_{oh})\cdot\tau_{d\_STPV\_blind}(n,t_{oh},A_{PV})$$

$$E_{STPV}(n,t_{oh},A_{PV}) := E_{b\_STPV}(n,t_{oh},A_{PV}) + E_{d\_STPV}(n,t_{oh},A_{PV}) + E_{g\_STPV}(n,t_{oh},A_{PV})$$

Effective illuminance of window viewing section

$$E_{b\_win}(n,t_{oh}) := E_b(n,t_{oh})\cdot\tau_{b\_win\_blind}(n,t_{oh})$$

$$E_{d\_win}(n,t_{oh}) := E_d(n,t_{oh})\cdot\tau_{d\_win\_blind}(n,t_{oh})$$

$$E_{g\_win}(n,t_{oh}) := E_g(n,t_{oh})\cdot\tau_{d\_win\_blind}(n,t_{oh})$$

$$E_{win}(n,t_{oh}) := E_{b\_win}(n,t_{oh}) + E_{d\_win}(n,t_{oh}) + E_{g\_win}(n,t_{oh})$$

Initial luminous existances of surfaces in the room:

Only the STPV and window viewing section have intial luminances

Beam :

$$M_{o\_b}(n,t_{oh},A_{PV}) := \begin{pmatrix} E_{b\_STPV}(n,t_{oh},A_{PV}) \\ E_{b\_win}(n,t_{oh}) \\ 0 \\ 0 \\ 0 \\ 0 \\ 0 \\ 0 \end{pmatrix}$$

Diffuse :

$$M_{o\_d}(n, t_{oh}, A_{PV}) := \begin{pmatrix} E_{d\_STPV}(n, t_{oh}, A_{PV}) + E_{g\_STPV}(n, t_{oh}, A_{PV}) \\ E_{d\_win}(n, t_{oh}) + E_{g\_win}(n, t_{oh}) \\ 0 \\ 0 \\ 0 \\ 0 \\ 0 \\ 0 \end{pmatrix}$$

Final luminous exitance of all surfaces:

Identity matrix:

$I := \text{identity}(8)$

Multiple reflections matrix:

Beam:

$\rho_{1b}(n, t_{oh}, A_{PV}) := \rho_{b\_STPV}(n, t_{oh}, A_{PV})$

$\rho_{2b}(n, t_{oh}) := \rho_{b\_win}(n, t_{oh})$

$$TT_b(n, t_{oh}, A_{PV}) := \begin{pmatrix} F_{11}\cdot\rho_{1b}(n, t_{oh}, A_{PV}) & F_{12}\cdot\rho_{1b}(n, t_{oh}, A_{PV}) & F_{13}\cdot\rho_{1b}(n, t_{oh}, A_{PV}) & F_{14}\cdot\rho_{1b}(n, t_{oh}, A_{PV}) & F_{15}\cdot\rho_{1b}(n, t_{oh}, A_{PV}) & F_{16}\cdot\rho_{1b}(n, t_{oh}, A_{PV}) & F_{17}\cdot\rho_{1b}(n, t_{oh}, A_{PV}) & F_{18}\cdot\rho_{1b}(n, t_{oh}, A_{PV}) \\ F_{21}\cdot\rho_{2b}(n, t_{oh}) & F_{22}\cdot\rho_{2b}(n, t_{oh}) & F_{23}\cdot\rho_{2b}(n, t_{oh}) & F_{24}\cdot\rho_{2b}(n, t_{oh}) & F_{25}\cdot\rho_{2b}(n, t_{oh}) & F_{26}\cdot\rho_{2b}(n, t_{oh}) & F_{27}\cdot\rho_{2b}(n, t_{oh}) & F_{28}\cdot\rho_{2b}(n, t_{oh}) \\ F_{31}\cdot\rho_3 & F_{32}\cdot\rho_3 & F_{33}\cdot\rho_3 & F_{34}\cdot\rho_3 & F_{35}\cdot\rho_3 & F_{36}\cdot\rho_3 & F_{37}\cdot\rho_3 & F_{38}\cdot\rho_3 \\ F_{41}\cdot\rho_4 & F_{42}\cdot\rho_4 & F_{43}\cdot\rho_4 & F_{44}\cdot\rho_4 & F_{45}\cdot\rho_4 & F_{46}\cdot\rho_4 & F_{47}\cdot\rho_4 & F_{48}\cdot\rho_4 \\ F_{51}\cdot\rho_5 & F_{52}\cdot\rho_5 & F_{53}\cdot\rho_5 & F_{54}\cdot\rho_5 & F_{55}\cdot\rho_5 & F_{56}\cdot\rho_5 & F_{57}\cdot\rho_5 & F_{58}\cdot\rho_5 \\ F_{61}\cdot\rho_6 & F_{62}\cdot\rho_6 & F_{63}\cdot\rho_6 & F_{64}\cdot\rho_6 & F_{65}\cdot\rho_6 & F_{66}\cdot\rho_6 & F_{67}\cdot\rho_6 & F_{68}\cdot\rho_6 \\ F_{71}\cdot\rho_7 & F_{72}\cdot\rho_7 & F_{73}\cdot\rho_7 & F_{74}\cdot\rho_7 & F_{75}\cdot\rho_7 & F_{76}\cdot\rho_7 & F_{77}\cdot\rho_7 & F_{78}\cdot\rho_7 \\ F_{81}\cdot\rho_8 & F_{82}\cdot\rho_8 & F_{83}\cdot\rho_8 & F_{84}\cdot\rho_8 & F_{85}\cdot\rho_8 & F_{86}\cdot\rho_8 & F_{87}\cdot\rho_8 & F_{88}\cdot\rho_8 \end{pmatrix}$$

$$M_b(n, t_{oh}, A_{PV}) := \left[\left(I - TT_b(n, t_{oh}, A_{PV})\right)^{-1}\right] \cdot M_{o\_b}(n, t_{oh}, A_{PV})$$

Diffuse :

$$\rho_{1d}(A_{PV}) := \rho_{d\_STPV}(A_{PV})$$

$$\rho_{2d} := \rho_{d\_win}$$

$$TT_d(A_{PV}) := \begin{pmatrix} F_{11}\cdot\rho_{1d}(A_{PV}) & F_{12}\cdot\rho_{1d}(A_{PV}) & F_{13}\cdot\rho_{1d}(A_{PV}) & F_{14}\cdot\rho_{1d}(A_{PV}) & F_{15}\cdot\rho_{1d}(A_{PV}) & F_{16}\cdot\rho_{1d}(A_{PV}) & F_{17}\cdot\rho_{1d}(A_{PV}) & F_{18}\cdot\rho_{1d}(A_{PV}) \\ F_{21}\cdot\rho_{2d} & F_{22}\cdot\rho_{2d} & F_{23}\cdot\rho_{2d} & F_{24}\cdot\rho_{2d} & F_{25}\cdot\rho_{2d} & F_{26}\cdot\rho_{2d} & F_{27}\cdot\rho_{2d} & F_{28}\cdot\rho_{2d} \\ F_{31}\cdot\rho_3 & F_{32}\cdot\rho_3 & F_{33}\cdot\rho_3 & F_{34}\cdot\rho_3 & F_{35}\cdot\rho_3 & F_{36}\cdot\rho_3 & F_{37}\cdot\rho_3 & F_{38}\cdot\rho_3 \\ F_{41}\cdot\rho_4 & F_{42}\cdot\rho_4 & F_{43}\cdot\rho_4 & F_{44}\cdot\rho_4 & F_{45}\cdot\rho_4 & F_{46}\cdot\rho_4 & F_{47}\cdot\rho_4 & F_{48}\cdot\rho_4 \\ F_{51}\cdot\rho_5 & F_{52}\cdot\rho_5 & F_{53}\cdot\rho_5 & F_{54}\cdot\rho_5 & F_{55}\cdot\rho_5 & F_{56}\cdot\rho_5 & F_{57}\cdot\rho_5 & F_{58}\cdot\rho_5 \\ F_{61}\cdot\rho_6 & F_{62}\cdot\rho_6 & F_{63}\cdot\rho_6 & F_{64}\cdot\rho_6 & F_{65}\cdot\rho_6 & F_{66}\cdot\rho_6 & F_{67}\cdot\rho_6 & F_{68}\cdot\rho_6 \\ F_{71}\cdot\rho_7 & F_{72}\cdot\rho_7 & F_{73}\cdot\rho_7 & F_{74}\cdot\rho_7 & F_{75}\cdot\rho_7 & F_{76}\cdot\rho_7 & F_{77}\cdot\rho_7 & F_{78}\cdot\rho_7 \\ F_{81}\cdot\rho_8 & F_{82}\cdot\rho_8 & F_{83}\cdot\rho_8 & F_{84}\cdot\rho_8 & F_{85}\cdot\rho_8 & F_{86}\cdot\rho_8 & F_{87}\cdot\rho_8 & F_{88}\cdot\rho_8 \end{pmatrix}$$

$$M_d(n, t_{oh}, A_{PV}) := \left[\left(I - TT_d(A_{PV})\right)^{-1}\right] \cdot M_{o\_d}(n, t_{oh}, A_{PV})$$

The horizontal illuminance on the workplane after infinite interreflections:

$$E_{workplane}(t_{oh}, n, A_{PV}) := \sum_{i=1}^{8} \left(M_b(n, t_{oh}, A_{PV})_i \cdot f_i\right) + \sum_{i=1}^{8} \left(M_d(n, t_{oh}, A_{PV})_i \cdot f_i\right)$$

APPENDIX VI J

Power required for luminaires to achieve desired illuminance on workplane

Lumen method to select lumianires required to supplement daylighting

Cavity ratios for this specific room:

$$FCR := \frac{5 \cdot WPH \cdot (LT + WT)}{LT \cdot WT} \qquad FCR = 2.333$$ Floor cavity ratio

$$RCR := \frac{5 \cdot (HT - WPH - h_{ceiling}) \cdot (LT + WT)}{LT \cdot WT} \qquad RCR = 8.75$$ Room cavity ratio

$$CCR := \frac{5 \cdot (h_{ceiling}) \cdot (LT + WT)}{LT \cdot WT} \qquad CCR = 0.583$$ Ceiling cavity ratio

Effective reflectances:

$\rho_{c\_eff} := .73$ Using figure 9-27 in IESNA 2000 the percentage effective ceiling reflectance is determined, using CCR of 0.6 and base reflectance of 0.8

$\rho_{f\_eff} := .2$ Using figure 9-27 in IESNA 2000 the percentage effective ceiling reflectance is determined, using FCR of 2.4 and base reflectance of 0.2

Coefficient of utilisation:

$CU := .395$ Using a RCR of 9, ceiling reflectance of 0.7, wall reflectance of 0.6, and a floor reflectance of 0.2 and luminaire 24 in IESNA 2000

Workplane area:

$A_{wp} := (LT \cdot WT) = 12 m^2$

Lumens required assuming no light coming from daylight (worse case)

$$\phi_{initial} := \frac{E_{desired} \cdot A_{wp}}{CU \cdot LLF}$$

$$N_{lum\_initial} := \frac{\phi_{initial}}{N_{tubes} \cdot Lm_{tube} \cdot EFF}$$

$N_{lum\_full} := 2$ If 300 lx is required on the workplane 2 luminaires are required. If 500lx is desired, 3 luminaires are required

Number of luminaires required to supplement daylight:

Luminaires are daylight controlled and will only turn on if workplane illuminance is not at the desired level

For automatic dimming control of lighting:

$$E_{required\_lamps}(n, t_{oh}, A_{PV}) := \begin{cases} 0 \text{ if } E_{workplane}(t_{oh}, n, A_{PV}) \geq E_{desired} \\ \left(E_{desired} - E_{workplane}(t_{oh}, n, A_{PV})\right) \text{ otherwise} \end{cases}$$

Fractional electric lighting output:

$$f_L(n, t_{oh}, A_{PV}) := \max\left[0, \left(\frac{E_{desired} - E_{workplane}(t_{oh}, n, A_{PV})}{E_{desired}}\right)\right]$$

Fractional electric lighting input power:

$$f_p(n, t_{oh}, A_{PV}) := \begin{cases} f_{pmin} \text{ if } f_L(n, t_{oh}, A_{PV}) < f_{Lmin} \\ \dfrac{f_L(n, t_{oh}, A_{PV}) + \left(1 - f_L(n, t_{oh}, A_{PV})\right) \cdot f_{pmin} - f_{Lmin}}{1 - f_{Lmin}} \text{ otherwise} \end{cases}$$

$$\phi_{required}(n, t_{oh}, A_{PV}) := \frac{E_{required\_lamps}(n, t_{oh}, A_{PV}) \cdot A_{wp}}{CU \cdot LLF}$$

$$N_{lum\_required}(n, t_{oh}, A_{PV}) := \frac{\phi_{required}(n, t_{oh}, A_{PV})}{N_{tubes} \cdot Lm_{tube} \cdot EFF}$$

For active on/off control of lighting:

$$E_{required\_lamps}(n, t_{oh}, A_{PV}) := \begin{cases} 0 \text{ if } E_{workplane}(t_{oh}, n, A_{PV}) \geq E_{desired} \\ E_{desired} \text{ otherwise} \end{cases}$$

Fractional electric lighting input:

$$f_p(n, t_{oh}, A_{PV}) := \begin{cases} 0 \text{ if } E_{workplane}(t_{oh}, n, A_{PV}) \geq E_{desired} \\ 1 \text{ otherwise} \end{cases}$$

$$N_{lum\_required}(n, t_{oh}, A_{PV}) := N_{lum\_full}$$

Power required for the lighting:

$$P_{lamps}(t_{oh}, n, A_{PV}) := N_{lum\_required}(n, t_{oh}, A_{PV}) \cdot P_{tube} \cdot N_{tubes} \cdot f_p(n, t_{oh}, A_{PV})$$

APPENDIX VI K

Power generated from photovoltaic cells

Standard test conditions:

$I_{STC} := 1000 \frac{watt}{m^2}$ Irradiance at STC

$T_{STC} := 25$ Cell temperature at STC

$I_o := 800 \frac{watt}{m^2}$ Reference irradiance

Cell temperature of the PV:

$$T_{cell}(n,t) := T_o(n,t) + \left(I_t(n,t)\right) \cdot \left(\frac{NOCT - 20}{I_o}\right)$$ (Messenger 2000)

Efficiency loss due to temperature deviation from STC:

$$\Delta\eta_{temp}(n,t) := \eta_{STC} \cdot \left[\eta_{power\_temp} \cdot \left(T_{cell}(n,t) - T_{STC}\right)\right]$$

Overall PV efficiency:

$$\eta(n,t) := \eta_{STC} - \Delta\eta_{temp}(n,t)$$

$$P_{PV}\left(t,n,A_{PV}\right) := I_t(n,t) \cdot A_{PV} A_1 \cdot \eta(n,t)$$

APPENDIX VII

Heat transfer through façade-
MathCAD simulation model

A- Model inputs
B- Heat transfer coefficients
C- U values
D- Solar heat gain coefficients
E- Total heat gain through façade

APPENDIX VII A

Inputs for thermal model:

All data is taken from the prototype window.

Design day measured glazing temperatures:

These temperatures were measured with thermocouples placed throughout the glazing. The values are input for each analysis and were taken at solar noon for the given design day.

$T_{g1} := 28$	Outer glazing- exterior (g1- c)
$T_{g2\_STPV} := 34.1$	Outer glazing- interior behind PV (g2-b)
$T_{g2\_win} := 28.2$	Outer glazing- interior behind clear (g2-d)
$T_{g3\_STPV} := 28.1$	Inner glazing- exterior behind PV (g3-b)
$T_{g3\_win} := 28.8$	Inner glazing- exterior behind clear (g3-d)
$T_{g4\_STPV} := 27.7$	Inner glazing- interior behind PV (g4-b)
$T_{g4\_win} := 28.5$	Inner glazing- interior behind clear (g4-d)
$T_{room} := 23.9$	Room temperature

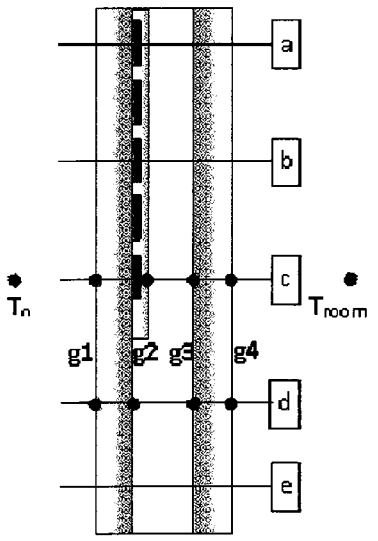

Design day outdoor conditions:

$T_o := 21.9$ Exterior temperature

$v_o := 4$ Wind velocity

$\theta := 68.094\,deg$ Angle of incidence

$I_b := 30.3 \cdot \frac{watt}{m^2}$ Exterior beam radiation incident on surface

$I_d := 238.5 \frac{watt}{m^2}$ Exterior diffuse radiation incident on surface

$I_g := 59.8 \frac{watt}{m^2}$ Exterior ground reflected radiation incident on surface

$I_t := 328.6 \frac{watt}{m^2}$ Exterior total radiation incident on surface

$p := 1$ Pressure (atm)

$degC \equiv 1$

Glazing properties:

$L := 50 \cdot mm$ Length of cavity

$h_{int} := 10 \cdot \frac{W}{m^2 \cdot K}$ Estimated interior film coefficient

$A_1 := 1.248 m^2$ Area of STPV section

$A_2 := 1.008 m^2$ Area of viewing section

$A_{pv} := 0.61$ Area ratio of PV in upper section

Solar absorptances of the individual layers as a function of angle of incidence of the sun
These values are taken from the measured on Jan.7 and Jan. 10

$\alpha_{EVA\_b} := .0116\theta^2 - .0042\theta + .050$ EVA & g1- Beam

$\alpha_{EVA\_d} := .05$ EVA & g1- Diffuse

$\alpha_{lowe2\_b} := -.1335\theta^3 + .2734\theta^2 - 0.1404\theta + .127$ g2 behind STPV- Beam

$\alpha_{lowe2\_d} := 0.12$ g2 behind STPV- Diffuse

$\alpha_{clear\_b} := .0274\theta^2 - .0091\theta + .08$ g1- Beam

$\alpha_{clear\_d} := 0.1$ g1- Diffuse

$\alpha_{lowe\_b} := -.1501\theta^3 + .3122\theta^2 - .165\theta + .137$ g2 behind viewing section- Beam

$\alpha_{lowe\_d} := 0.13$ g2 behind viewing section- Diffuse

$\alpha_{clear\_PV\_b} := .002\theta^2 + .0222\theta + .077$ g1 in front of PV- Beam

$\alpha_{clear\_PV\_d} := .104$ g1 in front of PV- Diffuse

$\alpha_{PV\_eff\_b} := -.6087\theta^3 + 1.0573\theta^2 - 0.628\theta + .906$ Effective PV- Beam

$\alpha_{PV\_eff\_d} := .712$ Effective PV- Diffuse

Solar transmittances of entire window as function of angle of incidence of the sun

$\tau_{EVA\_b} := -.6418\theta^3 + 1.0008\theta^2 - .5789\theta + .823$ EVA section (EVA + g1 + g2)- Beam

$\tau_{EVA\_d} := .2776$ EVA section (EVA + g1 + g2)- Diffuse

$\tau_{PV\_b} := 0$ PV section (PV + g1 +g2) - Beam

$\tau_{PV\_d} := 0$ PV section (PV + g1 +g2) - Diffuse

$\tau_{win\_b} := -.7102\theta^3 + 1.1406\theta^2 - .6738\theta + .877$ Window section (g1 +g2)- Beam

$\tau_{win\_d} := .5005$ Window section (g1 +g2)- Diffuse

$\tau_{clear\_b} := .8626$ for theta <60deg Clear front glazing (g1)- Beam

$\tau_{clear\_b} := .5781\theta + 1.594$ for theta >60deg

$\tau_{clear\_d} := .8487$ Clear front glazing (g2)- Diffuse

APPENDIX VII B

Heat transfer coefficients

Convective heat transfer coefficient for vertical cavity- STPV section: (Athienitis 1999)

$$Tm\_STPV := \left(\frac{T_{g2\_STPV} + T_{g3\_STPV}}{2} + 273 \right)$$ Mean temperature

$$a\_STPV := \frac{100 \cdot degC}{Tm\_STPV}$$

$$k_{air\_STPV} := \frac{0.002528 Tm\_STPV^{1.5}}{Tm\_STPV + 200} \cdot \frac{watt}{m \cdot K}$$ Thermal conductivity of air

$$Ra\_STPV := 2.737 \cdot (1 + 2 \cdot a\_STPV)^2 \cdot a\_STPV^4 \cdot \left(T_{g2\_STPV} - T_{g3\_STPV}\right) \cdot \left(\frac{L}{mm}\right)^3 \cdot p^2$$ Rayleigh number

$$Nu1_{STPV} := 0.0605 (Ra\_STPV)^{\frac{1}{3}}$$ Nusselt numbers

$$Nu2_{STPV} := \left[1 + \frac{0.104 (Ra\_STPV)^{0.293}}{\left[1 + \left(\frac{6310}{Ra\_STPV} \right)^{1.36} \right]^3} \right]^{\frac{1}{3}}$$

Convective heat transfer coefficient of the STPV section:

$$hc_{cav\_STPV} := \frac{k_{air\_STPV}}{L} \cdot if\left(Nu1_{STPV} > Nu2_{STPV}, Nu1_{STPV}, Nu2_{STPV}\right)$$

Convective heat transfer coefficient for vertical cavity- window viewing section:

$$Tm\_win := \left(\frac{T_{g2\_win} + T_{g3\_win}}{2} + 273 \right)$$ Mean temperature

$$a\_win := \frac{100 \cdot degC}{Tm\_win}$$

$$k_{air\_win} := \frac{0.002528 Tm\_win^{1.5}}{Tm\_win + 200} \cdot \frac{watt}{m \cdot K}$$ Thermal conductivity of air

$$Ra\_win := 2.737 (1 + 2 \cdot a\_win)^2 \cdot a\_win^4 \cdot \left(T_{g3\_win} - T_{g2\_win}\right) \cdot \left(\frac{L}{mm}\right)^3 \cdot p^2$$ Rayleigh number

$$Nu1_{win} := 0.0605 (Ra\_win)^{\frac{1}{3}}$$ Nusselt numbers

$$Nu2_{win} := \left[1 + \frac{0.104 (Ra\_win)^{0.293}}{\left[1 + \left(\frac{6310}{Ra\_win}\right)^{1.36}\right]^3}\right]^{\frac{1}{3}}$$

Convective heat transfer coefficient of the window viewing section:

$$hc_{cav\_win} := \frac{k_{air\_win}}{L} \cdot if\left(Nu1_{win} > Nu2_{win}, Nu1_{win}, Nu2_{win}\right)$$

Radiative heat transfer coefficient for vertical cavity:

$\varepsilon_1 := 0.9$ Emissivity of outer pane- facing cavity

$\varepsilon_2 := 0.1$ Emissivity of inner pane- facing cavity

$$\sigma := 5.67 \cdot 10^{-8} \cdot \frac{watt}{m^2 \cdot K^4}$$ Stefan-Boltzmann constant

For the STPV section:

$$hr_{cav\_STPV} := \frac{4 \cdot \sigma \cdot (Tm\_STPV \cdot K)^3}{\left(\frac{1}{\varepsilon_1} + \frac{1}{\varepsilon_2} - 1\right)}$$

For the window section:

$$hr_{cav\_win} := \frac{4 \cdot \sigma \cdot (Tm\_win \cdot K)^3}{\left(\frac{1}{\varepsilon_1} + \frac{1}{\varepsilon_2} - 1\right)}$$

Total heat transfer coefficient for vertical cavity:

$$h_{cav\_STPV} := hc_{cav\_STPV} + hr_{cav\_STPV} = 1.931 \frac{kg}{K \cdot s^3}$$

$$h_{cav\_win} := hc_{cav\_win} + hr_{cav\_win} = 1.222 \frac{kg}{K \cdot s^3}$$

APPENDIX VII C

U values

Front clear glazing: g1

$t_{g1} := 6 \cdot mm$ Thickness

$k_{g1} := .78 \cdot \frac{W}{m \cdot K}$ Thermal conductivity

Photovoltaic layer: pv

$t_{pv} := .1 \cdot mm$ Thickness

$k_{pv} := 168 \cdot \frac{W}{m \cdot K}$ Thermal conductivity

EVA layer: EVA

$t_{EVA} := 2 \cdot mm$ Thickness

$k_{EVA} := .116 \cdot \frac{W}{m \cdot K}$ Thermal conductivity

Inner glazing: g2

$t_{g2} := 6 \cdot mm$ Thickness

$k_{g2} := .78 \cdot \frac{W}{m \cdot K}$ Thermal conductivity

U value of PV section:

$$U_{pv} := \frac{1}{\frac{1}{h_{ext}} + \frac{t_{g1}}{k_{g1}} + \frac{t_{pv}}{k_{pv}} + \frac{t_{EVA}}{k_{EVA}} + \frac{1}{h_{cav\_STPV}} + \frac{t_{g2}}{k_{g2}} + \frac{1}{h_{int}}} \qquad U_{pv} = 1.38 \frac{1}{K} \cdot \frac{W}{m^2}$$

U value of EVA section:

$$U_{EVA} := \frac{1}{\frac{1}{h_{ext}} + \frac{t_{g1}}{k_{g1}} + \frac{t_{EVA}}{k_{EVA}} + \frac{1}{h_{cav\_STPV}} + \frac{t_{g2}}{k_{g2}} + \frac{1}{h_{int}}} \qquad U_{EVA} = 1.38 \frac{1}{K} \cdot \frac{W}{m^2}$$

U value of clear viewing section:

$$U_{win} := \frac{1}{\frac{1}{h_{ext}} + \frac{t_{g1}}{k_{g1}} + \frac{1}{h_{cav\_win}} + \frac{t_{g2}}{k_{g2}} + \frac{1}{h_{int}}} \qquad U_{win} = 0.992 \frac{1}{K} \cdot \frac{W}{m^2}$$

PV area weighted U value:

$$U_{eff\_PV} := \frac{U_{pv} \cdot A_{pv} \cdot A_1 + U_{EVA} \cdot (1 - A_{pv}) \cdot A_1}{A_1} \qquad U_{eff\_PV} = 1.38 \frac{1}{m^2 \cdot K} \cdot W$$

APPENDIX VII D

Solar Heat gain coefficients:

Inward flowing fractions:

$$N_{1\_STPV} := \frac{U_{eff\_PV}}{h_{ext}} \qquad N_{2\_STPV} := \frac{h_{ext} + U_{eff\_PV}}{h_{ext}}$$

$$N_{1\_win} := \frac{U_{win}}{h_{ext}} \qquad N_{2\_win} := \frac{h_{ext} + U_{win}}{h_{ext}}$$

The amount of radiation the PV layer absorbs is equal to the absorptance of the layer minus the electricity produced from the PV.

$\eta_{STC} := .11$ Efficiency of PV at standard test conditions

$\eta_{power\_temp} := .005$ Power temperature coefficient

$NOCT := 45$ Nominal operating cell temperature

$T_{o\_NOCT} := 25$ Outdoor temperature at NOCT

$I_{STC} := 1000 \frac{watt}{m^2}$ Irradiance at Standard test conditions

$T_{STC} := 25$ Cell temperature at sandard test conditions

$I_o := 800 \frac{watt}{m^2}$ Reference irradiance

Cell temperature of the PV:

$$T_{cell} := T_o + I_t \cdot \left(\frac{NOCT - 20}{I_o} \right) = 32.169$$ Check this temperature with Tg2_STPV

Efficiency loss due to temperature deviation from STC:

$$\Delta\eta_{temp} := \eta_{STC} \cdot \left[\eta_{power\_temp} \cdot (T_{cell} - T_{STC}) \right]$$

$$\eta := \eta_{STC} - \Delta\eta_{temp}$$

Overall absorptance of PV layer

$$\alpha_{PV\_beam} := \left[(\alpha_{PV\_eff\_b}) \cdot (1 - \eta) + (\alpha_{clear\_PV\_b}) \right]$$

$$\alpha_{PV\_diffuse} := \left[(\alpha_{PV\_eff\_d}) \cdot (1 - \eta) + (\alpha_{clear\_PV\_d}) \right]$$

Solar heat gain coefficient of PV section:

Note that the absorptance of the layer directly behind the PV is zero

$$SHGC_{PV\_beam} := \tau_{PV\_b} + N_{1\_STPV} \cdot \alpha_{PV\_beam} + N_{2\_STPV} \cdot 0$$

$$SHGC_{PV\_diffuse} := \tau_{PV\_d} + N_{1\_STPV} \cdot \alpha_{PV\_diffuse} + N_{2\_STPV} \cdot 0$$

Solar heat gain coefficient of EVA section:

$$SHGC_{EVA\_beam} := \tau_{EVA\_b} + N_{1\_STPV} \cdot \alpha_{EVA\_b} + N_{2\_STPV} \cdot \alpha_{lowe2\_b}$$

$$SHGC_{EVA\_diffuse} := \tau_{EVA\_d} + N_{1\_STPV} \cdot \alpha_{EVA\_d} + N_{2\_STPV} \cdot \alpha_{lowe2\_d}$$

Solar heat gain coefficient of the window viewing section:

$$SHGC_{win\_beam} := \tau_{win\_b} + N_{1\_win} \cdot \alpha_{clear\_b} + N_{2\_win} \cdot \alpha_{lowe\_b}$$

$$SHGC_{win\_diffuse} := \tau_{win\_d} + N_{1\_win} \cdot \alpha_{clear\_d} + N_{2\_win} \cdot (\alpha_{lowe\_d})$$

Overall area weighted solar heat gain coefficient:

$$SHGC_{eff\_beam} := \frac{SHGC_{PV\_beam} \cdot (A_1 \cdot A_{pv}) + SHGC_{EVA\_beam} \cdot [A_1 \cdot (1 - A_{pv})] + SHGC_{win\_beam} \cdot A_2}{A_1 + A_2}$$

$$SHGC_{eff\_diffuse} := \frac{SHGC_{PV\_diffuse} \cdot (A_1 \cdot A_{pv}) + SHGC_{EVA\_diffuse} \cdot [A_1 \cdot (1 - A_{pv})] + SHGC_{win\_diffuse} \cdot A_2}{A_1 + A_2}$$

APPENDIX VII E

Heat gain through facade

Thermal energy flow (instantaneous energy flow due to indoor-outdoor temperature difference)

Total:

$$Q_{th} := \left[\left(U_{eff\_PV} A_1\right) + \left(U_{win} A_2\right)\right] \cdot \left(T_o - T_{room}\right) \cdot K$$

STPV section:

$$Q_{th\_PV} := U_{pv} \cdot A_1 \cdot A_{pv} \cdot \left(T_o - T_{room}\right) \cdot K$$

$$Q_{th\_EVA} := U_{EVA} \cdot A_1 \cdot \left(1 - A_{pv}\right) \cdot \left(T_o - T_{room}\right) \cdot K$$

Window viewing section:

$$Q_{th\_win} := U_{win} \cdot A_2 \cdot \left(T_o - T_{room}\right) \cdot K$$

Solar energy flow (instantaneous energy flow due to solar radiation)

Total:

$$Q_{sol} := SHGC_{eff\_beam} \cdot \left(A_1 + A_2\right) I_b + SHGC_{eff\_diffuse} \cdot \left(A_1 + A_2\right) \cdot \left(I_d + I_g\right)$$

STPV section:

$$Q_{sol\_PV} := SHGC_{PV\_beam} \cdot \left(A_1 \cdot A_{pv}\right) I_b + SHGC_{PV\_diffuse} \cdot \left(A_1 \cdot A_{pv}\right) \cdot \left(I_d + I_g\right)$$

$$Q_{sol\_EVA} := SHGC_{EVA\_beam} \cdot \left[A_1 \cdot \left(1 - A_{pv}\right)\right] I_b + SHGC_{EVA\_diffuse} \cdot \left[A_1 \cdot \left(1 - A_{pv}\right)\right] \cdot \left(I_d + I_g\right)$$

Window viewing section:

$$Q_{sol\_win} := SHGC_{win\_beam} \cdot \left(A_2\right) I_b + SHGC_{win\_diffuse} \cdot \left(A_2\right) \cdot \left(I_d + I_g\right)$$

Total instantaneous energy flow:

$$Q_{facade} := Q_{th} + Q_{sol}$$